ANTINEUTRINO-BASED SAFEGUARDS FOR ULTRA-HIGH BURNUP FAST REACTORS

A Thesis
Presented to
The Academic Faculty

by

Christopher Stewart

In Partial Fulfillment
of the Requirements for the Degree
Doctor of Philosophy in the
Nuclear & Radiological Engineering Program

Georgia Institute of Technology
May 2016

ANTINEUTRINO-BASED SAFEGUARDS FOR ULTRA-HIGH BURNUP FAST REACTORS

Approved by:

Anna Erickson, Committee Chair
Nuclear & Radiological Engineering Program
Georgia Institute of Technology

Anna Erickson, Advisor
Nuclear & Radiological Engineering Program
Georgia Institute of Technology

Nolan Hertel
Nuclear and Radiological Engineering
Georgia Institute of Technology

Patrick Huber
Department of Physics
Virginia Polytechnic Institute and State University

Bojan Petrovic
Nuclear and Radiological Engineering
Georgia Institute of Technology

Adam Stulberg
School of International Affairs
Georgia Institute of Technology

Date Approved: 22 February 2016

To my parents, Michael and Janet, who cleared the way for me to pursue my dreams.

ACKNOWLEDGEMENTS

I would like to thank my committee for their help and support. Professor Huber, in particular, was instrumental in moving the research forward, providing both up-to-date antineutrino yield estimates and the basis for the statistical comparison framework.

I have had the great fortune of educators who have gone above and beyond to nurture my sense of wonder and my excitement for studying the world around me and deciphering its puzzles. I will never forget when Terry Johnson, my high school physics teacher, handed me the first of what would become many extracurricular problems in pattern recognition, deduction, and model development. Dr. Brau, my undergraduate advisor, and Dr. Jarvis introduced me to the world of structured research; Dr. Stacey focused me toward solving large-scale engineering problems. Perhaps most importantly, Dr. Erickson—by demanding excellence in process and product—taught me how to push myself harder than I ever have before while maintaining the context and goal of strife lest the flame of my passion for research sputter and fade. She pushed me to my breaking point and, with one conversation, helped reforge me into a better, stronger, and more determined person. I will forever be thankful for her efforts, patience, and influence.

TABLE OF CONTENTS

LIST OF TABLES

LIST OF FIGURES

SUMMARY

Since the first observation of antineutrinos from beta decay of the fission products inside a nuclear reactor in 1956, the design and operating experience of antineutrino detectors near reactors has increased to the point where monitoring the reactor's power level and progression through its burnup cycle has become possible. With the expected increase in world nuclear energy capacity, including the dissemination of reactor technologies to non-nuclear states, the need for safeguards measures which are able to provide continuous, near-real-time information about the state of the core, including its isotopic composition, in a tamper- and spoof-resistant manner is evident. Near-field (20 m from the core) antineutrino detectors are able to fulfill this demand without perturbing normal reactor operation, without requiring instrumentation which penetrates the reactor vessel, and without displacing other plant structures.

Two sodium-cooled long-life fast reactors that are characteristic of next-generation reactors which are attractive for installation in non-nuclear states, one large and one small power rating, have been modeled throughout their reference burnup cycles using MCC-3 and DIF3D/REBUS. Various diversions of fissile material from the core designed to obtain weapons-usable material for the purpose of nuclear proliferation were studied as perturbed core states. The difference in detector event rates between the reference and perturbed states was used to determine the probability that a particular diversionary activity would be apparent before the material could be converted into a weapon. These data indicate which types of diversion antineutrino safeguards are particularly strong against and how the technology might be implemented in current and future international policies concerning nuclear proliferation.

CHAPTER I

INTRODUCTION

1.1 Nuclear power expansion

The expansion of nuclear power generation in the nuclear states is a key element in the reduction of carbon emissions originating from those nations. However, with many non-nuclear states on the cusp of rapid industrialization and economic expansion, the gains made in emissions reduction by the nuclear states could be more than outstripped by the increase in these developing nations[22, 34, 26]. These states, which will soon need large-scale electricity generation for the first time in their history, represent an enormous energy market into which the nuclear industry would like to expand; the low operating cost of nuclear power and the emphasis on modular design of the Gen-IV reactors[6] are attractive features which make such an expansion mutually beneficial.

A rapidly rising portion—35% as of 2005—of the human population lives in freshwater-scarce regions[31], and desalination plants offer the ability to purify brackish and sea waters to mitigate shortages[42]. Nuclear energy is a good candidate for supplying process heat in desalination plants because the waste heat shed through tertiary cooling loops is at the ideal temperature for these processes[37]. This heat must be shed to facilitate safe reactor operation, and would normally be sent to the plant's ultimate heat sink; it is essentially free to use.

In developed economies there is increasing incentive and means to adapt the electric grid to smooth out its daily load cycle across all 24 hours[21]. A large part of this incentive is due to the shift to electric cars which are both most efficiently and conveniently charged at night when grid load is low[16]. Implementation of a smart

grid which uses energy storage technologies at both the grid and residential scales can also more evenly distribute the load[21]. The transition to a load cycle with less variation can take maximum advantage of the high economic efficiency provided by base load generation via nuclear power.

However, a prime barrier to the expansion of nuclear power in general, and in non-nuclear states in particular, is the propensity for the distribution of nuclear material and technology to result in the proliferation of nuclear weapons[26, 10].

1.2 Proliferation concerns

Because nuclear energy requires the development of either the capability to enrich uranium, obtain and reprocess spent (plutonium-bearing) fuel, or the use of heavy-water- or graphite-moderated reactors which use natural uranium fuels with low burnup at discharge (and therefore relatively weapons-usable plutonium), it is beneficial from a non-proliferation perspective to have fuel cycle states (those with such capability already established) provide reactor facilities and fabricated fuel directly to a user state, potentially in turnkey format, and to take back spent fuel for reprocessing or disposal[59]. Doing so allows for expanded nuclear energy capacity without increasing the number of actors with the technology required to produce either highly enriched uranium (HEU) or weapons-usable plutonium. Nonetheless, the use—as intended—of uranium in a nuclear reactor unavoidably generates ^{233}U and/or ^{239}Pu *in situ*. Even with the most proliferation-resistant format of nuclear energy expansion, the supplied material must still be accounted for during its time in the user state. Any expansion of nuclear energy production, under any format, must therefore be accompanied by robust safeguards and transparency of nuclear plant operation and nuclear material transfer and use.

1.3 Current safeguards regime

Currently, nuclear materials are reported by each nation possessing them to the International Atomic Energy Agency (IAEA), which then verifies the reported amounts, locations, and uses through sampling, on-site inspections, and checking operations records. For reactor fuel, the combination of the reactor power history and visual identification of the unique stamped number on each assembly, as well as checks for broken seals indicating unauthorized access are the main methods used to ensure that the reported values are accurate[17]. However, since these inspections have significant periods of time between them and are vulnerable to spoofing, several weeks may elapse between a successful diversion and its discovery. Depending on the readiness of the actor performing the diversion to use the material, the discovery may well be too late to prevent its use; for plutonium obtained from current forms of spent fuel, the estimated time for conversion to a weapon is 1-3 months, and for low-enriched uranium (LEU) it is 3-12 months[23]. The amount of each material that constitutes one significant quantity (SQ) is 8 kg for plutonium from irradiated fuel and 75 kg of ^{235}U in LEU[23]. These quantities can be obtained via removal of a few fuel assemblies from a commercial power reactor. For some diversions, a single assembly is enough—highlighting the necessity of high sensitivity in the application of safeguards technologies.

1.4 Development of antineutrino detectors for safeguards

As the number of nations engaging in nuclear energy use grows and the fuel cycle becomes more complex and internationalized, the stresses on the safeguards infrastructure will only increase[60]. Two of the most valuable qualities which new safeguards technologies can possess are the capability for always-on, real-time monitoring and

the integrity of the data provided. There are proposed operator-independent monitoring methods employing near-core ($\sim$ 20 m) antineutrino detection which are always on and approach real-time, limited by the time required to obtain sufficiently fine statistics to discern between reactor states[9]. The use of an always-on monitor independent of the reactor operator, in addition to observing the current reactor state, offers the benefit of verifying the operating history itself, and thereby placing an upper bound on the amount of fissile material generated[12, 8].

1.4.1 Safeguards-relevant properties of antineutrinos

Nuclear reactors produce a copious electron antineutrino ($\bar{\nu}_e$) flux which results from the β^- decay of the fission fragments (Equation 1). On average, approximately six such decays occur per fission; at $\sim$ 200 MeV released per fission, there are $O\left(10^{20}\right)$ antineutrinos generated per second per $\mathrm{GW_{th}}$.

$$ {}^{A}_{Z}X \rightarrow {}^{A}_{Z+1}Y + \beta^- + \bar{\nu}_e \tag{1} $$

Because the fission product distribution varies slightly depending on the isotope fissioned and, to a lesser extent, the neutron spectrum in the reactor, the antineutrino flux and energy spectrum is dependent upon the fission rates of each isotope in the reactor (Figure 1). Using this dependence and a known initial fuel composition and reactor neutron spectrum, it is therefore possible to produce a reference detector signal which should occur as a function of burnup[13] and compare the measured signal to determine if there is substantial deviation in either magnitude or spectrum which would indicate that a diversion of fuel has taken place, even if it has been replaced by a reactivity-equivalent substitute intended to spoof other means of detection.

Despite the extremely low interaction cross section (less than 10^{-40} cm^2) of neutrinos with matter, such a large antineutrino flux results in a sufficient detection rate for

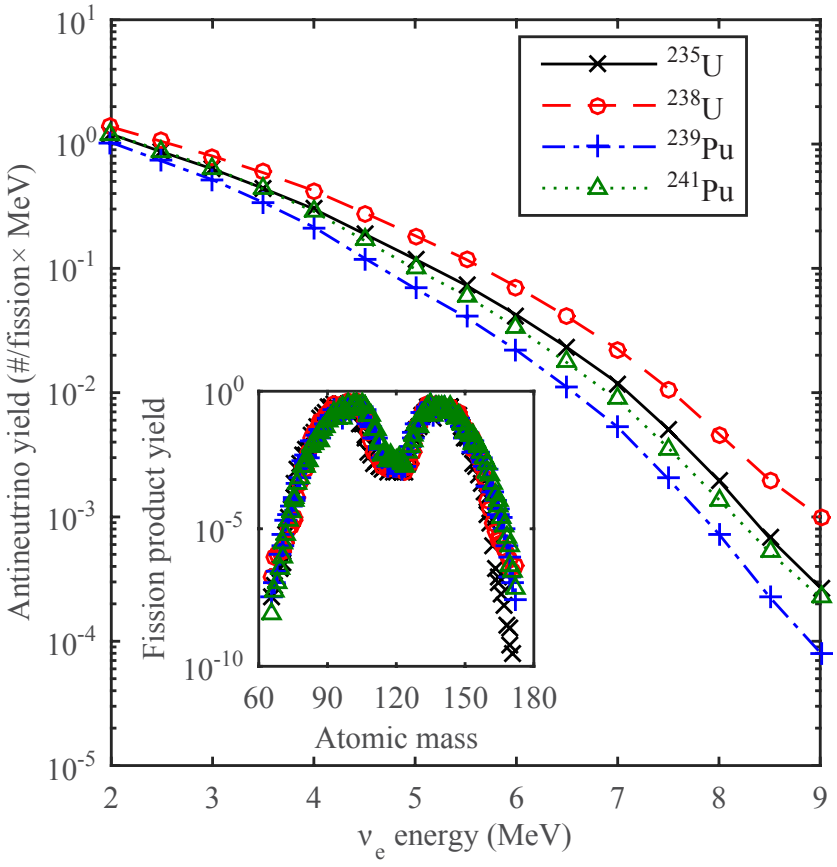

Figure 1: Antineutrino yield per fission per MeV for four primary isotopes (data provided by Patrick Huber, May 13, 2014) with (inset) cumulative fission product yields for the four primary isotopes (data compiled from JENDL FP Fission Yields Data File 2011).

application to reactor monitoring[8]. In fact, the low cross section renders them effectively unshieldable, thus providing an extremely transparent window into the reactors operating status without requiring the radiation-hardened electronics necessary for in-core instrumentation.

1.4.1.1 Tracking of reactor power changes

As the origin of the reactor's antineutrino flux is the decay of its fission products, the intensity of the reactor antineutrino source is directly proportional to its power—or, more precisely, the residual decay heat in the core. The core decay heat drops by an order of magnitude in ~ 3 hours following a full shutdown[46], allowing for hour-scale determination of the off/on status of the reactor and hour- to day-scale determination of a change in its operating power. This capability was demonstrated experimentally for a commercial thermal reactor with the SONGS-1 detector[8].

1.4.1.2 Tracking evolution of core fissile makeup with burnup

SONGS-1 also demonstrated the ability of 1 m^3-scale antineutrino detectors to effectively monitor the makeup of a reactor with known initial conditions as it progressed through its burnup cycle[13]. The primary driver for burnup-induced change in a reactors antineutrino spectrum is the gradual shift from fissioning ^{235}U to fissioning bred-in ^{239}Pu; the former yields more antineutrinos per fission, and has a harder antineutrino spectrum.

Furthermore, analysis performed by P. Huber[15] indicates that, had the technology existed at the time, a slightly larger (several m^3) antineutrino detector could have provided crucial information on the core loading and operational history of the DPRK test reactor which was used to produce weapons-grade plutonium and which was hastily disassembled immediately prior to the arrival of International Atomic Energy Agency (IAEA) inspectors in order to obscure such information.

1.4.1.3 Oscillation

Over reactor-detector standoffs relevant to single-plant antineutrino safeguards, oscillation of the flavor to mu or tau is negligible[2, 3], so the antineutrino flux reaching the detector is virtually identical to the one generated by the fission products, with only inverse-square geometric attenuation affecting its magnitude. The small deficit from full survival probability in flight from source to detector is the same for both the reference and nearly any perturbed-state reactor antineutrino spectrum, so difference calculations such as the ones performed when comparing reference and perturbed states will substantially mitigate the miniscule error incurred by ignoring oscillation.

1.4.1.4 The inverse beta decay reaction

The most mature technology for detecting electron antineutrinos relies on the inverse beta decay (IBD) reaction[58]:

$$\bar{\nu}_e + p \rightarrow e^+ + n \tag{2}$$

This reaction has a cross section on the order of 10^{-43} cm^2 and a threshold energy of 1.8 MeV which reduces the number of detectable antineutrinos produced per fission to approximately 1.92 for ^{235}U and 1.45 for ^{239}Pu[28]. The cross section for the IBD reaction as a function of energy shown in Figure 2 overlaid with a typical spectrum per fission event. The difference in detection rate between the two primary fissile isotopes present in most reactors is illustrated in Figure 3.

The IBD reaction does not occur for neutrinos; therefore sources of neutrinos are automatically excluded from detectors which use this method, thus reducing the background event rate. This property is particularly valuable for reactor monitoring purposes: reactors produce almost exclusively antineutrinos and the proton chain in the sun produces exclusively neutrinos; therefore detectors which use the IBD reaction automatically exclude solar neutrinos (since they, like antineutrinos, cannot

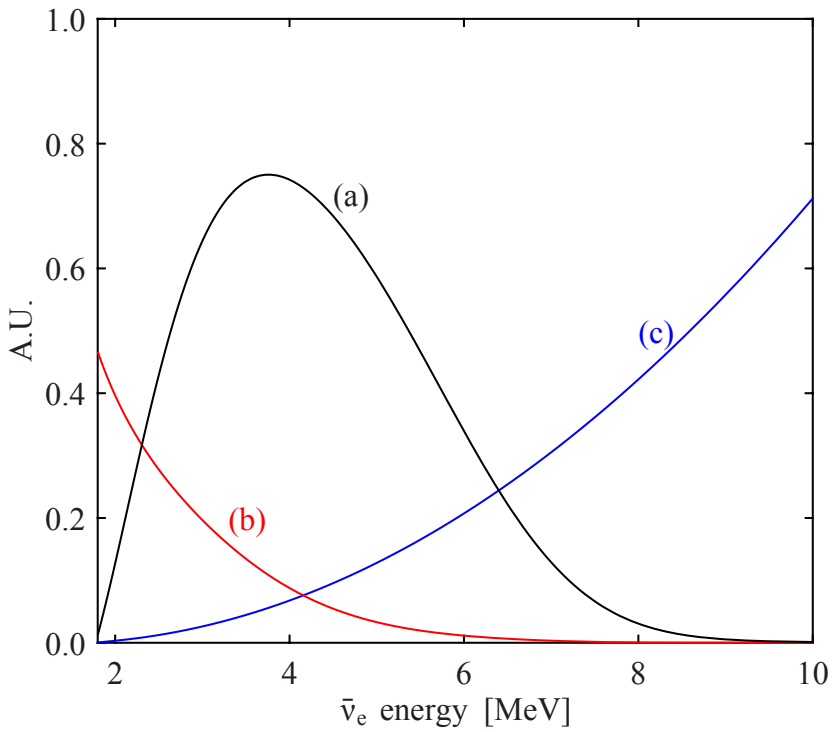

Figure 2: Detection spectrum (a) of reactor antineutrino flux spectrum (b) due to the energy dependence of the IBD cross section (c).

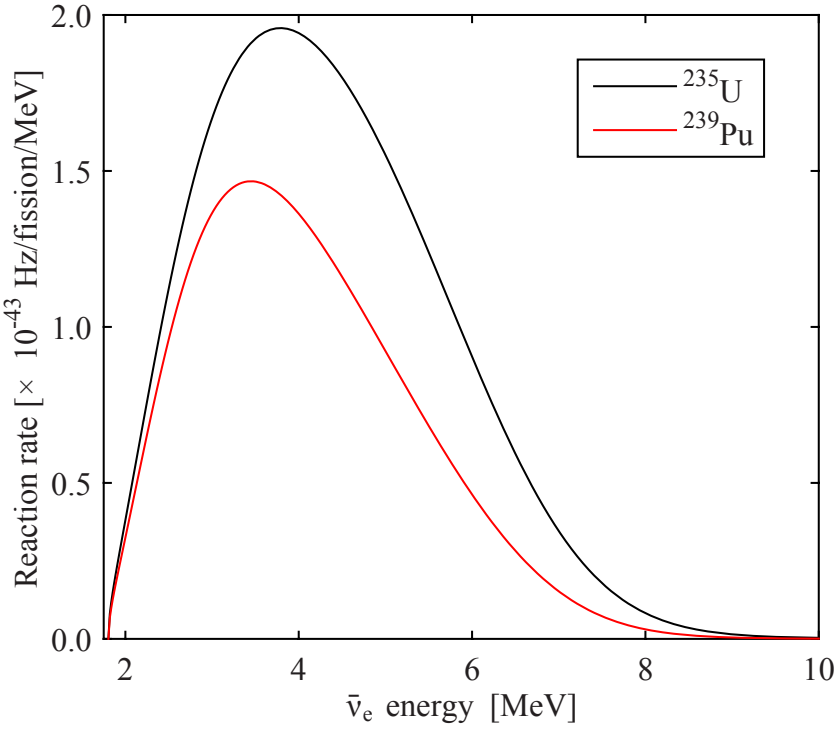

Figure 3: Product of IBD cross section and reactor antineutrino spectrum for ^{235}U and ^{239}Pu. The reaction rates for ^{239}Pu are lower and the spectrum has a lower peak energy.

be adequately shielded).

CHAPTER II

THE ROLE OF ANTINEUTRINO SAFEGUARDS IN NONPROLIFERATION POLICY

Antineutrino detectors of varying size and range offer the hope of monitoring nuclear-related activities including covert use of declared reactor facilities, operation of clandestine reactors, and remote detection of detonations. These capabilities shape its incorporation into both the enforcement of current treaties and agreements as well as the language and scope of future nonproliferation-related documents. While detection of clandestine reactors and nuclear detonations requires large-scale construction of detector networks with efficiency and background rejection exceeding current technology, near-field monitoring of declared reactors via small, on-site detectors is attainable in the near term [7]. Their safeguards relevance is limited to plutonium-based weapons, however, as their measurement requires a large antineutrino source such as an operating reactor—they would not be able to detect a uranium enrichment facility regardless of proximity. Bernstein et al [7] identify three areas of research into near-field reactor monitoring necessary to promote inclusion within a comprehensive safeguards regime:

1. Safeguards Analysis R&D, primarily the efficacy of monitoring non-PWR reactor types and combination of antineutrino-based data with other safeguards information,

2. R&D toward sensitivity gains of the detectors themselves, including detector efficiency improvements and background rejection as well as modeling of the antineutrino source behavior and reduction in uncertainty, and

3. R&D that facilitates deployment of detectors.

To address some of these needs, reactor antineutrino sources which have fuel cycle behavior markedly different than the LWR's used in experiments demonstrating the capabilities of near-field monitoring have been chosen. In particular, they are reactor types which may see deployment to non-nuclear states and therefore represent a unique proliferation vector. The historical and policy context of such reactor deployments and their monitoring is observed.

2.1 Current and proposed nuclear nonproliferation policy

2.1.1 Nonproliferation Treaty

Historically, the fear of nuclear weapon proliferation has been the driver of multiple international treaties and agreements, the most sweeping of which is the Non-Proliferation Treaty[53] (NPT). The NPT recognizes the right of nations to pursue nuclear technologies for peaceful applications, provided no effort is made to acquire or develop the capability to deploy nuclear weapons, while simultaneously directing those nations which had acquired nuclear weapons prior to ratification or accession to reduce their stockpiles of weapons and ultimately to fully disarm.

The success of the NPT depends to a high degree on the ability of international bodies to monitor nations production, use, and disposal of nuclear material; currently this is done in a declaration-verification scheme in which each nation declares its stores, transfers, operational records, etc., and these are checked against data gathered by inspectors deployed to declared sites[53]. In this way, nations adherence to the NPT or demonstration of a lack thereof is established through snapshots of their nuclear program. These can also be taken together with tracking and accounting on secondary goods which could be used to construct and operate non-declared facilities to establish limits on the level to which a nation may be subverting the NPT.

Antineutrino detectors operated as near-field reactor monitors would provide exclusion of proliferation paths which include removal of plutonium from a reactor. If combined with the exclusion of enrichment facilities operating on uranium above a particular enrichment, the reactor's inventory is protected against weaponization while within, as any uranium diverted from the reactor's core would require subsequent enrichment to achieve weapons-usable material.

2.1.2 Plutonium management and disposition agreement

In service to the disarmament pillar of the NPT, the United States and the Russian Federation signed the Plutonium Management and Disposition Agreement[54] (PMDA). The PMDA dictates the timeline for the disposal through fissioning of weapons-grade plutonium left over from previous dismantling of the nuclear stockpiles of the US and former USSR. Both are planning on blending the plutonium with uranium to form mixed oxide (MOX) fuels; the US, with its lack of a large-scale fast reactor fleet, will use its MOX fuel in light water reactors, while Russia plans to use its high-power-rating BN-series fast reactors to accomplish the same task[19]. Although each still maintains an appreciable nuclear arsenal, the recent cooling of US-Russia relations may present a scenario in which one or both parties might prefer to re-deploy higher warhead counts. The necessity of the ability of each party to continually verify, without assuming the deployment of an inspection team, that the fuel loaded into the reactors slated for disposal missions contains the correct amount of blended weapons-grade plutonium should not be underestimated.

2.1.3 Fissile material cutoff treaty

The proposed Fissile Material Cutoff Treaty, opposed primarily by Pakistan [32], would seek to place a cap on the amount of separated weapons-grade material each nation may possess, thereby placing an upper limit on the rate at which an arsenal may be accumulated. While most of the enforcement of such a treaty would, logically,

occur at the used fuel storage and reprocessing facilities, a way of circumventing such measures includes alteration of reactor inventory so as to reprocess material at a clandestine facility. Continuous verification of reactor inventories via antineutrino detection would provide assurance that plutonium slated to remain in a reactor until discharge does so without requiring extremely frequent inspections, the intrusiveness are a key sticking point in opposition to such a treaty [44]. The non-intrusiveness to normal operations of which antineutrino detectors are capable and restriction to plutonium, while not excluding uranium-based weapons, may provide a mechanism to limit at least some forms of further proliferation by weapons states. Pakistan has indicated in the past that it would consider a bilateral agreement with India to such an end [32], and if one were to be drawn up, parts of it might look similar to the PMDA in terms of verification mechanisms with respect to antineutrino monitoring—assurance that the initial core inventory is sufficiently close to what is declared and that it remains in the core for the declared burnup.

2.2 Lasting consequences of peaceful transfer

While the NPT has been generally successful at preventing large-scale proliferation of nuclear weapons across the glove, past provisions of nuclear equipment and technology for ostensibly peaceful purposes have resulted in steps toward weaponization. Optimism in any peaceful deployment to a non-nuclear state must be tempered by the reality that equipment which can be repurposed toward producing a nuclear weapon and the knowledge to use it tend to last much longer than the governments to which they are provided, whether that turnover is due to normal operation of a nation's governing process or a more revolutionary event. Both Iran and the DPRK were provided with nuclear technology in a manner not dissimilar from currently proposed provisions of reactors for power generation.

2.2.1 Democratic People's Republic of Korea

To date, there has been only one instance of withdrawal from the NPT, when the Democratic Peoples Republic of Korea (DPRK) acknowledged that it had used a test reactor and spent fuel processing facility to produce and weaponize plutonium[53]. The DPRK has had four successful nuclear tests, in 2006, 2009, 2013, and most recently, on January 6$^{\text{th}}$, 2016. The most recent detonation was claimed by the DPRK to have been a thermonuclear device[40], although the resulting seismic activity (5.1 on the Richter Scale) was about an order of magnitude less severe than known underground thermonuclear tests[55] and was more similar to that of previous DPRK tests, suggesting that either the device was actually a boosted fission bomb or that the fusion stage did not achieve its intended increase in total bomb yield. Atmospheric sampling in the coming weeks will be needed to provide information on the level of fusion reactions which actually took place. Regardless of the type of device, the continuation of nuclear testing combined with missile development implies that device miniaturization with the aim of ballistic missile armament is one of the DPRK's ambitions.

2.2.2 Iran

Iran, in a situation that mirrors some of the beginning of the DPRK withdrawal from the NPT and subsequent proliferation, has taken steps toward obtaining uranium-based nuclear weapons capability using a combination of declared facilities and clandestine facilities (most notably uranium enrichment at Fordrow). The most significant difference between the DPRK nuclear timeline and that of Iran is the willingness of Iran to negotiate away from its prior move to easily weaponizable material, thus increasing its breakout period—the minimum time necessary to finish developing and building a weapon—and culminating in the 2015 Joint Comprehensive Plan of Action (JCPOA) [18] between Iran and the P5+1 (the UN permanent security council

members plus Germany).

Iran's nuclear program began under the Atoms for Peace [36] program in 1957, when the nation was considered a US ally, and entailed the provision of LEU fuel and technical assistance by the US. This approach strongly resembles proposed provider-user framework for nuclear energy in non-nuclear states, and demands caution that facilities installed under such a framework cannot be assumed to be accessible to international inspection teams indefinitely. The termination of amicable US-Iran relations with the 1979 Iranian revolution and the context in which its nuclear program was initiated are relevant to any proposed construction of nuclear facilities in non-nuclear weapons states.

The recent events surrounding Iran's nuclear program, the negotiations, and the subsequent JCPOA between Iran and the P5+1 give some indication into what international safeguards bodies consider an "acceptable" breakout period for a country with a history of sparring with the IAEA and in possession of technical experience related to delivery systems for nuclear warheads.

In addition to dismantling most of Iran's uranium enrichment infrastructure and eliminating its stockpile of uranium on the cusp of 20% ^{235}U, the JPCOA requires Iran to submit discharged fuel for disposal, thus precluding the acquisition of a plutonium weapon via reprocessing irradiated fuel. However, since there are at least several months between consecutive core discharges, the need for more frequent verification of the core inventory is necessary. Should the integrity of the core inventory be compromised between discharges, it would provide immediate information regarding the completeness of Iran's declared facilities—as they would not risk detection to divert material without the propensity to use it before the next discharge.

The measures taken in the JPCOA have increased Iran's estimated breakout timeline from a few months to over a year, likely longer for plutonium-based weapons[35].

Supposing that one year represents an acceptably short confirmation time that safeguards attempts have failed—whether the indication is through determination that nuclear material has been diverted or through detection of a test detonation—, technology which allows such a determination for at least some modes of nuclear material diversion prior to one year after the fact should be of value to safeguards entities. Even should Iran disable monitoring technology as late as possible to buy time, the installation of continuous monitoring apparatus would thereby provide warning that clandestine efforts were underway prior to seismic readings after detonation and allow a chance at preventing the acquisition of a weapon. Safeguards analysis of antineutrino detectors which would fulfill a continuous monitoring purpose has been extended past the standard three month conversion period for plutonium sourced from irradiated fuel to a full year of reactor operation in order to assess their value in this context.

2.3 Advantages of antineutrino monitoring

The prospect of using antineutrino detectors to produce a continuous, if statistically complicated, image of an operating reactor's inventory has numerous advantages promoting inclusion to some degree in nuclear safeguards. The primary motivating factors for inclusion of antineutrino technology in verification of nonproliferation policy, some of which have already been mentioned in discussion, are the continuous nature of the provided information and the non-intrusiveness of its ascertainment. Real-time information is provided which bridges the knowledge integrity gap in the time between in-person inspections. In addition to the obvious advantages of possessing continuous information, this may be used with a focus on the integrity of knowledge of certain facilities to guide efficient inspection team deployments. Detectors which are always-on but removed from the reactor vessel provide a less-intrusive monitoring mechanism to verification efforts that may provide an additional tier of policy action

on the part of nations that lies between allowing and disallowing IAEA inspection teams to enter a country. Tiered enforcement may be written to take advantage of this if a sufficient distinction can be achieved.

CHAPTER III

SOURCE AND DETECTOR CASE STUDIES

3.1 Reactor antineutrino sources

Because of the proliferation concerns with fast reactor deployment, there has been significant effort spent designing fast reactors with proliferation-resistant features. Among the most widely adopted of these are the elimination of blanket zones and the use of non-oxide fuel forms which are capable of high burnup and are resistant to diversion during reprocessing. Some designs are built with a once-through fuel cycle in mind which fissions the fuel to very high burnup over several years, even multiple decades, at the end of which the spent fuel is not reprocessed. These designs are very attractive for deployment in non-nuclear states specifically because the reactor vessel does not need to be opened for any reason other than maintenance during the intervening years. The near-elimination in refueling logistics increases reactor uptime and saves money, but more importantly, removes pathways for diversion of material during refueling or transit.

In order to sustain critical operation for such a long time, however, these designs almost universally contain blanket or very low-enrichment zones in which fissile plutonium is bred to offset depletion of the initial fissile loading. Because the fast neutron spectrum has relatively low capture/fission ratios across all of the actinides, but particularly in ^{239}Pu, the bred plutonium can remain weapons-grade for years. Therefore, real-time monitoring is particularly desirable for these designs to ensure that nuclear material has not been diverted during a maintenance shutdown, which will inevitably occur. Two reactor designs which bear these characteristics—one with

a small power rating and one with a large rating more in line with the current commercial fleet—have been chosen for the role of reactor antineutrino source.

3.1.1 UCFR-1000

The UCFR-1000[51], the design for which was developed by the Ulsan Institute of Science and Technology (UNIST) in conjunction with Argonne National Laboratory (ANL), has been selected as the large, high-power-rating core. The UCFR-1000 is a U-10Zr-fueled core with a low-enriched uranium (LEU) starter zone on top of which sits a 300 cm fertile region containing natural uranium. During operation, the burn zone propagates upward at about 5 cm/year as plutonium is bred into the fertile zone and depleted fuel is left behind, consistent with the CANDLE[47] burnup scheme. It is intended to operate on a once-through cycle which lasts 60 years at full power. The major core parameters, taken from the design paper, are shown in Table 1, and the core layout, assembly cross-section, and axial enrichment zoning are shown in Figure 4, Figure 5, and Figure 6, respectively.

An additional motivation for choosing the UCFR-1000 is that the axial progression of the burn zone causes the geometric attenuation of the antineutrino flux to slowly change—opening the door for use of relative signal strength among multiple detectors to track progression once the core has completely transitioned to burning ^{239}Pu is complete.

Due to the very large heavy metal inventory of the core, removal of nuclear material which yields 1 SQ of plutonium will constitute a sub-1% change in total HM inventory, and depending on the location from which material is obtained, may change slightly more or less than this fraction of the fissile isotope inventory. Since, in practice, antineutrino detection resides firmly in the regime of poor counting statistics, discrimination of such small changes is quite difficult and requires many-day count integration periods. This is one of the primary challenges with respect to detecting

Table 1: Parameters of the UCFR-1000 core.

Parameter	Value (293 K)
Power rating (MW_{th}/MW_e)	2600/1000
Cycle length (Effective Full-Power Years)	60
Fuel form	U-10Zr
Initial HM loading (t)	201
Specific power density (MW/t)	12.9
Volumetric power density (W/cm^3	81.0
# Fuel assemblies	378
Assembly pitch (cm)	16.5
Fuel pin diameter (cm)	1.49
Fuel smeared density (cm)	74.5
Uranium enrichment of driver/blanket (%)	12.3/Natural
Active core height (cm)	360
Fuel pin overall length (cm)	460

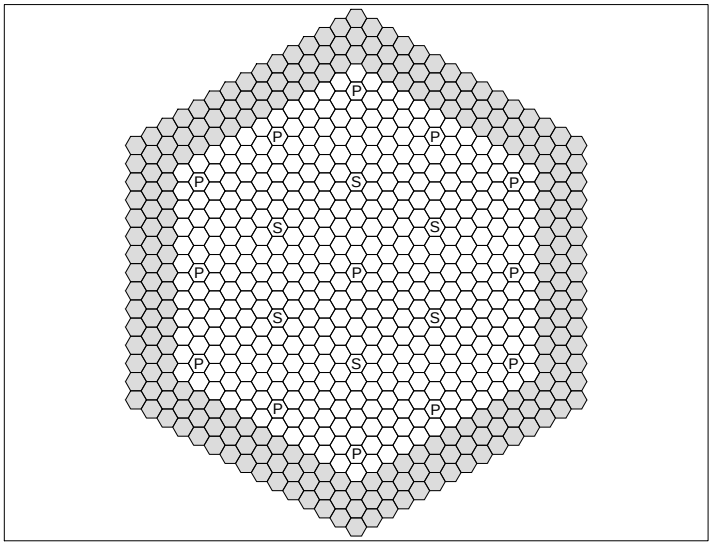

Figure 4: Layout of the assemblies in the UCFR-1000. Reflector assemblies are in grey. Letters indicate control assembly positions: "P" for primary control and "S" for secondary control.

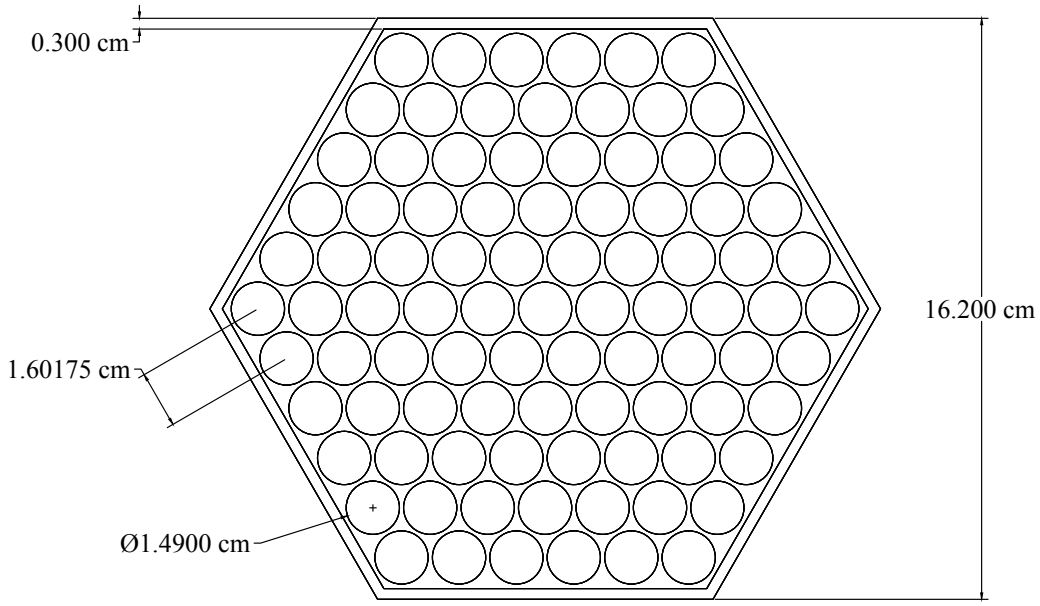

Figure 5: Cross-cut view of a UCFR-1000 fuel assembly (to scale).

partial-core diversions. The low magnitude of the change in fuel is offset somewhat by the UCFR's high thermal power rating.

3.1.2 AFR-100

The AFR-100[30], developed at ANL, has been chosen for the small, low-power-rating fast reactor design; it is a 250 MW_{th} sodium cooled fast core designed for a 30-year, once-through cycle. The major parameters of the AFR-100 are provided in Table 2, and the core layout is shown in Figure 7.

The AFR-100 shares the assembly and pin design cross section (Figure 5) with the UCFR-1000, but instead of a tall core with distinct starter and fertile regions at the beginning of cycle, the AFR-100 has the more traditional pancaked geometry of fast reactors. To achieve a balanced coolant exit temperature and power distribution, it has an onion-type enrichment scheme (Figure 8) which propagates the burn zone from the periphery of the reactor toward the center. The propagation is symmetric,

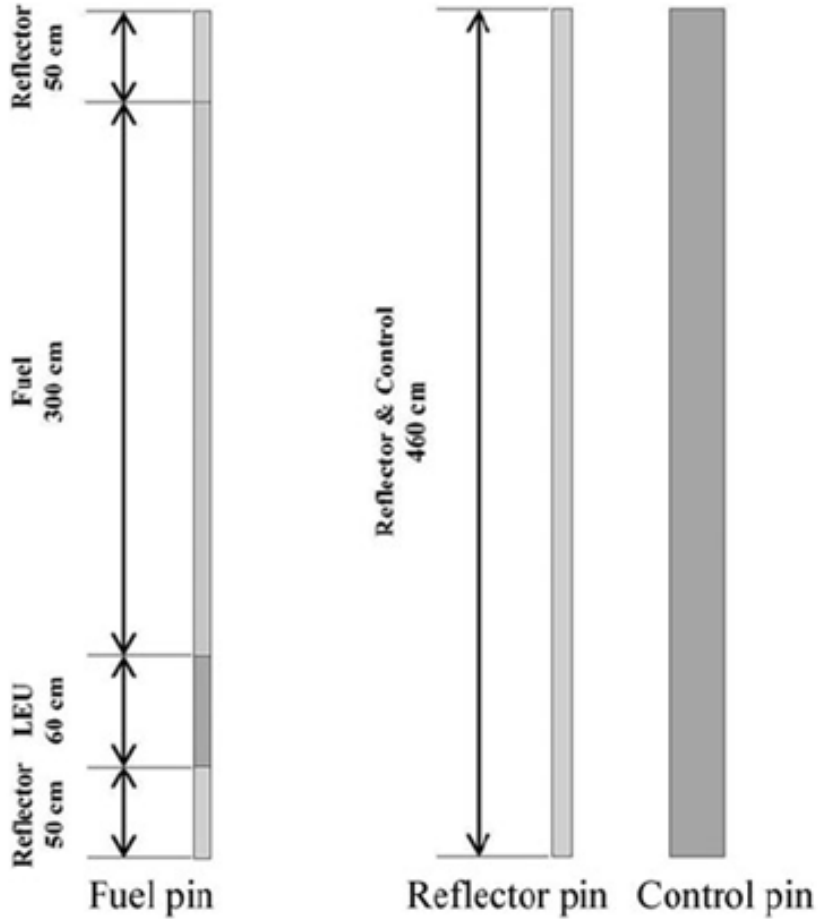

Figure 6: UCFR-1000 fuel, reflector, and assembly axial zoning.

Table 2: AFR-100 core parameters.

Parameters	Values (293 K)
Power rating (MW_{th}/MW_e)	250/100
Cycle length (EFPY)	30
Fuel form	U-10Zr
Initial heavy metal inventory (t)	24.64
Number of fuel assemblies	150
Assembly pitch (cm)	16.5
Fuel pin diameter (cm)	1.49
Fuel smeared density (%)	75
Core average enrichment (%)	13.47
Active core height (cm)	110

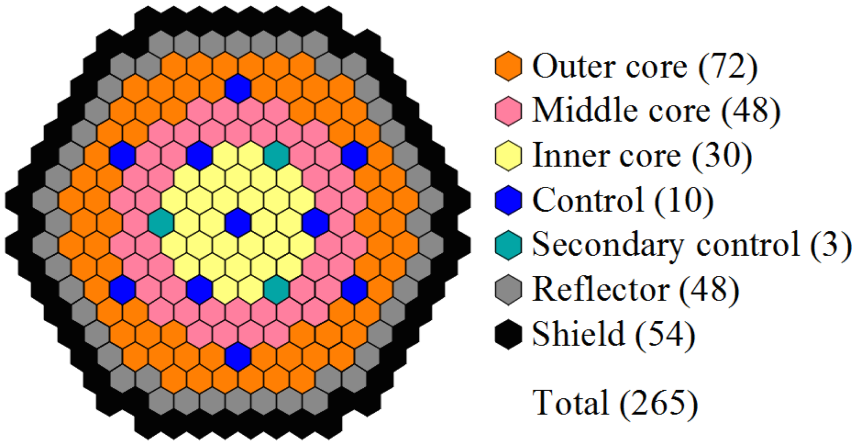

Figure 7: Layout of the assembly types in the AFR-100.

much slower, and the effect much less pronounced than in the UCFR-1000, primarily due to the small core volume, but also the more gradual enrichment differences. The change in geometric attenuation of the antineutrino flux is negligible.

One of the primary constraints for the design of the AFR-100 was that it must fit in a small core barrel (3.0 m diameter). This constraint resulted in the inclusion of only one layer each of reflector and shield assemblies. To avoid excessive radiation damage to the reactor vessel and core support structures, the traditional B_4C shielding material was mixed with $ZrH_{1.6}$ in order to enhance neutron moderation. Softening the neutron spectrum increases the absorption rate in the shield assembly, primarily

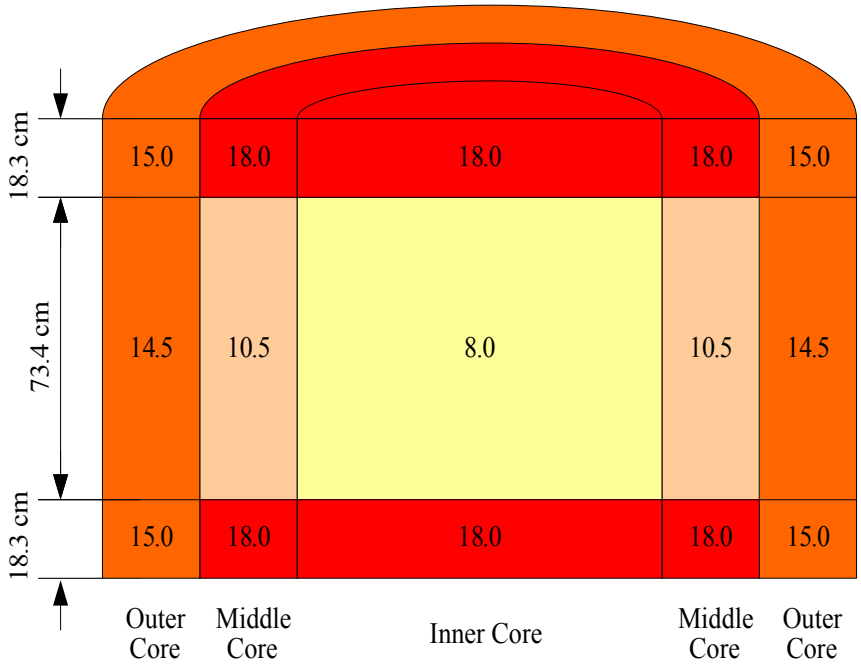

Figure 8: Enrichment zoning of the LEU starter fuel for the AFR-100.

in ^{10}B, as well as reducing the damage per neutron which interacts in structural materials. The improved shielding comes at the cost of slightly reducing the albedo of the combined reflector+shield.

The AFR provides challenges for safeguards via antineutrino detection in essentially the opposite manner of the UCFR. The small core volume means that a 1-SQ removal represents a much higher fraction of the total core heavy metal inventory, easing discrimination. This is countered by the order of magnitude lower power rating, and therefore antineutrino source strength, of the reactor. In addition, the conversion from ^{235}U to ^{239}Pu is less drastic since the "low" enrichment zone is still 8% ^{235}U rather than the 0.71% found in the UCFR, subsequently making burnup tracking more difficult.

3.2 Detector

The choice of detector was motivated by the desire to keep to near-field antineutrino detector experience so as to not extrapolate too egregiously upon the capabilities of detectors which would be installed at the earliest a few years from now. This excluded the physics experiments geared toward solar and stellar neutrino characterization and more toward oscillation experiments, many of which use commercial-scale nuclear reactors as their source of pure electron antineutrinos. A new focus in neutrino oscillation physics in the search for a sterile neutrino is near-field behavior of the antineutrino flux emitted from a reactor; to achieve very short baselines, test reactors are being used as sources. The few-meter separation from a test reactor has the added bonus of providing a high detector event rate that will help further improve precision on antineutrino yields from the fissions of some isotopes, particularly ^{235}U, since many test reactors are fueled with HEU and therefore fission almost exclusively this fuel isotope from initial loading to final discharge.

3.2.1 PROSPECT

A detector based heavily on the Phase-I (AD-I) and Phase-II (AD-II) detectors for the PROSPECT project[5] has been adopted for antineutrino safeguards calculations. The PROSPECT detectors are slated to deploy in the High Flux Isotope Reactor (HFIR) in late 2016 (AD-I) and 2019 (AD-II) with the objectives of precisely measuring the HFIR antineutrino spectrum, searching for short-range neutrino oscillation via motion of AD-I along a track that spans distances of 7-12 m from the core, and probing for eV-scale sterile neutrinos[5]. The safeguards-relevant parameters of PROSPECT AD-I and AD-II are provided in Table 3.

Multiple prototypes in increasing sizes similar to AD-I and AD-II have previously been constructed by the PROSPECT team in order to test proof-of-concept, detector properties, and backgrounds. Various shielding materials and configurations have

Table 3: PROSPECT AD-I and AD-II parameters used for the basis of the safeguards detector, obtained from [5].

Parameter	Value
Antineutrino Detector I (AD-I)	
Proton density	5.5e28 $^{\text{No.}}/_{\text{m}^3}$
Total target mass	2940 kg
Fiducialized target mass	1480 kg
Efficiency in fiducial volume	42%
Energy Resolution	$^{4.5\%}/\sqrt{E}$
Signal:Background (near, far)	3.1, 1.8
Closest distance to core (near, far)	6.9 m, 9.4 m
Antineutrino Detector II (AD-II)	
Total target mass	$\sim$ 10 ton
Fiducialized target mass	$\sim$ 7 tons
Signal:Background	3.0
Closest distance to core	15 m

resulted in a multi-layer shield consisting of water bricks, polyethylene (some of it borated), and lead bricks. The final shielding volume is approximately 1/4 of the AD-I volume[5].

3.2.1.1 Segmentation

The PROSPECT antineutrino detectors are segmented into rectangular prisms measuring approximately 15 cm $\times$ 15 cm $\times$ 120 cm, which are mounted in a grid with pitch based on their width. Between each segment is an optical divider; the remaining interstitial space is used to house calibration sources and to run fiber optic cables which carry signals from the adjacent segments[5]. Segmentation allows for segment-scale position resolution within the detector. This data can be leveraged to reduce background relative to a similarly-sized, non-segmented detector by giving the power to reject particles which interact over several segments based on directionality. The use in concert, of what are essentially an array of very small antineutrino detectors, improves the signal to background ratio to above unity[5].

3.2.1.2 Scintillator

Many previously-developed near-field antineutrino detectors have used Gd-doped water as the scintillation medium[12, 8, 13]; ^{157}Gd is stable and absorbs thermal neutrons with a cross section of about 255000 barns[14]. However, it does so via an (n, γ) reaction, and the resulting photon has E = 7.9 MeV, high enough that it would frequently deposit its energy across several segments. Therefore, another isotope was sought to act as a neutron capture agent in order to provide the characteristic positron-neutron coincidence behavior of IBD.

The EJ-309 liquid scintillator developed by Eljen Technology[52] was chosen by the PROSPECT team. This xylene-based compound was doped with ^{6}Li to capture the low-energy neutron released in the IBD reaction. ^{6}Li has a very high neutron absorption cross section—on the order of thousands of barns for thermal neutrons[14]—and the reaction products are heavy nuclei which deposit their energy over a very short range ($<$ 1 mm):

$$n +^{6} Li \rightarrow \alpha + t + 4.78 \text{ MeV} \tag{3}$$

3.2.1.3 Synergy with antineutrino safeguards

The deployment timeline of both phases of PROSPECT is shorter than the expected inclusion of antineutrino safeguards into new reactor facilities (approx. 10 years). Detector operation experience will contribute heavily toward further development and deployment of antineutrino detectors for safeguards purposes—indeed, one stated purpose of PROSPECT is to provide safeguards-usable data—as well as expand the knowledge of short-baseline neutrino physics which might affect the expected detector signal in normal operation and in diverted-material cases. AD-I and AD-II will provide very high-quality data on the ^{235}U component of the reactor antineutrino flux[5] at safeguards-relevant baselines.

The AD-II detector is similar to the simulated safeguards detector both in size and placement relative to the reactor and surface. Developments introduced for Phase II of PROSPECT and the assumptions and estimations made by the PROSPECT team for AD-II have been taken into account when making judgements on the capabilities of the safeguards detector and the environment in which it operates.

3.2.2 Detector placement

The SONGS-1 antineutrino monitoring experiment[12, 8, 13] used otherwise unoccupied space in the tendon gallery for commercial PWR observations. In the spirit of remaining unobtrusive to normal reactor operation, the detectors are placed as close to the core as possible without requiring special consideration during plant construction, resulting in locations within the containment building but outside the chamber containing the reactor pressure vessel, guard vessel, etc. For commercial-scale PWR's, this approach usually results in a standoff of 20-25 m from the center of the core. Sodium-cooled fast cores are much more compact per unit power than PWR's, but prevailing designs use a large pool-type reactor vessel to provide additional thermal inertia during transient events.

Because the UCFR-1000 is a (very) preliminary design and there are no commercial-scale fast reactors in existence designed for decades-long burnup cycles, there is no available information on specific dimensions of a potential UCFR containment building. The core compactness and pool-type vessel sizing should roughly offset, so a standoff of 25 m is assumed for UCFR-1000 monitoring based on the SONGS-1 standoff from a reactor with similar power rating. It is possible that improvements in fast reactor experience prior to final design of a CANDLE-type reactor with a large power rating will result in a reduced vessel radius given the time between now and earliest possible deployment, but standoff reduction of more than about 5 m is unlikely due to physics-based safety considerations.

The AFR-100 is a much more mature design, and therefore effort has been put into designing its containment building, cooling systems, etc.; the plant layout plan for the AFR-100 allows detector placement approximately 17 m from the core center [29]. The AFR standoff serves as a soft validation of the 25 m estimate for the UCFR.

Three PROSPECT-like segmented antineutrino detectors will be symmetrically arranged around a circle with a radius of the minimum unobtrusive standoff to estimate the performance of an antineutrino detector suite. If necessary to distinguish such a particular arrangement in the discussion of named detectors from another established detector or project, the suite will be referred to as RETINA (**R**eactor **E**valuation **T**hrough **I**nspection of **N**ear-field **A**ntineutrinos), although it should be noted that RETINA is not a set-in-stone arrangement or detector design in the general sense.

3.3 Diversions

3.3.1 Criteria

3.3.1.1 Focus on plutonium

Preliminary analysis using a coarse-grained model of the UCFR-1000 indicated that the diversion of 1 SQ of LEU (75 kg of ^{235}U in LEU) from a freshly loaded core, with replacement of natural uranium, would be unable to be detected within the weapon conversion window ($<$ 12 months) via near-field antineutrino safeguards. The exceedingly small change in the isotopes undergoing fission resulted in a nearly-identical antineutrino flux. Furthermore, the uranium acquired would be 12.3% enriched, requiring significant further enrichment in order to yield HEU that is weapons-usable ($>$ 90% ^{235}U). A nation possessing the enrichment capacity to bring the stolen uranium to the required enrichment would likely have other more easily executed methods of obtaining the required material—whether through procuring uranium under the guise of overt peaceful use or through black market channels. The limited utility

of antineutrino safeguards against LEU diversions from LEU-fueled fast reactors in addition to the availability of other acquisition methods for the material motivates a focus on diversions of plutonium.

3.3.1.2 Plutonium amount and purity

The plutonium inventory of fast reactor assemblies which are not initially loaded with reactor-sourced plutonium has the quality of remaining relatively devoid of contaminant isotopes (^{240}Pu, ^{238}Pu, fission products, etc.) for a long time after one SQ has accumulated in the assembly. In order to offset losses during processing and avoid the possibility of acquiring too little material, diverting actors will attempt to maximize the amount of plutonium obtained. In the likely event that the entity using the material is still testing aspects of their nuclear capabilities, multiple-SQ diversions are more probable endeavors. However, since these represent larger changes to the core fissile inventory, most of the diversions considered are of the order of 1 SQ to scope the limits of antineutrino safeguards technology. Since diversions for use in radiological weapons can be almost arbitrarily small in terms of plutonium mass removed, only diversions with a lower bound of one SQ of plutonium are considered.

Contaminant effects offer an upper bound on material irradiation for consideration as prime targets for assembly-level diversion. The primary contaminant for plutonium-based nuclear weapons is ^{240}Pu because its large spontaneous fission rate greatly increases the chance of fizzling and reduces the energy release during detonation. Although kiloton-scale detonations are estimated to be possible with plutonium containing 15% ^{240}Pu by using very sophisticated implosion and boosting techniques[43], the generally used demarcation for identifying plutonium as weapons-grade is the inclusion of less than 7% ^{240}Pu, so that will be used as a criterion for selecting diversions. All ^{239}Pu-containing plutonium is considered "direct use material" by the IAEA[23] unless it contains over 80% ^{238}Pu, rendering its heat generation

prohibitive to further processing. As plutonium born of reactor-irradiated uranium only contains at most a few percent ^{238}Pu, this restriction will not apply when selecting diversions. The radiotoxicity induced by the accumulation of fission products in irradiated nuclear fuel is not considered here to be a limiting factor to a determined actor which may have access to adequate shielding, since fission products are chemically separated out during reprocessing. However, less-contaminated fuel is considered "more attractive" since the acquisition of shielding and equipment and the construction of facilities designed to make use of highly radiotoxic material is itself a vector for potential discovery by authorities.

3.3.1.3 Remaining undetected

Time-integration of the detector signal can be performed by the monitoring agency for arbitrary start- and end-points, but the weapon conversion times defined by the IAEA[23] provides a reasonable limit of three months after the occurrence of material diversion for detection. Simulation of a core perturbed by a diversion will continue up to a year after the diversion in order to provide quantification of the extent to which the technology must be improved to catch near misses and to identify replacement scenarios that result in a subcritical core—an obvious indication that something is awry.

To facilitate remaining undetected as long as possible, diversions are selected which constitute removal of a single assembly or a few assemblies which are not co-located. Keeping the removal to at most a few percent of the total number of fuel assemblies—378 in the UCFR and 150 in the AFR—minimizes the relative change in core fissile inventory. The removal of many assemblies also necessitates proportionally larger shielding, logistics, and reprocessing efforts, giving more time for the diversion to be detected prior to deployment of a weapon. When multiple assembles are removed, they are assumed to be distributed as widely as possible across the core.

Nuclear reactors operate in a highly non-linear problem space, and the effects of local flux hotspots/depressions and neutron spectrum shift which further alter the perturbed vector of fissioning isotopes are pronounced when the replacement assemblies are more tightly coupled.

In all reactors, there are areas of higher and lower neutron importance. Removal of an assembly in a high-importance region will more substantially affect the reactor than removal of a less important assembly. For fast reactors, the higher incidence of neutron leakage from the core usually means peripheral assemblies are less important. The flat enrichment scheme of the UCFR-1000 yields a zero-order Bessel function radial flux shape, confirming the lower importance of peripheral assemblies. In the AFR-100, the enrichment scheme has been devised to minimize this effect for control rod worth reasons[30], but the inward migration of the burn zone, faster depletion of the fissile material in the edge assemblies, and decrease in leakage factor through the cycle indicate that peripheral assemblies lose neutron importance and the central assembles gain it as burnup increases.

3.3.1.4 Early availability

A single-assembly diversion will be considered for both reactors which represents the first instance of one SQ of plutonium becoming obtainable via removal of one assembly. This is done as a measure of the decrease in breakout period caused by installation of a long-life fast reactor facility in a non-nuclear weapons state. With fairly few accumulated fission products, removing these assemblies also constitutes some of the easiest-handled irradiated material, especially compared to late-cycle diversions. If the actor is able to replace the diverted material with an LEU-bearing replacement assembly, it will most closely approximate the removed one (fissile isotope mostly ^{235}U, few fission products) for early-cycle diversions.

Table 4: UCFR-1000 diversion scenarios

ID		Location(s)	Burnup (EFPY)	Replacement
UCFR-1	a b	Ring 2, Assembly 1	2.17	LEU Natural Uranium
UCFR-2	a b	Ring 12, Assembly 1	12.42	LEU Natural Uranium
UCFR-3	a b	Ring 12, Assemblies 1, 12, 23, 34, 45, 56	12.42	LEU Natural Uranium

3.3.1.5 Testing at the limits of near-field antineutrino safeguards

In order to assess the limits of near-field antineutrino safeguards, diversions will focus on removals of one SQ of plutonium from the most peripheral assemblies where it is available and at the shortest irradiation time for which it is present. Replacement assemblies are assumed to be manufactured to be structurally and materially identical to the removed assemblies, including the use of reduced-activation and low-swelling steels. Although it is a near-certainty that these would be exceedingly difficult to obtain, machine, and use undetected in a timely manner, the focus is on the change in heavy metal inventory, so opening the door to a myriad of replacement possibilities which may require the operator to change zoned cooling, single control-rod position, etc., are beyond the scope of this evaluation.

3.3.2 UCFR-1000 diversion cases

The set of diversions considered for the UCFR-1000 are outlined below in Table 4.

3.3.2.1 UCFR-1a and UCFR-1b

Diversions UCFR-1a and UCFR-1b represent the earliest point at which 1 SQ of plutonium is available via removal of a single assembly from the UCFR-1000. This occurs in any of the center-adjacent assemblies (the core has $\pi/3$ rotational symmetry),

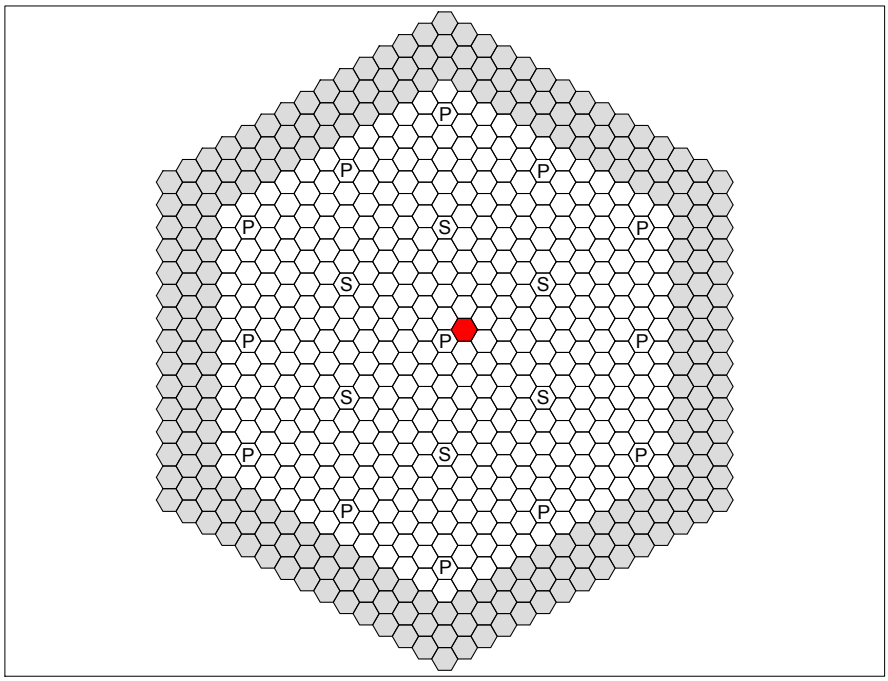

Figure 9: Location (red) of the diverted & replaced assembly for diversion scenarios UCFR-1a and UCFR-1b.

as these are the locations of highest flux. The plutonium vector is given in Table 5, and the assembly location is shown in Figure 9. The plutonium obtained via these diversions is not far from the 7% threshold of ^{240}Pu contamination.

3.3.2.2 UCFR-2a and UCFR-2b

Diversions UCFR-2a and UCFR-2b represent a patient actor who only needs one SQ and can reasonably wait until enough plutonium is available via diversion of a single corner assembly in order to select one with a low probability of being caught. The plutonium vector is given in Table 6, and the assembly location is shown in Figure 10. The plutonium is somewhat purer than that obtained from the UCFR-1a and UCFR-1b diversions due to the lower flux, and since the irradiation rate is about 15% as high,

Table 5: Plutonium vector for an assembly in Ring 2 of the UCFR-1000 at a burnup of 2.17 EFPY (diversions UCFR-1a and UCFR-1b).

Isotope	Mass (kg)	% of total
^{238}Pu	3.08×10^{-2}	0.38
^{239}Pu	7.53	93.04
^{240}Pu	5.07×10^{-1}	6.26
^{241}Pu	2.47×10^{-2}	0.31
^{242}Pu	1.08×10^{-3}	0.01
Total	8.10	

Table 6: Plutonium vector for a corner assembly (position 1) in Ring 12 of the UCFR-1000 at a burnup of 12.42 EFPY (diversions UCFR-2a and UCFR-2b).

Isotope	Mass (kg)	% of total
^{238}Pu	1.82×10^{-2}	0.23
^{239}Pu	7.55	93.95
^{240}Pu	4.49×10^{-1}	5.59
^{241}Pu	1.77×10^{-2}	0.22
^{242}Pu	6.49×10^{-4}	0.01
Total	8.04	

the concentration of surviving fission products is lower, potentially easing shielding requirements.

3.3.2.3 UCFR-3a and UCFR-3b

These diversions are essentially the same as UCFR-2a and UCFR-2b, but scaled up to include all corner assemblies, representing an actor who either needs more material or is willing to accept increased risk of detection in order to arm several weapons. Table 7 shows the plutonium obtained and Figure 11 the diverted assembly locations.

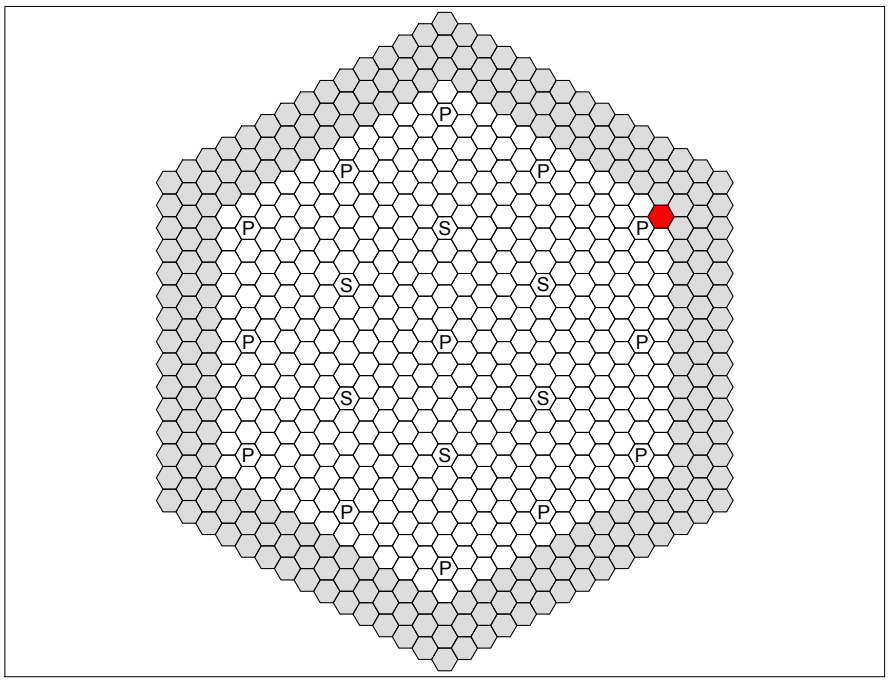

Figure 10: Location (red) of the diverted & replaced assembly for UCFR-2a and UCFR-2b.

Table 7: Plutonium vector for all corner assemblies in Ring 12 of the UCFR-1000 at a burnup of 12.42 EFPY (diversions UCFR-3a and UCFR-3b).

Isotope	Mass (kg)	% of total
^{238}Pu	0.11	0.23
^{239}Pu	45.3	93.95
^{240}Pu	2.70	5.59
^{241}Pu	0.11	0.22
^{242}Pu	3.90×10^{-3}	0.01
Total	48.21	

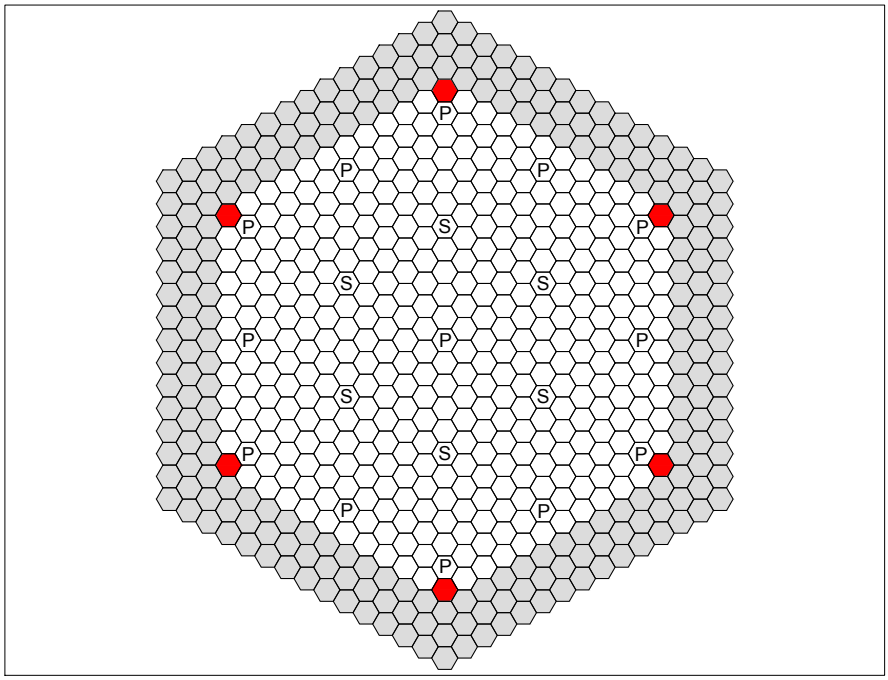

Figure 11: Locations (red) of the diverted & replaced assemblies for UCFR-3a and UCFR-3b.

Table 8: AFR-100 diversion scenarios

ID		Location(s)	Burnup (EFPY)	Replacement
AFR-1	a b	Ring 2, Assembly 2	15.75	LEU Natural Uranium
AFR-2	a b	Ring 8, Assemblies 2, 23	12.42	LEU Natural Uranium
AFR-3	a b	Ring 8, Assemblies 2, 16, 30	12.42	LEU Natural Uranium

3.3.3 AFR-100 diversion cases

The AFR-100 does not breed one SQ of plutonium into every assembly by the end of its burnup cycle; the chosen diversion scenarios instead focus on obtaining one SQ of plutonium via removal of one, two, and three assemblies that are either available as early as possible (scenarios 1a/b) or at the core periphery (scenarios 2a/b and 3a/b). The AFR-100 diversions are summarized in Table 8. For the scenarios with LEU replacement, the total fissile enrichment (^{235}U + ^{239}Pu + ^{241}Pu) present in the removed assembly at the time of diversion was rounded to the nearest integer percent to determine the ^{235}U enrichment each of the replacement fuel assembly macrozones. While a dedicated and sophisticated actor may be able to achieve greater precision in fuel fabrication, the returns on doing so are small compared to using LEU as opposed to natural uranium.

3.3.3.1 AFR-1a and AFR-1b

The flatter flux distribution, lower local power density, and lack of true blanket assemblies keeps one SQ of plutonium from being obtainable via a single-assembly diversion in the AFR-100 until 15.75 EFPY into the burnup cycle. At this burnup, three of the center-adjacent assemblies (the core has $^{2\pi}/_{3}$ rotational symmetry) host one SQ of weapons-grade plutonium. The plutonium obtained at this point is described in

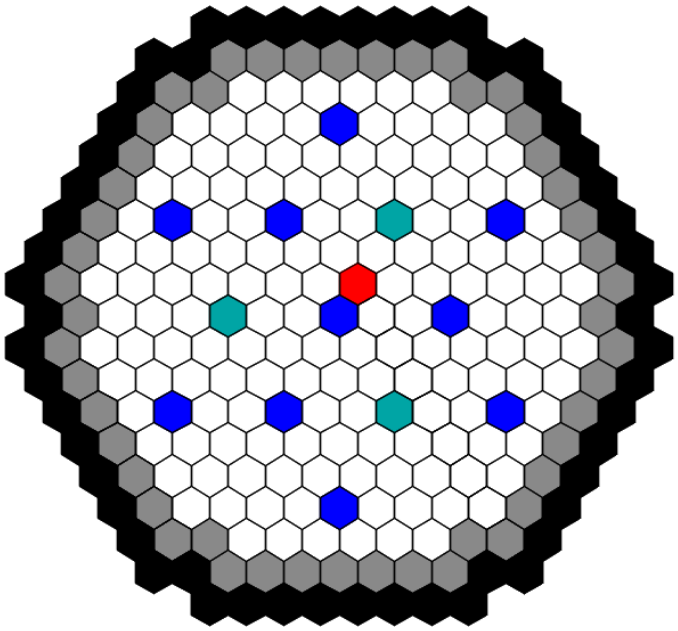

Figure 12: Location (red) of the diverted & replaced assembly for AFR-1a and AFR-1b.

Table 9, and the location of the withdrawn assembly is shown in Figure 12. The ^{235}U enrichment of the AFR-1a replacement assembly is 15% in the lower and upper fuel macrozones and 9% in the middle.

3.3.3.2 AFR-2a and AFR-2b

If a proliferator has access to an AFR-100 core late in its burnup cycle and is able to simultaneously divert two assemblies, 1 SQ can be obtained from the assemblies

Table 9: Plutonium vector for a center-adjacent assembly in the AFR-100 at a burnup of 15.75 EFPY (diversions AFR-1a and AFR-1b).

Isotope	Mass (kg)	% of total
^{238}Pu	2.50×10^{-2}	0.31
^{239}Pu	7.56	93.93
^{240}Pu	4.47×10^{-1}	5.55
^{241}Pu	1.62×10^{-2}	0.20
^{242}Pu	6.12×10^{-4}	0.01
Total	8.05	

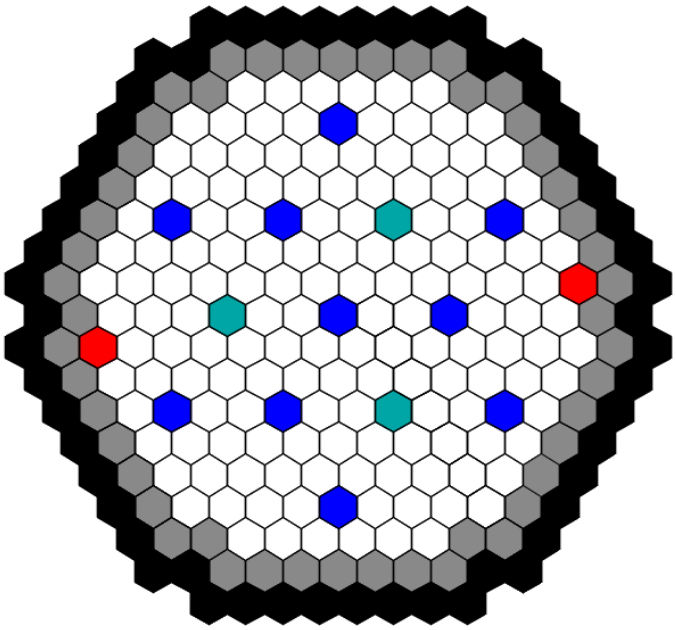

Figure 13: Locations (red) of the diverted & replaced assemblies for AFR-2a and AFR-2b.

at the edge of the core, where they will disturb the neutron flux distribution the least and provide the greatest chance of remaining undetected. Diversion scenarios AFR-2a and AFR-2b represent this situation. The plutonium obtained has superior purity to that from the center-adjacent assemblies obtained in scenarios AFR-1a/b, although the burnup (21.25 EFPY) is several years later in the cycle, so deploying an AFR-100 would not grant a proliferator a short breakout period in which they remain undetected for over two decades. The plutonium obtained from each of the two assemblies in these scenarios is described in Table 10, and the locations of the withdrawn assemblies are shown in Figure 13. The ^{235}U enrichment of the AFR-2a replacement assemblies is 14% in the upper and lower fuel macrozones and 13% in the middle.

3.3.3.3 AFR-3a and AFR-3b

If a proliferator wishes to act sooner than the timeline available in scenarios AFR-2a/b but has the capability to simultaneously remove three assemblies, the assemblies

Table 10: Plutonium vector for each of two peripheral assemblies in the AFR-100 at a burnup of 21.25 EFPY (diversions AFR-2a and AFR-2b).

Isotope	Mass (kg)	% of total
^{238}Pu	6.05×10^{-3}	0.15
^{239}Pu	3.91	97.00
^{240}Pu	1.13×10^{-1}	2.80
^{241}Pu	2.02×10^{-3}	0.05
^{242}Pu	3.78×10^{-5}	$<$ 0.01
Total	4.03	

Table 11: Plutonium vector for each of three peripheral assemblies in the AFR-100 at a burnup of 13.25 EFPY (diversions AFR-3a and AFR-3b).

Isotope	Mass (kg)	% of total
^{238}Pu	2.19×10^{-3}	0.08
^{239}Pu	2.62	98.15
^{240}Pu	4.68×10^{-2}	1.75
^{241}Pu	5.79×10^{-4}	0.02
^{242}Pu	6.84×10^{-6}	$<$ 0.01
Total	2.67	

at the core edge can provide 1/3-SQ of plutonium at 13.25 EFPY. The plutonium obtained by doing so (Table 11) is firmly in the "supergrade" category regardless of which definition—usually at least 95%-98% ^{239}Pu—is used. The assembly locations for these diversions are shown in Figure 14. The ^{235}U enrichment of the AFR-3a replacement assemblies is 14% throughout the active fuel region.

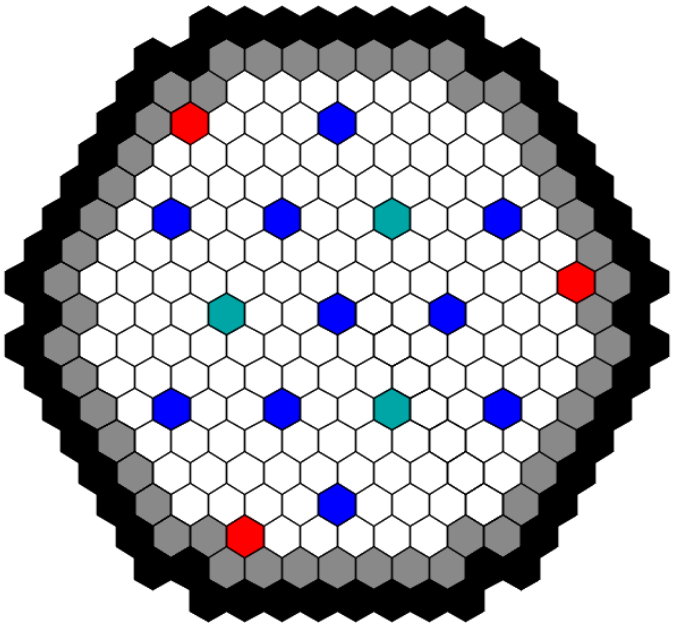

Figure 14: Location (red) of the diverted & replaced assembly for AFR-3a and AFR-3b.

CHAPTER IV

REACTOR MODELING METHODS, CALCULATION OF ANTINEUTRINO SOURCE AND DETECTOR SIGNAL, AND QUANTIFICATION OF UNCERTAINTY

4.1 Reactor modeling

The reactors were modeled using the Advanced Reactor Code (ARC) system developed and packaged by ANL. The ARC system is designed to quickly and accurately calculate various aspects of fast reactor neutronics, fuel cycles, and transient scenarios using high-fidelity deterministic solutions to the neutron transport equation. Its outputs are used to construct the antineutrino source which is incident upon the detector chosen for the case studies.

4.1.1 Lattice cell calculations

Lattice cell calculations were carried out in MC^2-3, a **m**ultigroup **c**ross section **c**ode which uses cross section libraries and a simplified reactor geometry to produce spatial- and energy-self-shielded effective cross sections for use in full-core neutronics calculations. Effective cross sections are necessary for deterministic solutions to the transport equation because solution-by-calculation methods do not automatically account for alterations to the neutron spectrum due to the presence of strongly interacting nuclei. In contrast, solution-by-demonstration methods such as Monte Carlo reactor simulations estimate these effects by simply executing the simulation.

4.1.1.1 Macro-zones

Traditionally, lattice cell calculations are carried out on a single reactor element of dimensions comparable to the neutron mean free path—this is usually a single fuel pin in thermal reactors and a fuel assembly in fast reactors. Reflective boundary conditions are enforced to simulate the leakage from and to adjacent elements which should, in reality, have nearly a identical composition, neutron spectrum, etc. A calculation is performed for each type of reactor cell since the neutron spectra in the fuel, blanket, reflector, shield, etc., will tend to differ significantly. While relatively efficient, the approximations required in the traditional become suspect near interfaces between different

A different approach which takes advantage of the increased computation power of modern machines and the long mean free path of neutrons in a fast reactor was taken with respect to representation of the various element types. Instead of only considering each lattice cell type in isolation, the reactor is divided into macro-zones over which material compositions and temperatures are averaged. These are then assembled within a simplified reactor geometry with cylindrical symmetry that preserves mass. By considering the arrangement of the macro-zones during the lattice cell calculations, leakage from one macro-zone to another is allowed to influence the effective cross sections. In addition, the macro-zone approach provides a consistent method for accommodating large-scale changes in flux distribution and fuel composition which may occur during burnup, particularly in ultra-high-burnup designs.

The macro-zone layout for the AFR-100 is dictated by the enrichment zoning (Figure 8). An additional lateral cut across the core mid-plane was made to restrict the temperature rise across any particular fuel macro-zone to about 50 K. The resulting zone structure has 4 axial sections of each of the inner, middle, and outer core assembly types, totaling 12 macro-zones.

In order to avoid imposing massive computational costs every time microscopic

cross sections need to be calculated, the total number of macro-zones in the UCFR-1000 is kept to 12. The flat enrichment scheme across the starter zone necessitates two radial sections to account for the Bessel-shaped radial flux distribution, and axial divisions are made every 60 cm up the fuel column such that the bottom inner and outer axial macro-zones contain the starter fuel and the rest contain sections of the fertile column.

4.1.1.2 Ultra-fine group calculation and condensation to broad group structure

The ultra-fine group (UFG) calculation was performed using ENDF-VII cross section libraries and the ANL2082 group structure. The neutron spectrum and self-shielded UFG microscopic cross sections were first estimated in each macro-zone via a 0-D (traditional) lattice cell calculation. These estimated UFG cross sections were then refined in the approximate RZ geometry described in the previous section. The TWODANT neutron flux solver was used to provide an S_{12} UFG flux solution with a maximum mesh spacing of 5 cm. This flux was used to produce self-shielded UFG cross sections and then to collapse the cross sections down to broad groups (ANL33 Structure) in preparation for full-core neutronics calculations.

4.1.2 Full-core neutronics and fuel cycle

Full-core calculations were carried out using VARIANT to supply high-fidelity neutron flux distributions in the ANL33 group structure obtained by solving the neutron transport equation via variational nodal methods. VARIANT has the advantage of retaining real assembly-level geometry (Hex-Z), but must use homogenized (smeared) compositions within each assembly mesh. Sub-assembly spatial fidelity is able to be partially retained by using the flux shape functions which are the minima of the variational nodal calculation. The flux distribution was used to deplete the fuel in the REBUS (**Re**actor **Bu**rnup **S**ystem) code, which solves the Bateman Equations for the isotopes of interest in the reactor. Fuel isotopes from ^{233}U (Z = 92, N = 141)

through ^{245}Cm (Z = 96, N = 149) were considered "of interest", as outside these bounds the concentrations and reaction rates are exceedingly small for a uranium-fueled fast reactor. Fission products were lumped according to the parent isotope undergoing fission and assigned averaged neutronic properties weighted by relative yield. Fissions of fuel isotopes above ^{241}Pu were lumped together because of their small individual concentrations.

The size of the depletion steps used to map the fuel cycle for each reactor was based on the relative power density in each reactor and the time scale over which diversions of interest would be evaluated. The AFR-100 has a low power density for a fast reactor (58.2 kW/L, compared to ∼300 kW/L for a typical SFR), so step size was set at 1/4 EFPY since this is the weapon conversion time for reactor-sourced plutonium. The UCFR-1000 has a listed power density approximately 30% higher than the AFR-100, but because the power is produced in a small fraction (∼1/6) of the core volume at any one time, 1/12-EFPY steps were used instead. The smaller step size also helps limit error in the flux distribution used to deplete the fuel that is introduced by motion of the burn zone.

4.1.3 Mid-cycle cross section updates

During early simulations of the UCFR-1000 burnup cycle, it became apparent that significant error was being introduced by using the BOC effective cross sections for the whole cycle. The factors causing this were twofold: motion of the burn zone causes the spatial flux distribution to change throughout the cycle, and conversion from burning ^{235}U to ^{239}Pu alters the relative magnitudes of cross section resonances, exacerbating early-cycle errors. These factors are much more significant in the UCFR-1000 than in the AFR-100 because the latter experiences a much smaller change in flux distribution and the conversion to burning ^{239}Pu is spread out over the entire cycle.

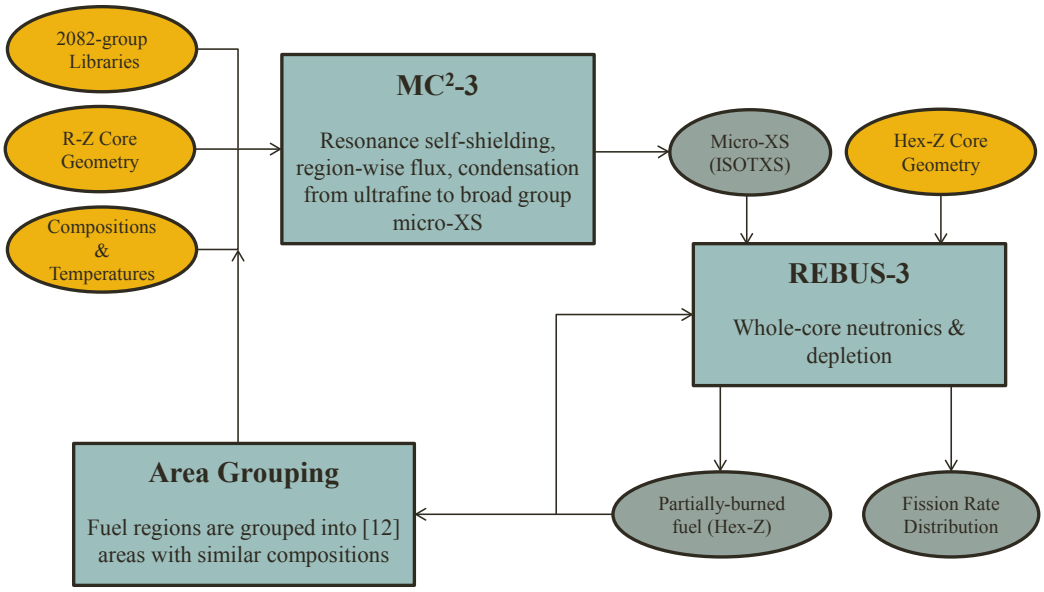

Figure 15: Calculation scheme used to map the fuel cycle of the AFR-100 and UCFR-1000. Rectangles indicate codes which perform the duties described within; ovals are data sets, with gold denoting user-defined data and grey denoting calculated data.

4.1.3.1 Update calculation scheme

In order to facilitate periodic updates to the effective microscopic cross sections, a script was written which averages the fine-grained fuel isotope data from the REBUS outputs at a particular interval across the spatial macro-zones. The entire lattice cell calculation process is repeated for each mid-cycle concentration, and the updated effective microscopic cross sections are recombined with the fine-grained isotope concentration data and used to continue fuel cycle calculations until the next update is required. Frequent updates are computationally expensive, so the interval between updates was kept to approximately the duration required for the burn zone peak to move from one axial mesh to the next. The calculation scheme for the fuel cycle mapping, including the actions required when updating the effective cross sections, is outlined in Figure 15.

4.1.3.2 UCFR update comparison

Because the rate of divergence between the UCFR fuel cycle data should be most pronounced during the beginning of the cycle, metrics from the first 15 EFPY were used to assess the case for periodic updates to the effective microscopic cross sections. Updates were performed every 1 EFPY, during which the burn zone propagates by at most about ∼5 cm (half the z-mesh used for region differentiation). The difference in the reactor eigenvalue, k_{eff}, illustrates the scale of the difference for integral effects (Figure 16). While the eigenvalues track each other for the first 3 EFPY, the burn zone propagates more quickly thereafter as fissile material is burned out of the starter region. The ∼1 EFPY separation between the local minima indicates a slower burn zone speed in the non-updated case. By 15 EFPY, the updated-case eigenvalue asymptotes, as one would expect from a flux distribution that moves upward into fertile material, depletes it as it moves through, and leaves behind material increasingly laden with reactivity poisons. In contrast, the non-updated case eigenvalue diverges from the expected asymptotic behavior. Under-predicting the reactor eigenvalue indicates an under-prediction of reactions with fissile isotopes and an over-prediction of reactions with non-fissile isotopes, most notably ^{238}U since it comprises the bulk of the fuel.

In addition to integral effects, neglecting to update effective cross sections also introduces a great deal of error into metrics which are of prime interest in nuclear safeguards. The inaccuracy in the plutonium inventory (Table 12) of the reactor by 10 EFPY into the cycle on the scale of 1 SQ—the same as the amount taken in some of the diversion scenarios.

The difference between the data indicate that periodic updates to the effective microscopic cross sections are necessary to ensure accuracy of the fuel cycle output data. For the reference fuel cycle, cross sections will be updated every 1 EFPY from 0 to 15 EFPY, then every 3 EFPY for the remainder of the cycle. The relaxed update

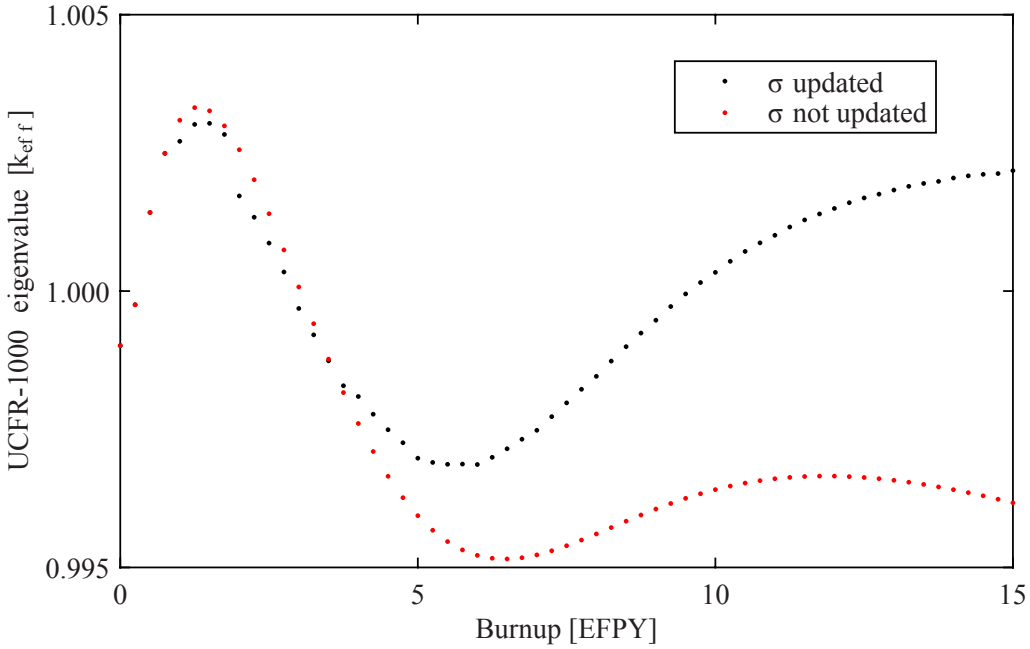

Figure 16: Comparison of the reactor eigenvalue for the UCFR-1000 between the fuel cycle simulations with updated and non-updated effective microscopic cross sections.

Table 12: Difference in the plutonium inventory between the updated and non-updated UCFR-1000 data.

	5 EFPY		10 EFPY	
Isotope	Diff(kg)	%	Diff(kg)	%
^{238}Pu	−0.02	−0.35	−0.11	−0.73
^{239}Pu	2.54	0.25	6.97	0.45
^{240}Pu	−0.37	−0.43	−2.13	−1.00
^{241}Pu	−0.09	−1.69	−0.44	−2.44
^{242}Pu	−0.01	−1.36	−0.05	−2.21

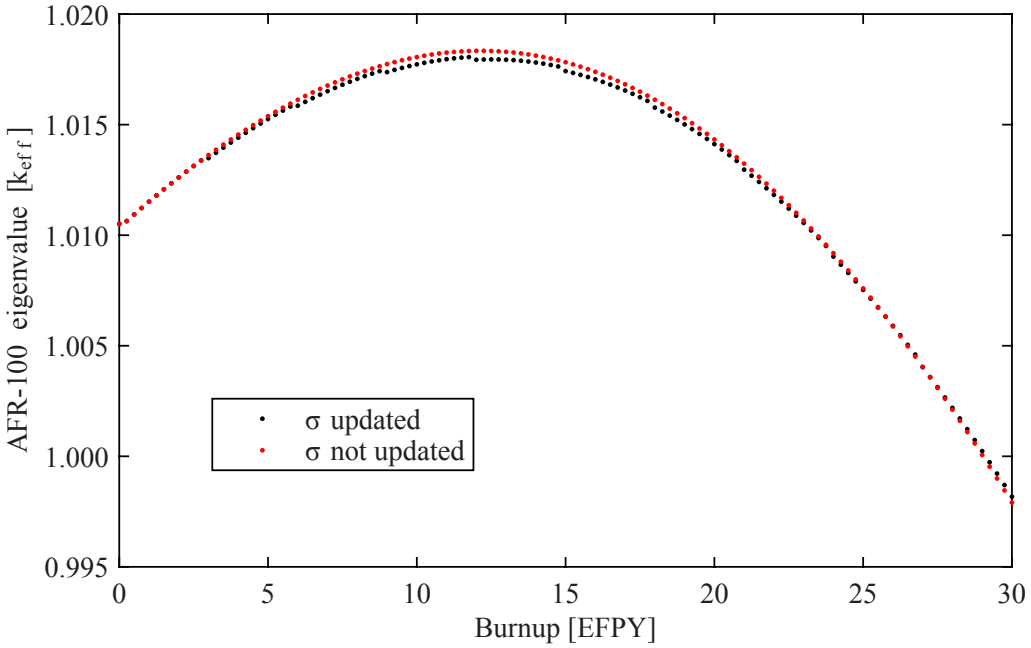

Figure 17: Comparison of the reactor eigenvalue for the AFR-100 between the fuel cycle simulations with updated and non-updated effective microscopic cross sections.

schedule past the first quarter of the burnup cycle is only possible because by that point the burn zone is propagating slowly upward and the change in fuel isotopes is slow compared to at BOC.

4.1.3.3 AFR update comparison

The AFR-100, contrary to the UCFR-1000, has very little difference between fuel cycle data resulting from periodic (every 3 EFPY) updates to effective microscopic cross sections and that resulting from a never-updated simulation. The burn zone motion is minute by comparison, and conversion from fissioning ^{235}U to ^{239}Pu is slower and of lower magnitude. The reactivity never varies more than 40 pcm during the cycle, and the k_{eff} curves lie on top of one another (Figure 17).

Similarly, the fission rates of the primary power-producing isotopes never varies by more than 0.2%, with ^{235}U and ^{239}Pu staying within 0.1% until the last 5 EFPY of the burnup cycle. The difference of each as a function of burnup is shown in Figure 18.

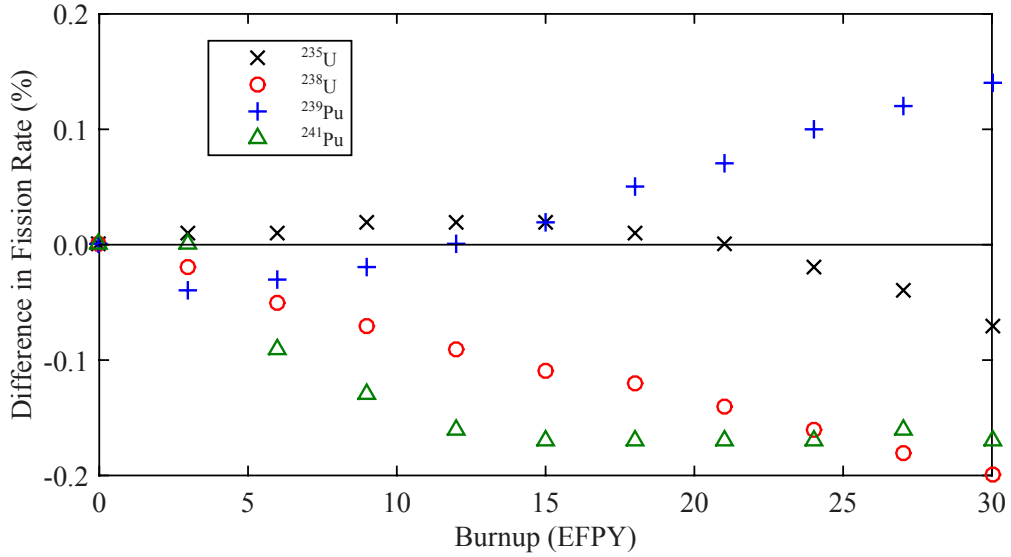

Figure 18: Comparison of the reactor eigenvalue for the AFR-100 between the fuel cycle simulations with updated and non-updated effective microscopic cross sections.

The lack of significant difference between the non-updated and updated cases indicates that mid-cycle updates to the effective microscopic cross sections are unnecessary for the AFR-100 fuel cycle mapping.

4.2 Construction of the antineutrino source and detector signal

4.2.1 Reactor antineutrino source

4.2.1.1 Building the source at reference points from antineutrino yield

The antineutrino yield data which comprise the non-reactor input to the antineutrino source calculation are aggregated from multiple experiments and theoretical beta decay calculations. Nearly all of the compiled experimental data to date on antineutrino yields from nuclear fission is the result of thermal fission of the primary isotopes responsible for power production in thermal reactors: ^{235}U, ^{239}Pu, and ^{241}Pu. The bulk of these data comes from measurement of the beta decay spectra associated with fission of these isotopes at the Institut Laue-Langevin (ILL) research

reactor [45, 57, 25, 56]. These measurements have been incorporated with an *ab initio* prediction which sums the contributions to the electron antineutrino flux from the individual beta decay pathways of the various fission products [33]. Recently, integral measurements for the antineutrino yield resulting from ^{238}U fission have been made [24] which generated data in a similar manner to that provided by the ILL measurements. To date, these are the only yield values which incorporate experimental measurement of fission product beta decays.

The yields and their uncertainties over the range of reactor antineutrinos measurable by inverse beta decay for the primary fissioning isotopes, compiled from Huber [27] for ^{235}U, ^{239}Pu, and ^{241}Pu and Haag et al. [24] for ^{238}U are in Table 13. The spectrum has been divided into 0.5-MeV wide energy bins; data with 250-keV binning has been weighted according to the antineutrino yield per fission.

The nominal antineutrino yields for the isotopes without experimental data, packaged into 0.5-MeV energy bins, were provided by Huber [27]. Aggregated with the ILL and Haag experimental results into a yield matrix $\mathbf{Y}$, these are used to calculate the nominal antineutrino spectrum (Eq. 4) emitted by the reactor with fission rate vector f at a particular burnup:

$$S = \mathbf{Y} f \tag{4}$$

4.2.1.2 Fitting event rate curves to span burnup cycle

Equation 4 provides the instantaneous reactor antineutrino source in each energy bin for all of the depletion steps in each reactor's fuel cycle. However, the timescale during which irradiated fuel can be converted to a weapon is similar to the gap between depletion steps. Therefore, although the reactor antineutrino source changes quite slowly, it is helpful to express the source in each bin as a function of burnup. Fitting smooth curves to the data also adds the capability to extrapolate or interpolate

Table 13: Nominal antineutrino yields and errors (primary isotopes). The tabulation starts at 2 MeV because of the 1.8 MeV energy threshold of the IBD reaction. Values marked with * were estimated from fitting curves to the available yield uncertainty data.

$\bar{\nu}_e$ Energy (MeV)	^{235}U (#/fission/MeV)	1σ (%)	^{238}U (#/fission/MeV)	1σ (%)
2.0	1.198	1.8	1.372	18.5 *
2.5	8.643×10^{-1}	1.9	1.047	9.2*
3.0	6.302×10^{-1}	1.9	8.002×10^{-1}	4.7
3.5	4.403×10^{-1}	2.0	5.882×10^{-1}	4.3
4.0	3.005×10^{-1}	2.1	4.217×10^{-1}	4.2
4.5	1.891×10^{-1}	2.4	2.795×10^{-1}	4.4
5.0	1.186×10^{-1}	2.6	1.831×10^{-1}	5.0
5.5	7.331×10^{-2}	2.8	1.183×10^{-1}	5.9
6.0	4.231×10^{-2}	3.2	7.111×10^{-2}	8.3
6.5	2.311×10^{-2}	3.5	4.089×10^{-2}	12.3
7.0	1.195×10^{-2}	3.9	2.237×10^{-2}	15.0
7.5	5.077×10^{-3}	4.8	1.079×10^{-2}	29.8
8.0	1.959×10^{-3}	6.4	4.650×10^{-3}	49.1 *
8.5	6.743×10^{-4}	7.2	1.987×10^{-3}	50.0 *
9.0	2.696×10^{-4}	9.2*	9.947×10^{-4}	50.0 *
$\bar{\nu}_e$ Energy (MeV)	^{239}Pu (#/fission/MeV)	1σ (%)	^{241}Pu (#/fission/MeV)	1σ (%)
2.0	1.028	2.6	1.199	2.5
2.5	7.286×10^{-1}	2.6	8.839×10^{-1}	2.3
3.0	5.159×10^{-1}	2.8	6.420×10^{-1}	2.4
3.5	3.388×10^{-1}	3.2	4.359×10^{-1}	2.5
4.0	2.146×10^{-1}	3.5	2.872×10^{-1}	2.6
4.5	1.207×10^{-1}	4.6	1.675×10^{-1}	3.3
5.0	6.882×10^{-2}	4.9	9.893×10^{-2}	3.5
5.5	4.057×10^{-2}	5.6	6.033×10^{-2}	3.8
6.0	2.198×10^{-2}	7.9	3.350×10^{-2}	4.8
6.5	1.105×10^{-2}	9.9	1.741×10^{-2}	5.7
7.0	5.289×10^{-3}	13.1	8.772×10^{-3}	6.2
7.5	2.020×10^{-3}	21.4	3.589×10^{-3}	8.4
8.0	7.279×10^{-4}	28.4	1.375×10^{-3}	11.7
8.5	2.268×10^{-4}	29.0	5.199×10^{-4}	13.0
9.0	8.106×10^{-5}	35.9 *	2.249×10^{-4}	16.9 *

diversion results, if necessary, based on the discrete data. The smoothness of the burnup dependency and the monotonically increasing or decreasing evolution of the fuel isotopes allows accuracy with a relatively low-order polynomial fit; the large excess of data points over fit coefficients ensures that little error is introduced during fitting. A 4^{th} order polynomial proved sufficiently precise, and because time is a reasonable proxy for burnup, the nomenclature for time dependence was used in lieu of adding yet another "b" to subscripts or function arguments.

4.2.2 Detector event rates

The expected burnup-dependent event rate $n_b\,(t)$ in each bin b at each depletion step is a function of the burnup-dependent reactor source $S_b\,(t)$ in that bin, geometric attenuation, number of target protons N_d in the scintillation medium, and the bin-averaged IBD cross section σ_b^{IBD} and intrinsic efficiency ϵ_b. The background term B_b is assumed to be constant in time.

$$n_b\,(t) = \frac{N_d}{4\pi L^2}\sigma_b^{IBD}\epsilon_b S_b\,(t) + B_b \tag{5}$$

4.2.2.1 Background

The PROSPECT team undertook extensive site-specific background characterization throughout the development of their AD-I and AD-II detector designs[4]. The main backgrounds for the IBD reaction with a reactor antineutrino source are reactor-correlated neutron and gamma fields which result from capture and scattering of the neutron flux in the reactor, coincident uncorrelated γ events originating in surrounding bedrock/soil, and cosmogenic fast neutrons which downscatter and subsequently capture in the ^{6}Li-doped scintillator. Measurements during prototyping indicated that passive shielding and time-, energy-, and position-based cuts, including pulse-shade discrimination and fiducialization, were sufficient to reduce the uncorrelated and reactor-correlated backgrounds to negligible levels[5]. The reactor-correlated

background, negligible for the PROSPECT team at ~ 7 m from a test reactor, should be at least as low for more distant installations near a power reactor that does not require perforations in shielding to allow for experimental equipment, etc.

The remaining IBD-like background due to cosmogenic neutrons was modeled by the PROSPECT team for the AD-I detector and compared to data gathered by one of the latest prototypes, PROSPECT-20. The data showed very good agreement well past the energy range considered for safeguards[5]. The passive shielding for other background sources in combination with reactor building features and Earth's atmosphere provide attenuation of cosmogenic neutrons which is not appreciably better than surface-level estimates of the cosmogenic fast neutron flux[5].

The variation due to altitude and depth of reactor installation are the primary factors which would decrease the cosmogenic flux. These vary enough from site to site that the AD-I background is used for background estimation without assuming any additional overburden from below-grade placement of the detector which would put it in the plane of the core. AD-II is to be sited 1 floor below AD-I, and will therefore experience slightly lower cosmogenic flux, and it is expected to achieve at least as good a signal-to-background ratio as AD-I[5]. The simulated safeguards detector, whose placement resembles PROSPECT AD-II to a high degree, will therefore use the AD-I background estimates as a conservative indicator of the background at a generic reactor site with the note that it would be reduced somewhat via below-grade placement or for sites close to sea level.

Estimation of the post-cut HFIR background data and uncertainties for the PROSPECT project[5] was performed via close-range (< 20 cm) optical techniques. The resulting data was shifted by the detector prompt ionization energy (1.293 MeV) to align with incident antineutrino energy and re-binned to match the energy structure used for safeguards calculations. The estimated data and resulting safeguards background

event rates due to cosmogenic fast neutrons are shown in Figure 19. The rates in Figure 19b are linearly scaled up to account for the higher fiducial mass of the safeguards detector (5 tons, compared to $\sim$ 1.5 tons for AD-I).

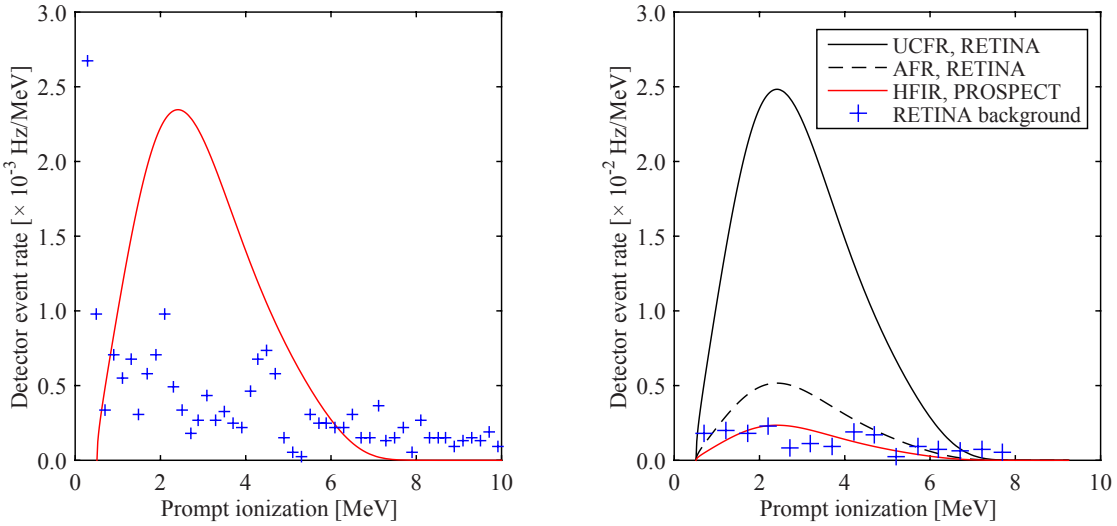

(a) Estimations PROSPECT AD-I background, recreated from Ashenfelter *et al.*[5].

(b) Background for safeguards calculations, converted and rebinned from the data in (a).

Figure 19: The estimates of PROSPECT AD-I background due to cosmogenic fast neutrons was used to approximate the background for antineutrino safeguards applications.

4.3 Quantification of Uncertainty

The uncertainties affecting the comparison calculation between the antineutrino signal from reference and perturbed reactor states arise from the following elements of the calculation: reactor physics uncertainty σ_{rp}, antineutrino yield uncertainty σ_{yields}, detector parameter uncertainty σ_{det}, reactor operating power uncertainty σ_{power} used for diversion masking, and the fitting errors for the burnup-dependent evolution of the calculated nominal reference and perturbed detector event rates $\sigma_{fit,ref}$ and $\sigma_{fit,div}$. These are combined in quadrature to produce the parameter σ_{norm} in the χ^2 goodness-of-fit calculation (Equation 13). Each uncertainty element may have multiple components, and for the reactor physics uncertainty these components show significant

correlations. Equation 6 details the level at which component uncertainties are combined in quadrature.

$$\sigma^2_{norm} = \sigma^2_{rp} + \sigma^2_{yields} + \sigma^2_{det} + \sigma^2_{fit,ref} + \sigma^2_{fit,div} + \sigma^2_{power} \tag{6}$$

4.3.1 Reactor physics uncertainties

The uncertainty on the reactor antineutrino source arising from the model of the reactor and its burnup cycle is propagated through the calculated isotopic fission rates (Equation 7). The antineutrino yield matrix $\mathbf{Y}$ is also the array of partial derivatives of the source with respect to each fission rate.

$$\mathbf{\Delta S_R} = \mathbf{Y}\left(\mathbf{\Sigma}\left(\mathbf{F}\right)\right)\mathbf{Y^T} \tag{7}$$

The fission rates are determined only by the initial-state reactor compositions, the microscopic cross sections for each interaction, the reactor thermal power, and the operating history of the reactor. The approach to propagating uncertainty on each of these as fuel depletion proceeds becomes complex due to the significant correlation and anti-correlation introduced through the imposition of a total thermal power output for the reactor. Because the energy release per fission varies only slightly between isotopes, a fission of one species almost exactly offsets one of another species. This trade-off in fission rates is compounded by the mutual exclusivity of the various reaction paths (inducing fission, radiative capture, inelastic and elastic scatter, n-2n, and other reactions) any given neutron can take. For example, an under-predicted ^{238}U capture cross section bears many similarities to an under-predicted ^{239}Pu fission-to-capture ratio because ^{238}U begins the plutonium production chain. However, it will quicken the burnout of ^{235}U since there is less plutonium available to produce power, whereas an over-predicted ^{239}Pu capture cross section will alter the fission rates of plutonium species relative to one another without impacting the share of

reactor power from plutonium fissions as significantly. This leads to significant non-diagonality in the fission rate covariance matrix $\mathbf{\Sigma}(\mathbf{F})$.

4.3.1.1 Monte Carlo method for estimating fission rate uncertainties

With the rise in computing power and information storage, a Monte Carlo approach can be taken to evaluating output sensitivity to uncertainty on reactor model inputs, such as the fuel loading and cross sections, rather than the cumbersome and tedious process of forward-propagating uncertainty along with the reactor burnup calculation; the Monte Carlo approach toestimating sensitivity has been outlined by ANL for estimating uncertainty on derived values [48]. In this method, many histories of the burnup cycle are generated with input parameters sampled from distributions of basic nuclear measurements in order to determine the sensitivity of desired outputs—in this case, the fission rates of each isotope—from variation of the inputs for the specific reactor under study. This approach has the advantage of simultaneously generating the covariance matrix $\mathbf{V}$ of the outputs, with elements (Eq. 8):

$$V_{ij} = \langle (f_{ik} - f_{i0})(f_{jk} - f_{j0}) \rangle_k \tag{8}$$

where i and j refer to the species, f is the relevant isotopic fission rate, and k denotes the Monte Carlo history (the zero subscript refers to the history with nominal inputs). A relative covariance matrix $\mathbf{R}$ is obtained by dividing the elements of $\mathbf{V}$ by the data generated using nominal inputs (Eq. 9):

$$R_{ij} = V_{ij}/(f_{i0} \times f_{j0}) \tag{9}$$

The distributions on the input parameters are constructed from the data compiled in the appendix of Palmiotti et al. [39]. For some of the rarer reactions, particularly (n,2n), the range values are sufficiently large to encounter negative cross sections

as a result of sampling; if this occurs, the distribution is re-sampled to avoid non-physical values. Although this artificially enhances the rate of higher-than-nominal cross sections assigned to these reactions, the small chance of triggering re-sampling combined with the—by definition—very small nominal value of the cross sections for these reactions, ensures that the effect on overall reactor calculations is negligible. Modifications to the cross sections, neutron yields, etc. were made at the broad-group level.

4.3.1.2 Initial fuel loading variation

Because VARIANT [38], the nodal transport code used to generate flux solutions for REBUS-3, homogenizes the reactor assembly within each axial mesh, the fuel loading was kept constant due to the negligible variation in fuel enrichment and composition at the assembly level resulting from this homogenization and the assumption that pins would be individually measured for weight and uranium enrichment during fuel production.

4.3.1.3 Reactor thermal power variation

The reactor thermal power is traditionally measured via a flowmeter in the steam loop, and although currently installed flowmeters are accurate to about 2%, new measuring techniques and equipment allow for up to an order of magnitude better determination of the reactor output [20]. The reactor thermal power was sampled with a 1σ value of 0.2% alongside the microscopic cross section as an input to each of the Monte Carlo burnup histories.

4.3.2 Antineutrino yield uncertainties

The nominal fission rates, because they are the partial derivatives of the antineutrino source with respect to the antineutrino yields, are used to calculate the contribution of uncertainty on the yield data to the uncertainty on the reactor antineutrino source

by weighting the bin yield uncertainty on each isotope Δy_i^b by the fraction of total fissions contributed by isotope i:

$$\Delta N_{\bar{\nu}}^b = \sum_i \Delta y_i^b f_i \tag{10}$$

This component of the uncertainty increases with burnup, chiefly due to the higher uncertainty on ^{239}Pu and ^{241}Pu yields than those resulting from fission of ^{235}U. The ^{238}U fission rate changes very little and the other actinides fission infrequently.

The experimentally measured thermal spectrum antineutrino yield data comes with relative errors, as shown in Table 13. It should be noted that there are errors missing for the yields at high energy for all isotopes and just above the IBD threshold for ^{238}U (marked with *). The missing error data has been estimated from fitting curves to the available yield uncertainty data with the acknowledgement that the ^{238}U yield experiment predicted a roughly 10% higher uncertainty at low energy due to increased background [24] and that the high uncertainty at higher energies is largely a consequence of the poor counting statistics due to lower yields in that energy range.

The lack of widespread fast reactor use in conjunction with the lack of significant funding directed toward antineutrino yield measurements has left the data on fast fission of common isotopes and all modes of fission on the rarer transuranic species sparse. The yields from these species are calculated via the *ab initio* summation method from the decay paths of their fission product distributions. Because the fission product yields of fast and thermal fission of the well-studied isotopes are very similar, predictions of the fast fission antineutrino yields for these isotopes only differ from their thermal-fission counterparts by $\sim$1%; the uncertainty data for thermal fission will therefore be used for these isotopes under the assumption that similarly precise data will become available with the adoption of fast reactor technologies. However, since there is a dearth of data for the fission product distributions of the higher actinides due to their relative scarcity in used nuclear fuel, the uncertainty on the

antineutrino yield per fission is roughly an order of magnitude higher than for isotopes for which experimental data is available. These isotopes have been conservatively assumed to bear 20% uncertainties on their yields below 7.0 MeV and 50% above that, with the restriction that yields cannot be negative.

4.3.2.1 Possible reduction in fast fission antineutrino yield data

An estimation of the magnitude of reduction in uncertainty on fast fission antineutrino yield data achievable by near-field observation of the AFR-100 by a 5-ton SONGS-like detector with 30% intrinsic efficiency was made in order to validate the use of thermal-spectrum errors where available. The uncorrelated background B for measurement via inverse beta decay was estimated to be about 6450 counts per day based on the uncorrelated background in the SONGS-1 experiment [8], evenly spread across all energy bins [1], while the correlated background is assumed to be mitigated to negligible levels via active shielding. The standoff from the core as well as the substantial neutron and gamma shielding between the core and detector should result in a negligible background from non-$\bar{\nu}_e$ reactor radiation. The detector measures the reactor antineutrino source for 10 years with the reactor at full nominal power.

The resulting data did not resolve the binned yield from any of the higher plutonium isotopes, even for observation extended to 30 EFPY. This is largely due to their very low fission rates through the beginning of the burnup cycle. On the other hand, precisions of the order of the current experimental data for thermal fission of ^{235}U and fast fission of ^{238}U are achievable in the center of the IBD event rate distribution (3.0-6.5 MeV) with *zero* prior knowledge of the yields. If observation is allowed to continue for the entire 30-year burnup cycle unabated, precisions on the order of 1-1.5% for ^{235}U, 3-4% for ^{238}U, and 10% for ^{239}Pu are achievable. The gains on the uranium isotopes are largely due to better statistics, but the improvement in the ^{239}Pu yield precision is attributable to its high fission rate in the latter half of

the burnup cycle. With that in mind, a reactor initially fueled with either blended reactor grade plutonium or downblended plutonium from weapons streams would be able to significantly decrease the calculated uncertainty on all plutonium isotopes. The use of a larger or more efficient detector would improve on the yield reductions by approximately a factor of $1/\sqrt{n}$ through better counting statistics due to a linear increase in detector event rates. Similarly, a reactor with a higher power output would linearly increase the antineutrino flux incident on the detector. Depending on advances in detector technology, the particular set of antineutrino yield observations made between now and the implementation of fast reactors, the power rating of the reactors, and their initial fueling, improved statistics and the incorporation of priors may be used to hasten the refinement of fast spectrum yield data by an order of magnitude.

4.3.3 Detector parameter uncertainty

The detector parameters which were considered to contribute to uncertainty on antineutrino-like event rates are the reactor-detector standoff, the number of target protons in the fiducial volume, the IBD cross section value, and the intrinsic efficiency. Because these arise from distinct physical phenomena, they are considered independent and are added in quadrature (Equation 11) to obtain the total contribution to uncertainty from the detector parameters.

$$\sigma_{det}^2 = \sigma_{standoff}^2 + \sigma_{prot}^2 + \sigma_{IBD}^2 + \sigma_{\epsilon}^2 \tag{11}$$

4.3.3.1 Reactor-detector standoff

The reactor-detector standoff is considered to be known to an absolute 1σ level of 1 cm. This is based on the assumptions that the detector and its ensemble of shielding structures has a well-known size, that it is placed adjacent to a wall in the containment building in an effort to minimize the standoff, and the construction of the containment

building is executed with the extreme precision usually associated with safety-related nuclear structures.

4.3.3.2 Number of target protons

The segmented structure of the detector allows for individual measurement of empty and filled liquid scintillator cells, providing high precision on the mass of scintillator in each segment. The variation in composition as-produced is not available in the EJ-309 documentation [52], but the use of calibration sources both prior to detector assembly and during reactor-off periods in concert with the scintillator mass data should provide a narrow envelope on the composition of each segment. The number of target protons is conservatively assumed to vary by 1% when considered across the entire fiducial volume, allowing for much greater variability on a per-segment basis.

4.3.3.3 Inverse beta decay cross section

The current uncertainty on the magnitude of the energy-dependent IBD cross section is reported to be 1.4% [58]. This value is used as a conservative estimate of the uncertainty on its magnitude that will exist some 5-10 years from present, when next-generation fast reactors might begin to see deployment. Some neutrino physics experiments, both ongoing and those about to enter their data collection phase, have reduction of IBD cross section uncertainty as a stated or implied goal of the program.

4.3.3.4 Detector intrinsic efficiency

The PROSPECT team has noted that efficiencies among the segments comprising the fiducial volume are largely consistent to percent-level 1σ deviations and that on-line calibration using inserted gamma and neutron sources as well as analysis of background levels can correct these deviations [5]. Despite the ability to correct variation in segment efficiency, a relative 1% uncertainty on detector intrinsic efficiency is retained to account for comparison with poorly-characterized background, the potential

malfunction of calibration equipment that degrades the confidence of the efficiency corrections, etc.

4.3.4 Fitting errors

The statistical errors produced by the polynomial fits to reactor sources and detector event rates in each energy bin as functions of burnup were produced along with the fits in MATLAB. These were normalized to the range of the fit (normalized root mean square error) and weighted by the fraction of the total source or event rate in each bin, then summed to produce each σ_{fit}. The normalization and weighting of the root mean square errors is laid out in Equation 12.

$$\sigma_{fit}(t) = \sum_{b} \left(\frac{n_b(t)}{\sum_b n_b(t)} \right) \left(\frac{RMSE(n_b(t))}{max(n_b) - min(n_b)} \right) \tag{12}$$

Although the fitting errors depend on the particular diversion scenario and the burnup at which the reference-diversion comparison is made, the fitting errors for all of the studied diversions vary tightly around about 2% of the value of the total calculated uncertainty on detector rates, σ_{norm}, and about 0.1% of the magnitude of the nominal detector event rates.

4.4 Comparison statistics

Once the reference detector signal has been compiled, the same process can be done to provide the nominal detector signal for each diversion case. The difference in detector signals between the reference and perturbed cases is the basis upon which determinations about the state of the reactor are made. The spectral differences are used to calculate a goodness-of-fit metric with a distribution that has significant penetration into the reference case probability space, but which diverges sharply from reference allowances for sub-optimal attempts to mask diversions.

4.4.1 Chi-square goodness of fit

A χ^2 goodness-of-fit statistic (Equation 13) can be calculated based on the difference between the integrated detector event rates of the reference ($n_b(t)$) and perturbed ($n_b'(t)$) states in each energy bin that allows for the reactor operator to attempt to reduce the difference between the reference state and its post-diversion state by operating at a different power level; this power manipulation is captured in the parameter x:

$$\chi^2 = \left(\sum_b \frac{\left(n_b - (1+x)\, n_b'\right)^2}{n_b} \right) + \left(\frac{x}{\sigma_{norm}} \right)^2 \tag{13}$$

The last term applies a penalty to account for the fact that continuous operation above or below the supposed nominal power (as this is the part of x which the operator can influence), under the assumption that an independent statement of the operating power is available, would also raise red flags for a deviation that is high relative to the uncertainty on the power measurement. The statistic, as formulated, essentially measures a worst-case scenario, in which the reactor operator and diverting actor have near-perfect information on the reactor state and the required information to best spoof detection via antineutrinos.

4.4.2 Accounting for variation about the nominal fit

The value of χ^2 calculated in Equation 13 applies to the mean of the diverted-case minimized bin difference; in reality, the world is not perfect, and the measured value is distributed about $T_0 = \chi^2$. It can be shown[11] that the corresponding statistic T is normally distributed:

$$T \sim N\left(T_0, 2\sqrt{T_0}\right) \tag{14}$$

The null hypothesis against which data is compared in this test, as with IAEA safeguards in general, is that no nuclear material has been lost. In this context, a

false positive (Type-I error) might result in falsely concluding that material has been diverted. Conversely, a false negative (Type-II error) happens when a diversion is concluded to not have occurred when, in fact, it has—this is referred to as the non-detection probability[23]. For a specified critical value of T^{α}_{crit} for which the Type-I error rate is α, the rate of Type-II errors (β) and the power of the test are:

$$\beta = \Phi\left(\frac{T^{\alpha}_{crit} - T_0}{2\sqrt{T_0}}\right) \tag{15}$$

$$\text{Power} = 1 - \beta \tag{16}$$

where $\Phi(x)$ is the cumulative distribution function of the standard normal distribution. Safeguards tests pre-select $\alpha = 0.05$ or lower in order to keep the frequency of false alarms low[23].

The acceptable thresholds for the power of safeguards measurements are 0.9 for high-probability events and 0.2 for low-probability events[23]—the lower threshold in the latter case represents the impetus for action on less certain data due to the generally high consequences of an ignored but real low-probability event. However, the normal distribution of the goodness-of-fit χ^2 results in Power = β = 0.5 at T_0 = T^{α}_{crit}, so should the diversion of material from a functioning reactor be classified as a low-probability event, it is likely that a reduced false-positive threshold would be employed to take advantage of data with non-negligible indication that immediate inspection and/or international intervention is required. However, regularly updated integration of detector events—one of the more intuitive ways to condense time-series safeguards data—would then give many false positives, depending on how often the metric is updated. For example, if the cumulative detector event count is updated daily and the safeguards discrimination has a false positive rate of 0.05, we should expect 18.25 false positive events per year according to the binomial distribution with

n = 365 and p = 0.05. In order to avoid frequent expensive action based on false-positive indications from antineutrino safeguards mechanisms alone, their data should be used in conjunction with other safeguards metrics to allow joint probabilities to guide inspector deployments or corrective measures.

4.5 Figures of merit

With the need for high discrimination power and fast detection times combined with the desirability of low false-positive rates, three metrics present themselves as attractive for consideration:

1. Certitude of non-diversion: for the maximum-allowed Type-I error rate and integration allowed over the entire duration of the relevant weapon conversion time (3 months for plutonium, 1 year for LEU), what is the probability that a diversion went undetected?

2. Speed of determination: for the maximum-allowed Type-I and Type-II error rates, what integration time for which the detector event difference produces the nominal $\chi^2 = T^{\alpha}_{crit}$?

3. Significance of determination: for the maximum-allowed Type-II error rate and integration allowed over the entire duration of the relevant weapon conversion time, what is the false positive rate?

CHAPTER V

REFERENCE FUEL CYCLE RESULTS AND UNCERTAINTY

There are three fuel cycle parameters which have prime relevance to antineutrino safeguards: core excess reactivity, isotopic fission rates, and plutonium inventory.

The excess reactivity of a core is an indication of how much fissile material can be removed from a core and the core still be able to maintain criticality. Both the AFR-100 and UCFR-1000 have a small beginning-of-cycle excess reactivity and use bred-in plutonium to offset the reactivity loss from the depletion of the initial charge of ^{235}U. The result is an extremely flat reactivity curve as a function of burnup that reactor design engineers tend to keep as close above critical as possible for safety purposes.

As mentioned prior, the fission rates of each isotope are the mechanism by which the measurable differences in reference and perturbed antineutrino signal can be ascertained. Finally, the plutonium inventory measures the amount and purity of the product to be gained by a diverting actor.

The total plutonium inventory of the core is a useful tool for core-level diversion scenarios; for assembly-level scenarios, it is an indication of the average plutonium content per assembly, with central assemblies usually having higher amounts of less pure plutonium. Peripheral assemblies, by contrast, tend to have lower amounts of plutonium in higher purities.

The uncertainty established via the Monte Carlo sampling of modeling inputs is reported alongside each of these parameters. The uncertainty on the isotopic fission

rates is afforded the most detail because these are necessary to calculate the uncertainty on the nominal event rates in the antineutrino detector. Because the perturbed core states simulated in each of the diversion scenarios are not substantially different from the reference cases at the whole-core level, the reference case uncertainties are also used for the perturbed state fission rate data. Convergence of the sample variances is used to determine that the variance estimates for these parameters obtained by averaging over all of the available Monte Carlo fuel cycle histories is representative of the true variances.

5.1 AFR-100 reference fuel cycle

The AFR-100 fuel cycle features a bowed reactivity curve typical of a fast breeder reactor. Its conversion ratio, however, is only about 0.8[30], implying less end-of-cycle plutonium inventory. This is reflected in the incomplete conversion from ^{235}U to ^{239}Pu in the isotopic fission rates, although the swing is more pronounced than in commercial LWR's.

5.1.1 Reactivity

The small excess reactivity throughout the AFR-100 burnup cycle is the result of two primary design decisions: to preserve passive shutdown capability even in the case of stuck control rods and to achieve an even coolant outlet temperature across the core[30]. These objectives drove the decision fot the onion enrichment scheme, and the resulting excess reactivity in combination with the small core size (150 total fuel assemblies) mean that diversion scenarios which do not replace (in the form of LEU) some of the stolen fissile material may render the core subcritical, even for scenarios which only involve a single assembly. The evolution of the core reactivity, measured via the reactor eigenvalue k_{eff}, as a function of burnup is shown in Figure 20. $k_{eff} > 1$ indicates supercriticality, $k_{eff} = 1$ criticality, and $k_{eff} <$ subcriticality. The eigenvalue

is calculated for the all rods out position of the control assemblies; these are partially inserted to achieve k = 1 during operation.

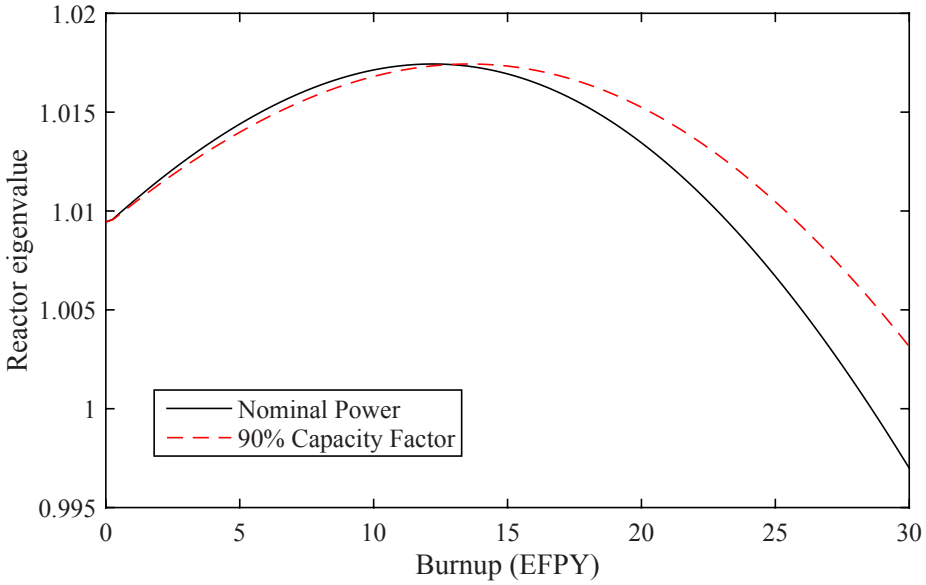

Figure 20: AFR-100 eigenvalue evolution in the all rods out condition. Operation with a smooth 90% capacity factor is shown for reference.

The reactor was designed with a 90% capacity factor in mind; full power with 100% capacity is used in the safeguards analysis because this is the only reasonably predictable outcome of a full maintenance shutdown which would facilitate a diversion in the first place. The protective value of low excess reactivity against diversions with a large net loss of fissile material will be most pronounced at the end of the burnup cycle, when excess reactivity is the lowest.

5.1.2 Fission rates

The evolution of the isotopic fission rates in the AFR-100 proceeds with ^{235}U dominating power production in the early cycle and ceding primacy to ^{239}Pu by the end of cycle. The transition from burning ^{235}U to ^{239}Pu is more complete than in typical modern commercial light water reactors, in which the isotopes typically do not quite reach equal power production. The fission rate of ^{238}U remained nearly constant

throughout the burnup cycle, and ^{240}Pu and ^{241}Pu were not produced in large enough quantities to contribute more than 1% and 0.28% of the total fissions, respectively.

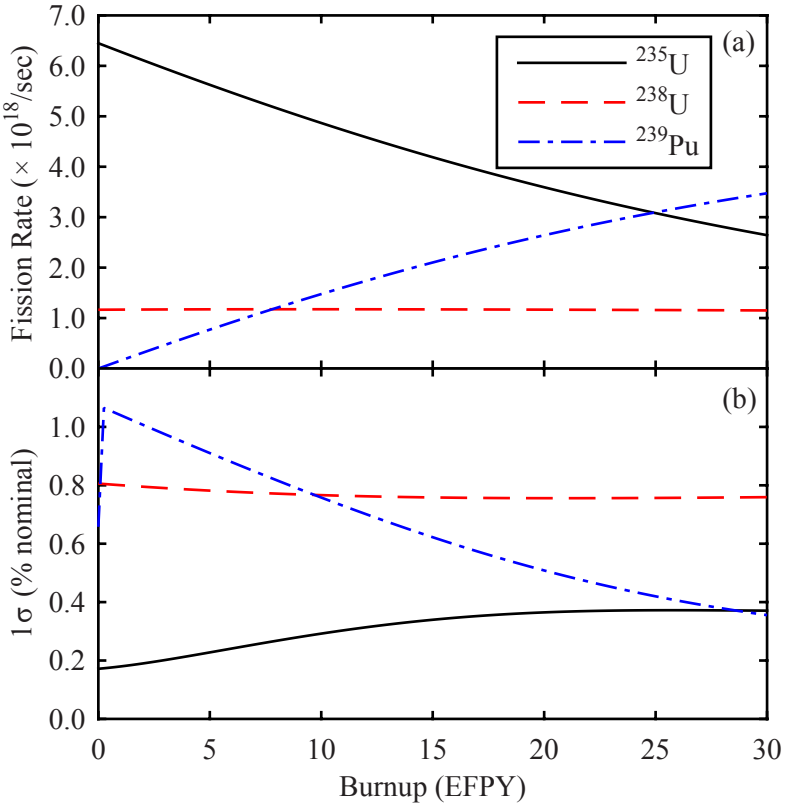

Figure 21: (a) Evolution of the fission rates of the primary power-producing fuel isotopes through the burnup cycle. (b) 1σ relative errors on the fission rates.

Should there be a diversion of plutonium from the core with LEU replacement, the fission rates will, for the most part, "reset" to the ratio exhibited by a lesser burnup. The magnitude of the reset is determined by the amount removed/replaced and, to a lesser extent, the location of the diverted assembly or assemblies. If the only available replacement fuel material is natural uranium, the location of the diversion will determine whether the fission rates, upon resuming operation, would resemble a regressed or progressed burnup. A local flux depression caused by diversion near the core center suppresses plutonium fission rates, regressing the burnup, while a depression in the periphery is more likely to suppress ^{235}U fission at least as much as

that of bred-in plutonium.

The uncertainties on the isotopic fission rates are expressed in the covariance matrices calculated via the method outlined in Section 4.3.1.1. Four burnups, the beginning-, middle-, and end- of-cycle, in addition to 1 EFPY were selected to illustrate the change in magnitude, particularly among the plutonium isotopes, as burnup progresses. The complex interdependence of the modifications to the reactor input parameters produces a large degree of non-diagonality in the covariance matrix spanning the fission rates of the heavy metal isotopes, as shown in Table 14. By the end of cycle, the off-diagonal elements for all isotope pairs has increased to similar magnitudes, as opposed to the beginning-of-cycle variation concentrated in the uranium isotopes.

5.1.3 Plutonium inventory

The AFR-100 lacks dedicated blanket assemblies that bear fuel with natural uranium enrichment. Instead, the breed-in of plutonium is fairly balanced across the core with the exception of the outer row of assemblies because the flux is propped up by the (at the lowest) 8% ^{235}U initial enrichment. This opens the door to a variety of diversion scenarios, in which the actor may choose an assembly at-will past mid-cycle with reasonable certainty to obtain 1 SQ of plutonium. Conversely, the distributed plutonium inventory prevents acquisition of 1 SQ without removing multiple assemblies until at least 15.75 EFPY, protecting the installation from use in proliferation schemes through the early cycle. Barring removal of a significant fraction of the core, adding an AFR-100 installation to a nation's energy production capacity should not significantly affect its breakout period without detection by a monitoring body.

The core-averaged plutonium content per assembly (Figure 22) only barely exceeds 1 SQ by the end of cycle, indicating that either mid- to late-cycle diversions of single central assemblies or mid- to late-cycle multiple-assembly diversions from the core

Table 14: Covariance matrices of AFR fission rates for selected burnups (primary isotopes). Correlation between the isotopic fission rates increases with increasing burnup. With the exception of the very beginning of irradiation, correlation between ^{235}U (and ^{238}U) and Pu isotopes is negative (the more fissions occur in ^{235}U (and ^{238}U), the fewer are required in Pu isotopes in order to compensate for constant power requirement.) Correlation between Pu isotopes is positive due to direct fission-capture relation (recall that ^{240}Pu and ^{241}Pu are produced by neutron capture on ^{239}Pu.)

0 EFPY	^{235}U	^{238}U	^{239}Pu	^{240}Pu	^{241}Pu
^{235}U	1.23×10^{32}	-9.01×10^{31}	-1.00×10^{24}	3.83×10^{22}	-4.93×10^{23}
^{238}U	-9.01×10^{31}	8.81×10^{31}	2.48×10^{23}	-1.76×10^{23}	-6.39×10^{23}
^{239}Pu	-1.00×10^{24}	2.48×10^{23}	1.99×10^{18}	1.39×10^{17}	1.04×10^{18}
^{240}Pu	3.83×10^{22}	-1.76×10^{23}	1.39×10^{17}	1.41×10^{17}	1.61×10^{17}
^{241}Pu	-4.93×10^{23}	-6.39×10^{23}	1.04×10^{18}	1.61×10^{17}	8.28×10^{18}
1 EFPY	^{235}U	^{238}U	^{239}Pu	^{240}Pu	^{241}Pu
^{235}U	1.27×10^{32}	-8.93×10^{31}	-4.86×10^{30}	-3.31×10^{27}	-5.74×10^{25}
^{238}U	-8.93×10^{31}	8.73×10^{31}	6.71×10^{29}	-1.01×10^{26}	-5.03×10^{24}
^{239}Pu	-4.86×10^{30}	6.71×10^{29}	2.68×10^{30}	1.90×10^{27}	3.24×10^{25}
^{240}Pu	-3.31×10^{27}	-1.01×10^{26}	1.90×10^{27}	3.53×10^{24}	4.79×10^{22}
^{241}Pu	-5.74×10^{25}	-5.03×10^{24}	3.24×10^{25}	4.79×10^{22}	1.60×10^{21}
15 EFPY	^{235}U	^{238}U	^{239}Pu	^{240}Pu	^{241}Pu
^{235}U	2.02×10^{32}	-3.98×10^{31}	-1.37×10^{32}	-1.64×10^{30}	-3.51×10^{29}
^{238}U	-3.98×10^{31}	7.90×10^{31}	-3.42×10^{31}	-4.59×10^{29}	-9.87×10^{28}
^{239}Pu	-1.37×10^{32}	-3.42×10^{31}	1.71×10^{32}	1.79×10^{30}	3.74×10^{29}
^{240}Pu	-1.64×10^{30}	-4.59×10^{29}	1.79×10^{30}	1.20×10^{29}	1.79×10^{28}
^{241}Pu	-3.51×10^{29}	-9.87×10^{28}	3.74×10^{29}	1.79×10^{28}	8.38×10^{27}
30 EFPY	^{235}U	^{238}U	^{239}Pu	^{240}Pu	^{241}Pu
^{235}U	9.60×10^{31}	-2.47×10^{30}	-7.70×10^{31}	-1.89×10^{30}	-8.11×10^{29}
^{238}U	-2.47×10^{30}	7.64×10^{31}	-6.51×10^{31}	-1.71×10^{30}	-5.89×10^{29}
^{239}Pu	-7.70×10^{31}	-6.51×10^{31}	1.52×10^{32}	1.40×10^{30}	5.29×10^{29}
^{240}Pu	-1.89×10^{30}	-1.71×10^{30}	1.40×10^{30}	1.23×10^{30}	2.61×10^{29}
^{241}Pu	-8.11×10^{29}	-5.89×10^{29}	5.29×10^{29}	2.61×10^{29}	2.50×10^{29}

periphery are the minimum acceptable options for an actor seeking weaponizable plutonium.

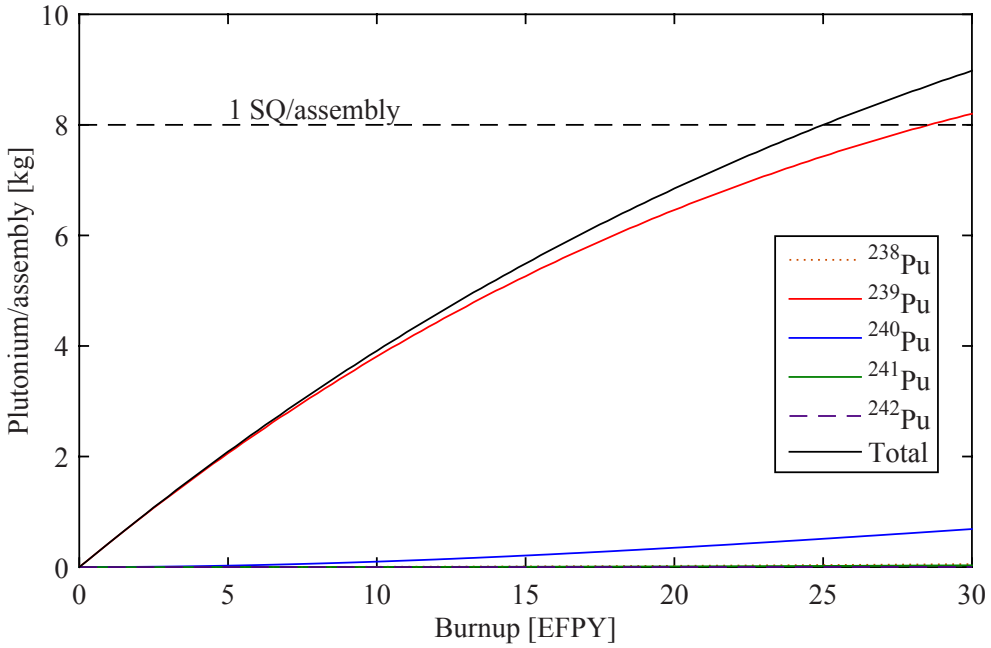

Figure 22: Core-averaged plutonium mass (kg) per assembly as a function of burnup.

5.1.4 Convergence of the Monte-Carlo sampled fuel cycle histories

At least 1000 fuel cycle histories are recommended [48] in order to reduce statistical variability of the generated elements of the covariance matrix, V_{ij}, to $\sim 3\%$. The convergence of the fission rate variances was checked by sampling n histories, averaging them, and taking the relative difference to the value of the "converged" variance obtained by using all 1000 histories. The AFR-100 data from the middle of the burnup cycle (15 EPFY)—when the bred-in isotopes have had sufficient time to accumulate substantially in the fuel— was used as a proxy for the whole dataset, as checking for convergence of the variances at all burnup steps becomes prohibitively computationally expensive once more than a couple hundred histories are amassed. Sampling n variances as described produces a chi-square distribution with $n-1$ degrees of freedom according to Equation 17:

$$\frac{s^2}{\sigma^2} \sim \frac{\chi^2_{n-1}}{n-1} \tag{17}$$

The convergence behavior of the variances for the primary power-producing isotopes in the AFR-100 as more histories are sampled is illustrated in Figure 23.

5.1.5 Antineutrino signal evolution

The progression of the isotopic fission rates in the AFR-100 manifests itself as a slowly diminishing signal to a nearby antineutrino detector. The steady transition to producing power through plutonium fission reduces the intensity of the reactor antineutrino source as burnup progresses (Figure 24). The relative errors on the antineutrino source increase steadily throughout the burnup cycle as core plutonium content increases. Although some of this increase is due to higher aggregate uncertainty on the fission rates themselves, the vast majority of the uncertainty on the reactor antineutrino source propagates from the expected antineutrino yield per fission. The large increase in antineutrino source uncertainty by the end of the burnup cycle results from the proportionally higher contribution from fissions of plutonium isotopes, for which the antineutrino yields are less certain.

The nominal signal in each detector of the RETINA suite is shown in Figure 25 as a function of burnup and given in Table 15 for various burnups. The smoothly diminishing source intensity is one of the features which would be disrupted by a potential proliferator who removes some bred-in plutonium. The reactor operator can offset this disruption by precisely adjusting the reactor power, but another feature of the signal evolution evades such attempts to dissemble: the signal on the high-energy side of the peak falls away more quickly than that on the low-energy side. This spectral evolution feature cannot be masked by manipulation of the reactor antineutrino source, and attempts to prop up the high-energy side of the spectrum via exposure of the detector to another coincident positron-neutron phenomenon would

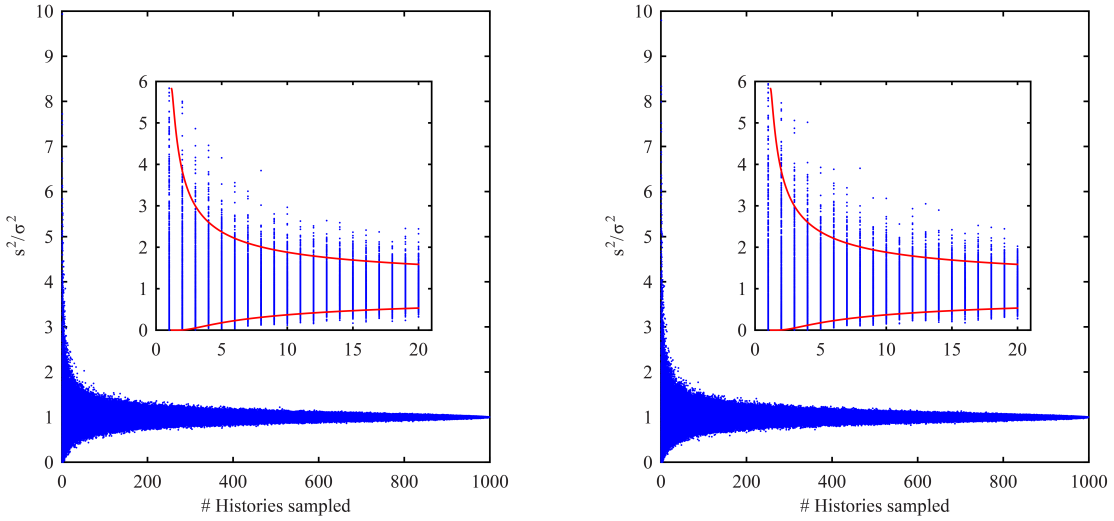

(a) ^{235}U

(b) ^{238}U

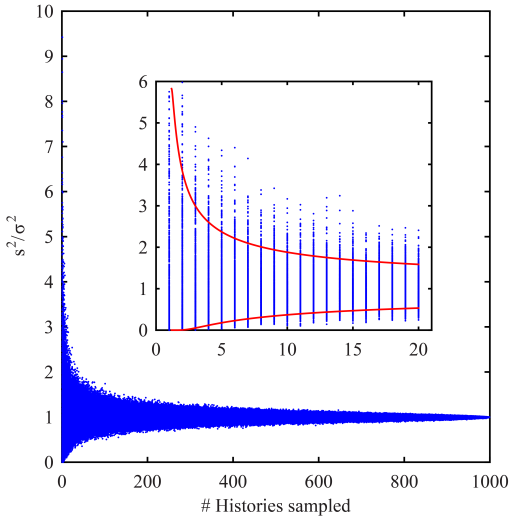

(c) ^{239}Pu

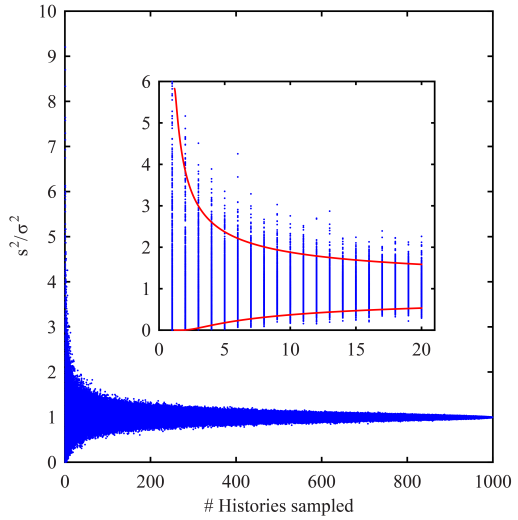

(d) ^{241}Pu

Figure 23: Convergence behavior of the sample variances for the fission rates of the primary power-producing isotopes in the AFR-100 at 15 EFPY. The calculated variance converges as more histories are sampled. The red curves on the enlarged axes display the 90% confidence interval for the sample variance.

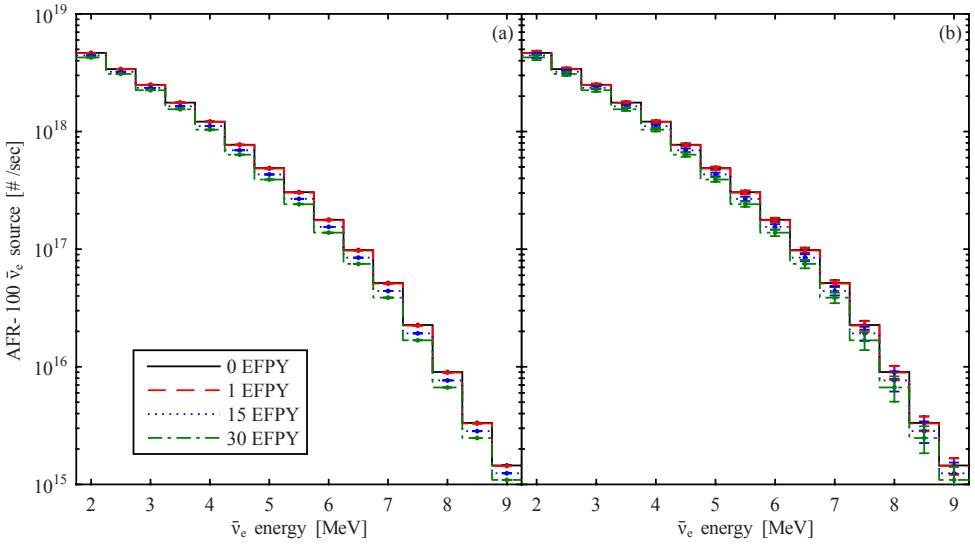

Figure 24: The reactor antineutrino source emitted by the AFR-100 at nominal power shown with (a) relative errors due to fission rate uncertainties, and (b) relative errors due to antineutrino yield uncertainties.

be made obvious as the second phenomenon drowned out the antineutrino signal.

5.2 UCFR-1000 reference fuel cycle

The UCFR-1000, in contrast with the AFR-100, undergoes a complete conversion to burning ^{239}Pu early in the cycle and relies on further ^{239}Pu production in the fertile column to continue its cycle. The in-place conversion and beginning of burn zone motion gives rise to somewhat exotic reactivity evolution with burnup in the first quarter of its fuel cycle, after which it continues in a nearly steady state. The plutonium inventory of the UCFR is more heterogeneous than in the AFR due to its simpler enrichment scheme, and because there is residual plutonium left behind as the burn zone progresses and the taller fuel elements, each assembly eventually accumulates far more plutonium. In addition, because there are 378 fuel assemblies in the UCFR compared to 150 in the AFR, there are more diversion options which are, in general, less disruptive to core operation.

Due to burnup code difficulties, only the first half of the fuel cycle could be

Table 15: Event rates in each detector of the RETINA suite due to the reactor antineutrino source emitted by the AFR-100 at various burnups and due to cosmogenic background estimated using the PROSPECT data. All count rates are in units of 10^{-3} $^{\text{counts}}/_{\text{sec}}$.

Bin	0 EFPY	5 EFPY	10 EFPY	20 EFPY	30 EFPY	Background
1	0.497	0.489	0.481	0.466	0.455	0.899
2	1.346	1.321	1.297	1.256	1.224	0.994
3	2.090	2.047	2.006	1.935	1.879	0.918
4	2.497	2.433	2.374	2.272	2.192	1.158
5	2.594	2.515	2.442	2.315	2.217	0.429
6	2.314	2.228	2.148	2.010	1.903	0.576
7	1.952	1.870	1.794	1.662	1.560	0.442
8	1.566	1.497	1.433	1.322	1.237	0.944
9	1.139	1.086	1.036	0.951	0.885	0.829
10	0.769	0.731	0.695	0.634	0.586	0.129
11	0.484	0.458	0.435	0.394	0.363	0.451
12	0.251	0.237	0.225	0.203	0.186	0.387
13	0.116	0.110	0.104	0.094	0.086	0.331
14	0.050	0.047	0.045	0.040	0.037	0.389
15	0.025	0.023	0.022	0.020	0.019	0.244

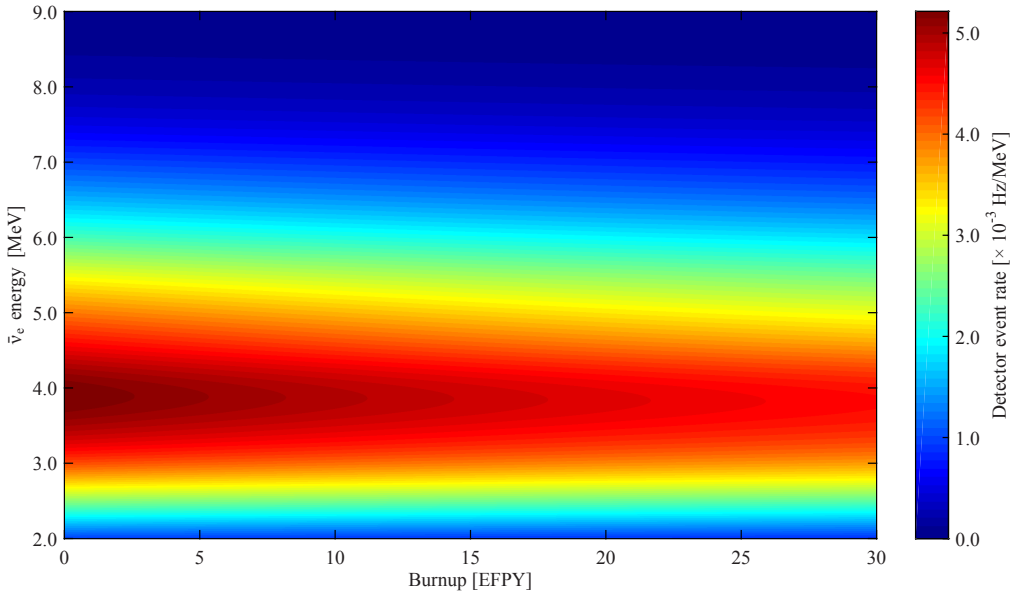

Figure 25: The expected detector signal diminishes in intensity and slightly shifts its peak to lower energy as burnup progresses in the AFR-100.

modeled, but as this is well into steady-state motion of the burn zone, the data from 15+ EFPY allows for study of diversions which should give insight into mid- to late-cycle diversion scenarios.

5.2.1 Reactivity

The large fertile column in the UCFR-1000 results in an almost perfectly flat reactivity burnup curve once the exotic S-curve behavior from initial conversion has finished. The UCFR then operates barely above critical—with only about 200 pcm excess reactivity according to the REBUS model. Figure 26 shows the first half of the UCFR reactivity evolution.

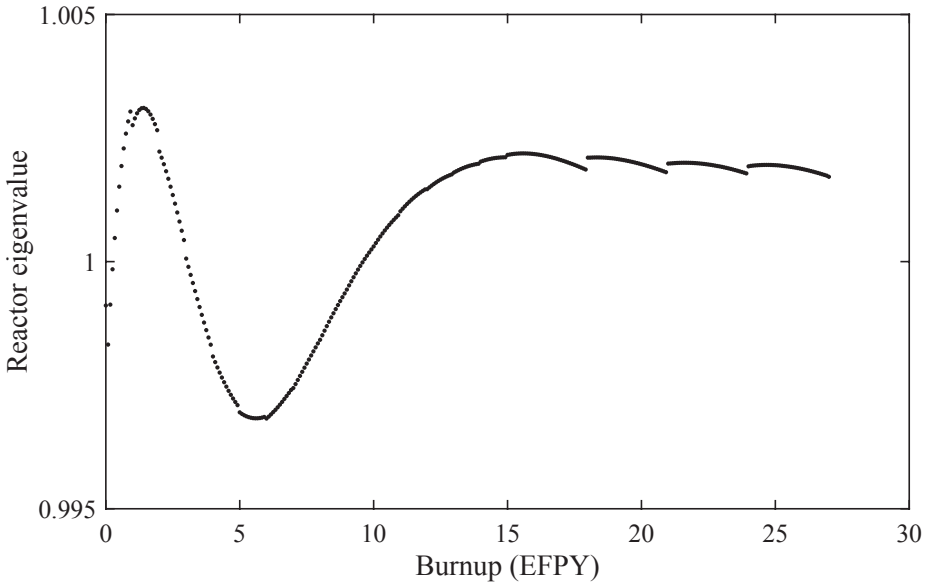

Figure 26: UCFR-1000 reactivity evolution in the all rods out condition. Discontinuities are present where microscopic fuel cross sections are updated; they appear large due to the small cycle $^{\delta k}/_{k}$, but are $O\,(10)$ pcm or less.

The temporary subcritical operation between 3 EFPY and 9.75 EFPY is a result of using ENDF/B-VII libraries and the MCC/REBUS codes with cross section updates. In the design paper, the reactor was modeled in MCNP and was able to maintain criticality, although it came very close[51] to the criticality condition with all control rods withdrawn. The S-curve reactivity evolution has the same shape as in the design

paper[51] and matches closely with preliminary data generated with the ERANOS 2.0 code package[41] and JEFF-2 cross section libraries (Figure 27), despite the greater duration between cross section recalculation for the preliminary data and the coarser spatial zoning when doing so. During construction of the REBUS model, access to ERANOS 2.1 and the JEFF-3.1 cross section libraries was briefly available, and they showed good agreement with the preliminary data. The offset in reactivity between ERANOS/JEFF and REBUS/ENDF is $\sim$ 400-600 pcm, which is consistent with benchmark comparisons performed in these codes with ENDF/B-VII.0 and JEFF-3.1[49]. The reactor fuel inventory was in very good agreement despite the offset in reactor eigenvalue[49].

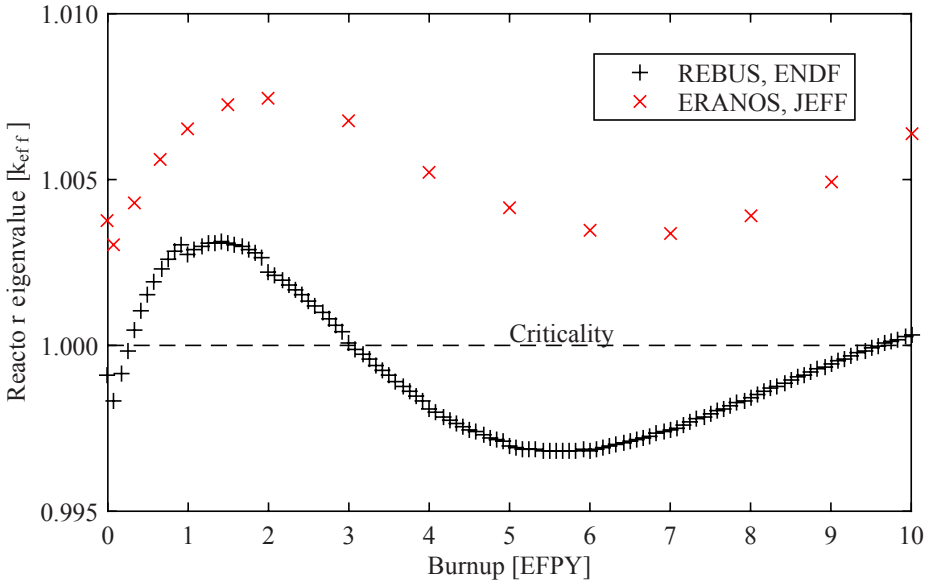

Figure 27: UCFR-1000 S-curve reactivity evolution as modeled in REBUS and ERANOS. The ERANOS data was used for preliminary indication of the efficacy of safeguards scenarios but the code was found to be too unwieldy to update cross sections while maintaining a very fine spatial mesh.

If the preliminary data more closely predicts the excess reactivity of a production UCFR-1000, the steady-state excess is still approximately half of the peak AFR-100 excess, indicating a very slim margin to subcriticality. Because the flat enrichment scheme creates an approximate chopped-Bessel radial flux shape, diversions of central

assemblies will likely require LEU-based replacement assemblies, while peripheral assemblies likely do not.

5.2.2 Fission rates

The UCFR-1000 quickly depletes its initial charge of ^{235}U and by about 2.75 EFPY into the burnup cycle is already burning more transuranic isotopes, primarily ^{239}Pu, than ^{235}U. After the transition, the fission rates of each isotope stabilize as the burn zone propagates upward at a steady rate and expose the neutron flux distribution to fresh fuel, leaving the higher actinides in the depleted fuel behind. Bumpiness in the relative errors around 6 EFPY is due to changes in microscopic cross sections during their periodic update at the beginning of substantial burn zone distribution above the first macro-zone demarcation.

The covariance matrices of the fission rates for the primary power-producing isotopes in the UCFR-1000 experience greater transformation than those for the AFR-100, again as a result of the complete depletion of ^{235}U. The matrices for burnups through the transition, as well as at 15 and 25 EFPY, are given in Table 16. By 10 EFPY, the majority of the off-diagonal elements are of the same order of magnitude, indicating significant interplay in the errors of several isotopes instead of just ^{239}Pu and ^{235}U.

5.2.3 Plutonium inventory

The UCFR-1000 relies on continuous production of new plutonium in order to maintain criticality, and because it does not fully deplete bred-in plutonium as the burn zone moves upward, the total plutonium inventory of the core steadily grows until final shutdown (Figure 29). While this is clearly a liability from a nonproliferation perspective, the plutonium vector of each assembly also becomes steadily less pure as ^{240}Pu accumulates from neutron capture on ^{239}Pu, complicating its use.

Table 16: Covariance matrices for the fission rates of the main power-producing isotopes in the UCFR-1000 for various burnups spanning the inventory transition and first half of steady-state operation.

0 EFPY	^{235}U	^{238}U	^{239}Pu	^{240}Pu	^{241}Pu
^{235}U	1.45×10^{34}	-1.35×10^{34}	-2.69×10^{26}	-8.77×10^{24}	-5.62×10^{26}
^{238}U	-1.35×10^{34}	1.28×10^{34}	1.06×10^{26}	-1.95×10^{25}	3.73×10^{26}
^{239}Pu	-2.69×10^{26}	1.06×10^{26}	1.73×10^{20}	8.70×10^{18}	1.13×10^{20}
^{240}Pu	-8.77×10^{24}	-1.95×10^{25}	8.70×10^{18}	9.35×10^{18}	1.51×10^{19}
^{241}Pu	-5.62×10^{26}	3.73×10^{26}	1.13×10^{20}	1.51×10^{19}	6.72×10^{20}
2 EFPY	^{235}U	^{238}U	^{239}Pu	^{240}Pu	^{241}Pu
^{235}U	3.99×10^{34}	-4.60×10^{33}	-3.04×10^{34}	-4.71×10^{32}	-1.48×10^{32}
^{238}U	-4.60×10^{33}	1.08×10^{34}	-5.32×10^{33}	-1.63×10^{32}	-3.60×10^{31}
^{239}Pu	-3.04×10^{34}	-5.32×10^{33}	3.34×10^{34}	5.55×10^{32}	1.57×10^{32}
^{240}Pu	-4.71×10^{32}	-1.63×10^{32}	5.55×10^{32}	2.59×10^{31}	5.81×10^{30}
^{241}Pu	-1.48×10^{32}	-3.60×10^{31}	1.57×10^{32}	5.81×10^{30}	2.77×10^{30}
5 EFPY	^{235}U	^{238}U	^{239}Pu	^{240}Pu	^{241}Pu
^{235}U	6.84×10^{33}	7.80×10^{32}	-5.30×10^{33}	-2.44×10^{32}	-1.60×10^{32}
^{238}U	7.80×10^{32}	1.06×10^{34}	-9.46×10^{33}	-6.13×10^{32}	-2.60×10^{32}
^{239}Pu	-5.30×10^{33}	-9.46×10^{33}	1.49×10^{34}	4.10×10^{32}	1.36×10^{32}
^{240}Pu	-2.44×10^{32}	-6.13×10^{32}	4.10×10^{32}	2.51×10^{32}	8.58×10^{31}
^{241}Pu	-1.60×10^{32}	-2.60×10^{32}	1.36×10^{32}	8.58×10^{31}	9.46×10^{31}
10 EFPY	^{235}U	^{238}U	^{239}Pu	^{240}Pu	^{241}Pu
^{235}U	1.64×10^{33}	-2.77×10^{32}	-1.55×10^{32}	-2.64×10^{32}	-2.88×10^{32}
^{238}U	-2.77×10^{32}	1.03×10^{34}	-7.76×10^{33}	-8.09×10^{32}	-3.65×10^{32}
^{239}Pu	-1.55×10^{32}	-7.76×10^{33}	1.05×10^{34}	-2.43×10^{32}	-4.12×10^{32}
^{240}Pu	-2.64×10^{32}	-8.09×10^{32}	-2.43×10^{32}	7.91×10^{32}	3.18×10^{32}
^{241}Pu	-2.88×10^{32}	-3.65×10^{32}	-4.12×10^{32}	3.18×10^{32}	4.90×10^{32}
15 EFPY	^{235}U	^{238}U	^{239}Pu	^{240}Pu	^{241}Pu
^{235}U	3.19×10^{32}	1.16×10^{31}	3.42×10^{32}	-2.01×10^{32}	-1.64×10^{32}
^{238}U	1.16×10^{31}	1.02×10^{34}	-7.61×10^{33}	-9.83×10^{32}	-5.13×10^{32}
^{239}Pu	3.42×10^{32}	-7.61×10^{33}	1.13×10^{34}	-6.48×10^{32}	-9.03×10^{32}
^{240}Pu	-2.01×10^{32}	-9.83×10^{32}	-6.48×10^{32}	1.12×10^{33}	4.49×10^{32}
^{241}Pu	-1.64×10^{32}	-5.13×10^{32}	-9.03×10^{32}	4.49×10^{32}	7.64×10^{32}
25 EFPY	^{235}U	^{238}U	^{239}Pu	^{240}Pu	^{241}Pu
^{235}U	3.48×10^{31}	5.58×10^{31}	1.53×10^{32}	-7.23×10^{31}	-3.87×10^{31}
^{238}U	5.58×10^{31}	1.02×10^{34}	-7.40×10^{33}	-1.10×10^{33}	-5.88×10^{32}
^{239}Pu	1.53×10^{32}	-7.40×10^{33}	1.24×10^{34}	-1.04×10^{33}	-1.28×10^{33}
^{240}Pu	-7.23×10^{31}	-1.10×10^{33}	-1.04×10^{33}	1.38×10^{33}	5.16×10^{32}
^{241}Pu	-3.87×10^{31}	-5.88×10^{32}	-1.28×10^{33}	5.16×10^{32}	9.25×10^{32}

The purest plutonium exists directly above the burn zone, and despite each assembly containing multiple SQ of plutonium by mid-cycle, the recoverable weapons-grade mass remains fairly constant after steady-state burn zone propagation has begun. To obtain several SQ of fissile material, a proliferator must choose between diverting multiple assemblies or constructing a weapon with fuel-grade plutonium—a considerably more precise task that results in a bomb with reduced yield. The average ^{240}Pu of the core is shown as a function of burnup in Figure 30. Assemblies in the core center will tend to have more, dirtier plutonium than average; the converse is true for assemblies on the core periphery.

5.2.4 Convergence of the Monte Carlo fuel cycle histories (UCFR)

The UCFR-1000 burnup cycle is much more computationally expensive to model than the AFR-100 due to its significantly larger size, longer burnup cycle, and the necessity for regular updates to the microscopic cross sections (each update requires several CPU-hours apiece and cannot be parallelized with the burnup calculation). Subsequently, only 95 Monte Carlo histories have been compiled, sufficient to reduce the statistical variation in the calculated uncertainties to $\sim 10\%$. The convergence behavior was checked at several points in the burnup cycle corresponding to the reported covariance matrices (Table 16). The convergence of the variances of the primary power-producing isotopes is shown in Figures 31-35. The variances appear to be converging as expected, and because the contribution of the antineutrino yields to the reactor antineutrino source uncertainty tends to dominate that of the fission rate uncertainties[50], any statistical fluctuations resulting from only using 95 histories instead of 1000 or more should be very small by comparison ($< 1\%$).

Table 17: Event rates in each detector of the RETINA suite due to the reactor antineutrino source emitted by the UCFR-1000 at various burnups and due to cosmogenic background estimated using the PROSPECT data. All count rates are in units of 10^{-3} $^{\text{counts}}/_{\text{sec}}$.

Bin	0 EFPY	2 EFPY	5 EFPY	10 EFPY	25 EFPY	Background
1	2.43	2.29	2.18	2.12	2.09	0.899
2	6.58	6.17	5.85	5.68	5.61	0.994
3	10.23	9.52	8.97	8.67	8.55	0.918
4	12.22	11.19	10.41	9.97	9.78	1.158
5	12.71	11.44	10.46	9.91	9.69	0.429
6	11.34	9.97	8.89	8.30	8.05	0.576
7	9.58	8.26	7.24	6.66	6.43	0.442
8	7.69	6.58	5.72	5.24	5.04	0.944
9	5.60	4.74	4.08	3.71	3.55	0.829
10	3.78	3.17	2.69	2.42	2.31	0.129
11	2.38	1.98	1.66	1.48	1.41	0.451
12	1.24	1.02	0.85	0.75	0.71	0.387
13	0.58	0.47	0.39	0.35	0.33	0.331
14	0.25	0.20	0.17	0.15	0.14	0.389
15	0.12	0.10	0.09	0.08	0.07	0.244

5.2.5 Antineutrino signal evolution

The UCFR-1000 reactor antineutrino source rapidly diminishes in the first ~ 5 years of full-power operation as the fission isotopic evolution proceeds and burn zone propagation begins. The majority of the shift to steady state behavior of the antineutrinos emanating from an operating UCFR-1000 has occurred by this point; the antineutrino source shown for 25 EFPY is almost exactly the same as the full-power source from 10 EFPY through final shutdown (60 EFPY).

The nominal signal in each detector of the RETINA suite due to the UCFR-1000 reactor antineutrino soruce is shown in Figure 25 and given at various burnups in Table 17. The reduction in peak count rates as well as the differential behavior of the high- and low-energy spectrum behavior is more striking than in the signal from the AFR-100. Disruption of the steady-state signal strength and spectrum shape after

the first $\sim$ 10 EFPY are clues that might indicate the removal of plutonium from the core.

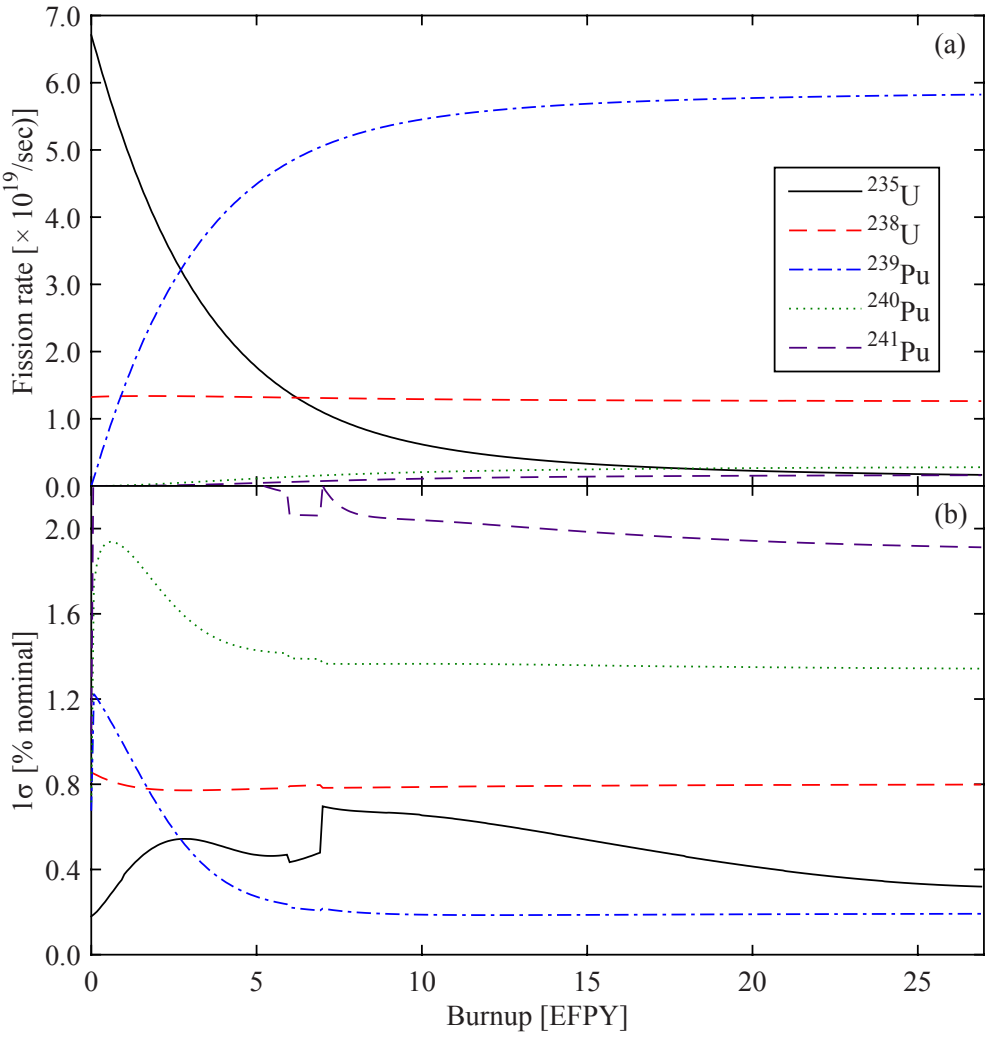

Figure 28: Evolution of the fission rates of the main power-producing isotopes in the UCFR-1000 during the first half of its burnup cycle (a) and their relative 1σ errors. Note the much lower rate of ^{235}U fissions compared to the AFR-100 once the initial fissile charge has been depleted.

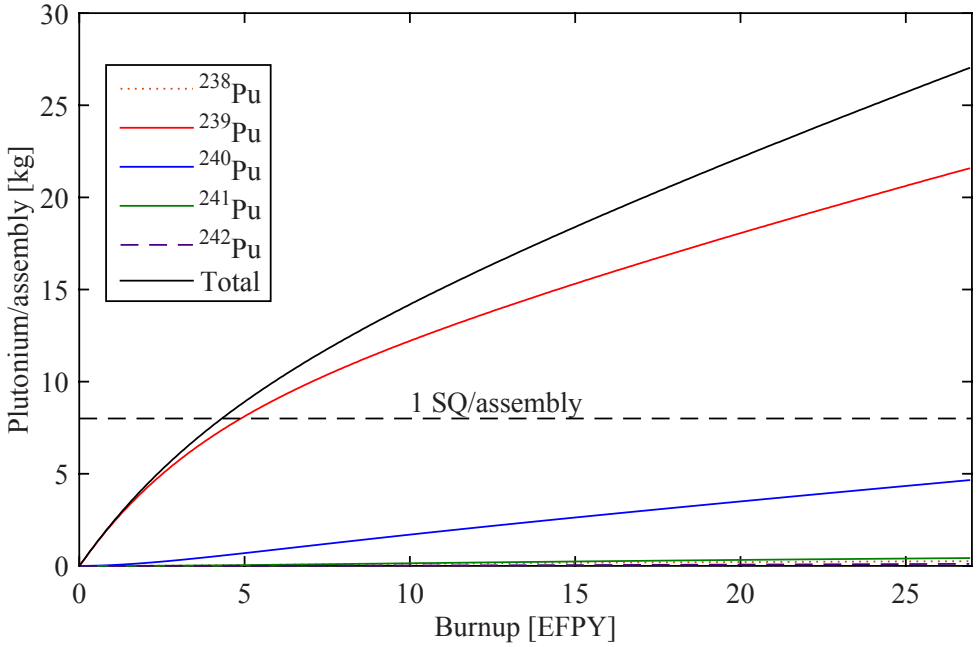

Figure 29: Core-averaged plutonium mass (kg) per assembly as a function of burnup. The average plutonium mass per assembly steadily grows throughout the burnup cycle due to burn zone motion but has substantially higher ^{240}Pu content than in the AFR-100.

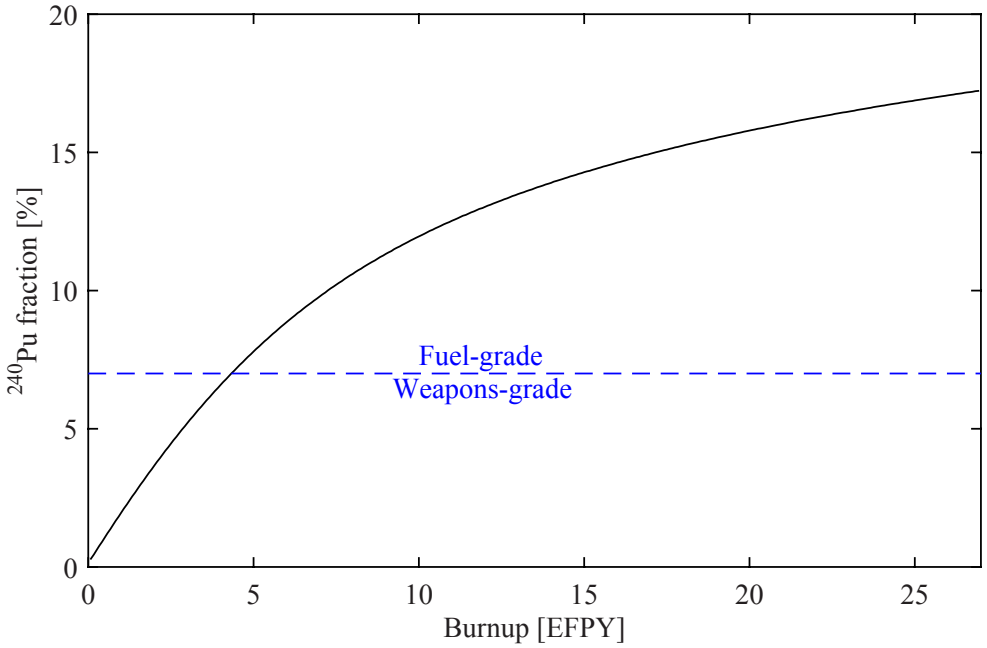

Figure 30: Core-averaged ^{240}Pu fraction of the UCFR-1000 as a function of burnup.

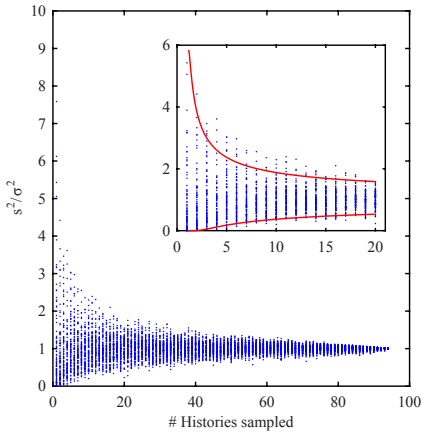

(a) BoC

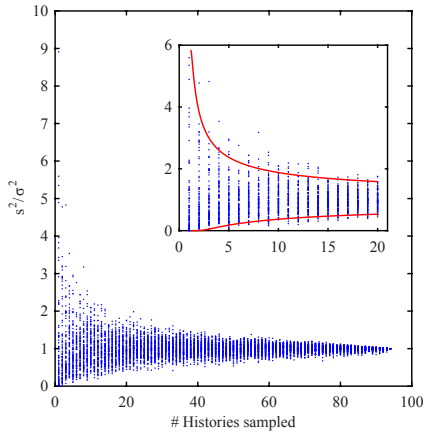

(b) 2 EFPY

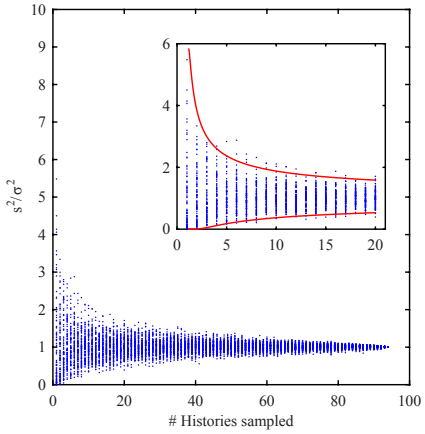

(c) 5 EFPY

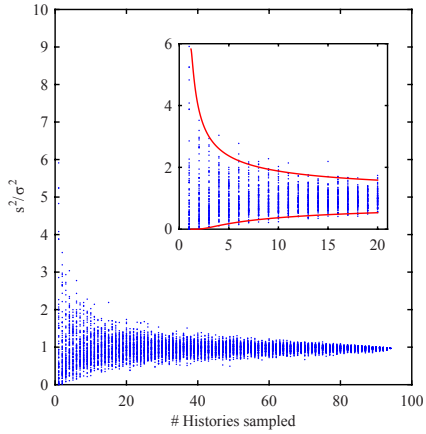

(d) 10 EFPY

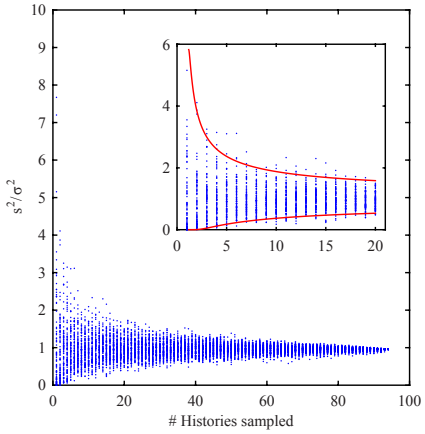

(e) 15 EFPY

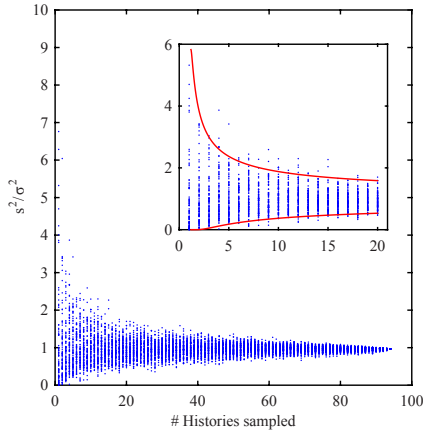

(f) 25 EFPY

Figure 31: Convergence behavior of the sample variances for the fission rates of ^{235}U in the UCFR-1000. The calculated variance converges as more histories are sampled. The red curves on the enlarged axes display the 90% confidence interval for the sample variance.

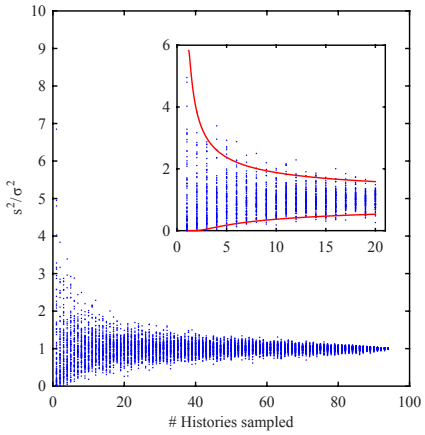

(a) BoC

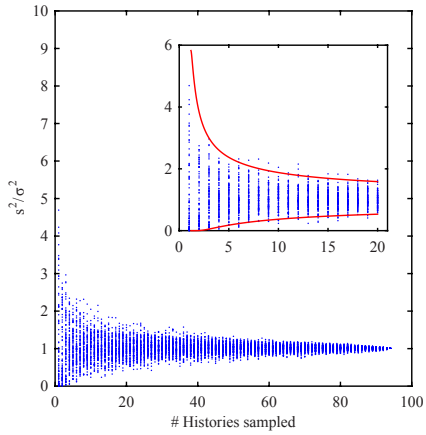

(b) 2 EFPY

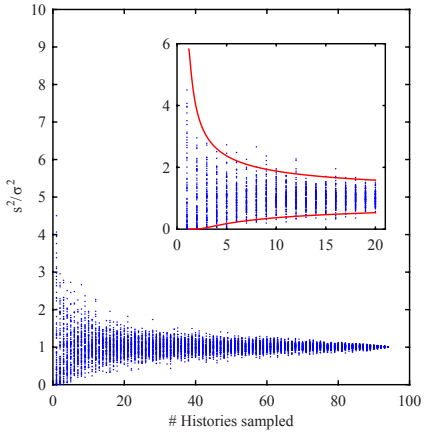

(c) 5 EFPY

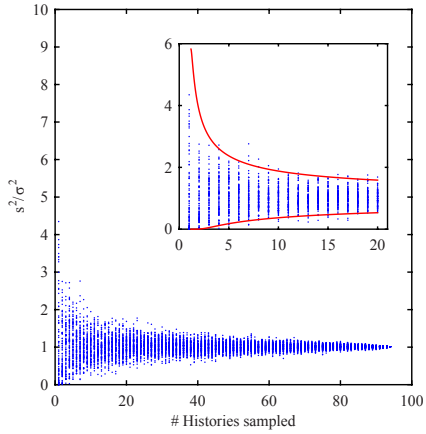

(d) 10 EFPY

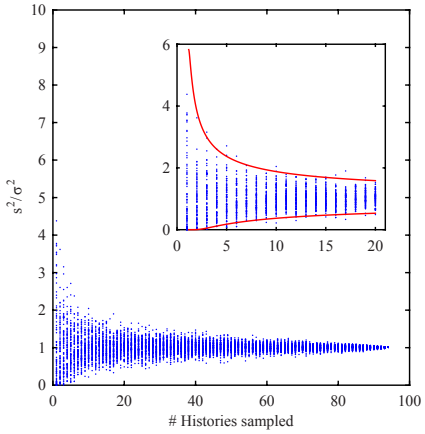

(e) 15 EFPY

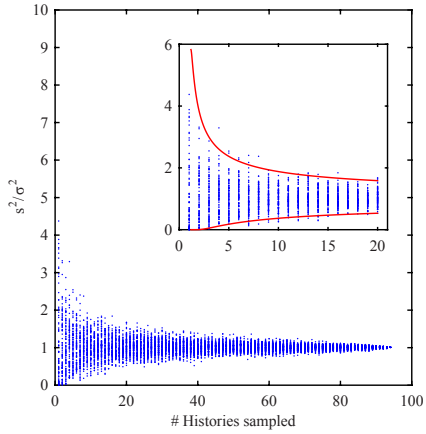

(f) 25 EFPY

Figure 32: Convergence behavior of the sample variances for the fission rates of ^{238}U in the UCFR-1000. The calculated variance converges as more histories are sampled. The red curves on the enlarged axes display the 90% confidence interval for the sample variance.

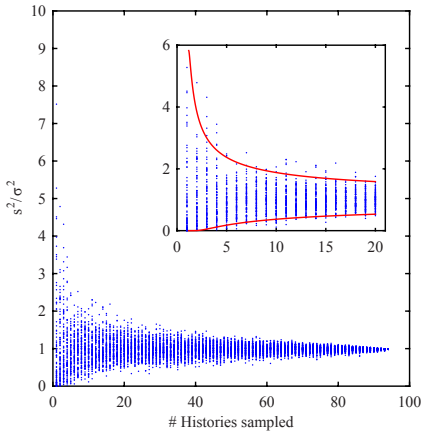

(a) BoC

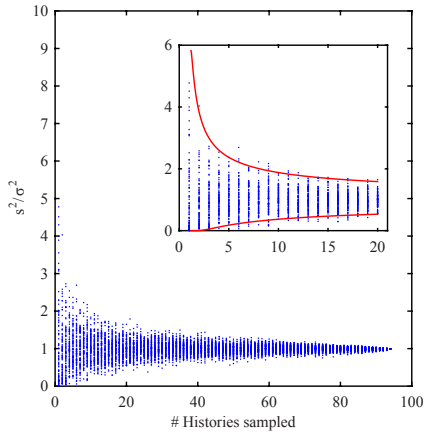

(b) 2 EFPY

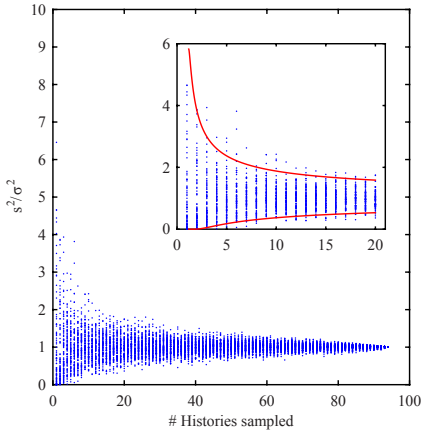

(c) 5 EFPY

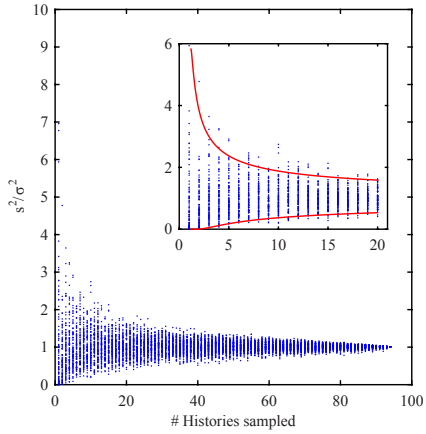

(d) 10 EFPY

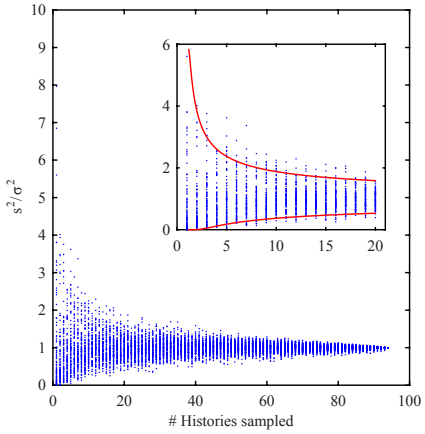

(e) 15 EFPY

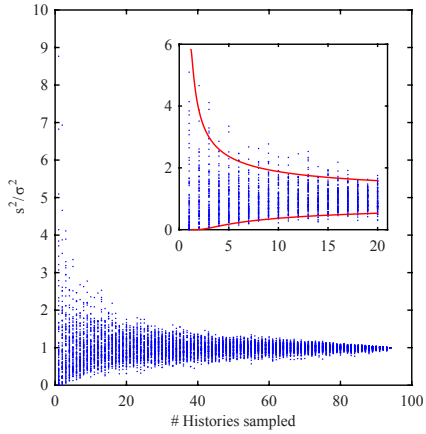

(f) 25 EFPY

Figure 33: Convergence behavior of the sample variances for the fission rates of ^{239}Pu in the UCFR-1000. The calculated variance converges as more histories are sampled. The red curves on the enlarged axes display the 90% confidence interval for the sample variance.

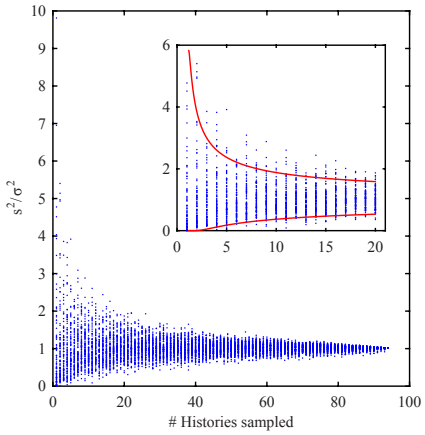

(a) BoC

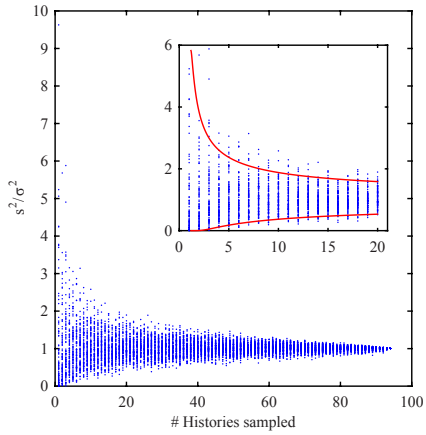

(b) 2 EFPY

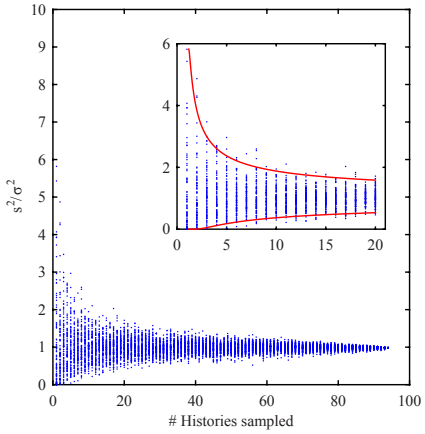

(c) 5 EFPY

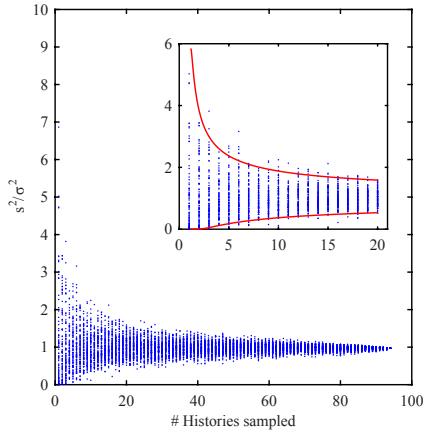

(d) 10 EFPY

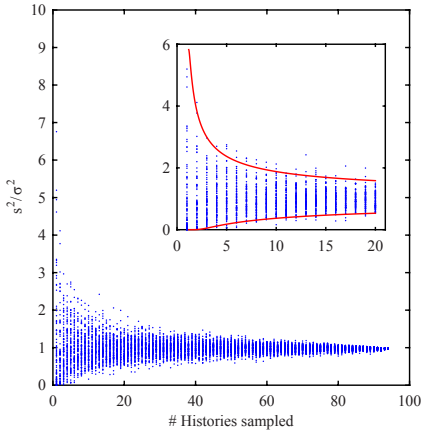

(e) 15 EFPY

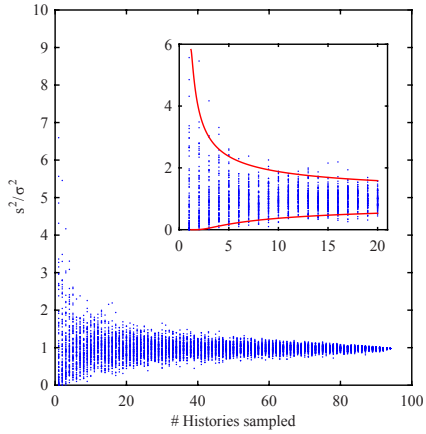

(f) 25 EFPY

Figure 34: Convergence behavior of the sample variances for the fission rates of ^{240}Pu in the UCFR-1000. The calculated variance converges as more histories are sampled. The red curves on the enlarged axes display the 90% confidence interval for the sample variance.

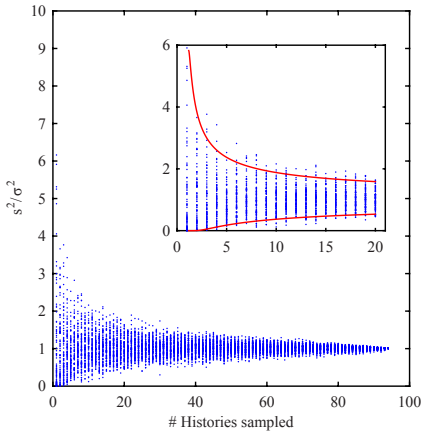

(a) BoC

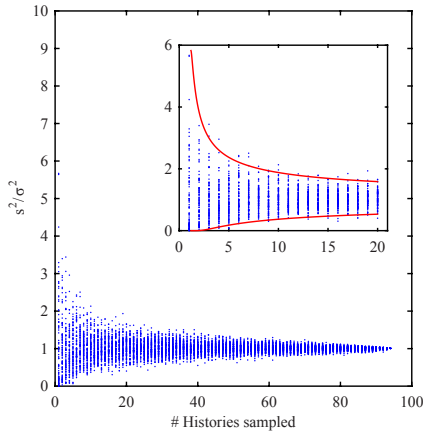

(b) 2 EFPY

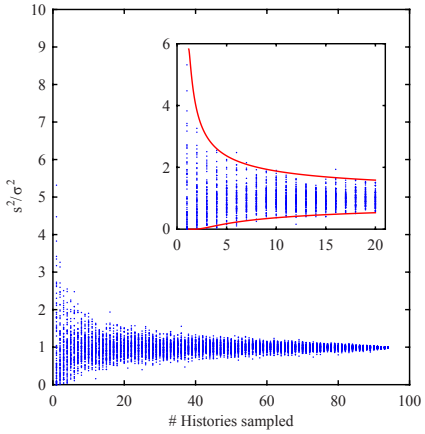

(c) 5 EFPY

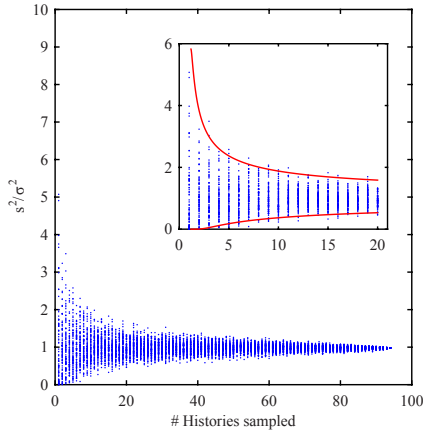

(d) 10 EFPY

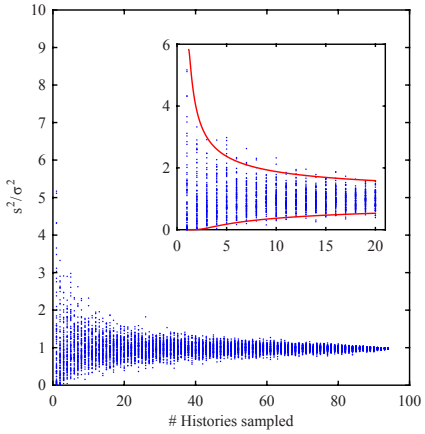

(e) 15 EFPY

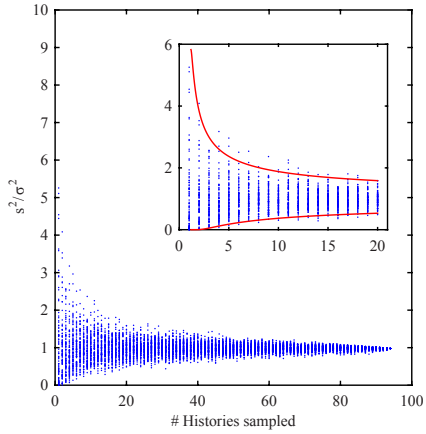

(f) 25 EFPY

Figure 35: Convergence behavior of the sample variances for the fission rates of ^{241}Pu in the UCFR-1000. The calculated variance converges as more histories are sampled. The red curves on the enlarged axes display the 90% confidence interval for the sample variance.

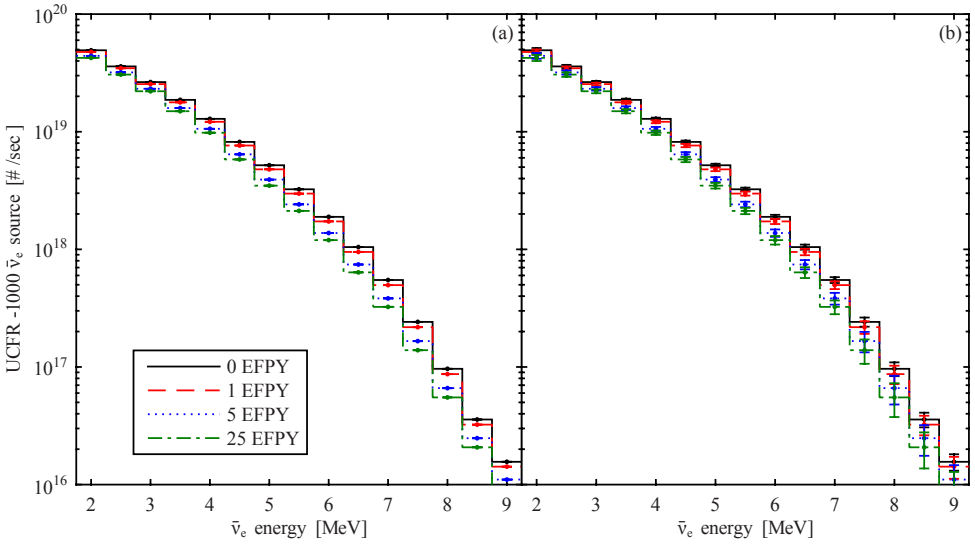

Figure 36: The reactor antineutrino source emitted by the UCFR-1000 at nominal power shown with (a) relative errors due to fission rate uncertainties, and (b) relative errors due to antineutrino yield uncertainties.

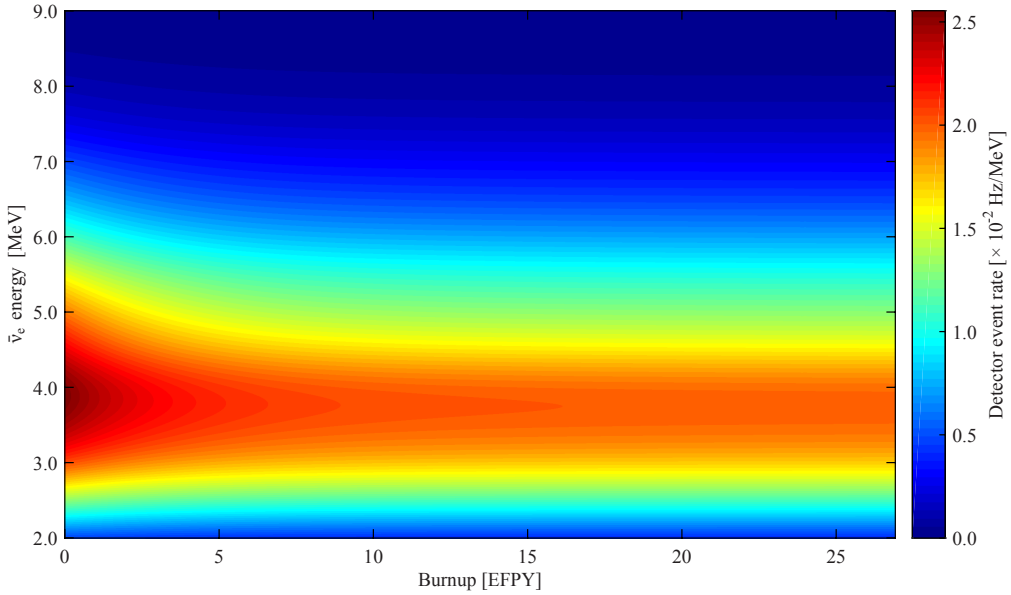

Figure 37: The expected detector signal quickly diminishes in the first few years of full-power operation, after which the signal is approximately constant as a function of burnup.

CHAPTER VI

DIVERSION SCENARIO RESULTS AND DISCUSSION

The results of the safeguards test sensitivity to the modeled diversion scenarios indicate that current-generation near-field antineutrino detectors are not quite up to the task of protecting against some of the most difficult-to-detect diversions of nuclear material from a long-life fast reactor. However, the safeguards performance in some of the core-center diversion scenarios approached the required sensitivity (20%) for low-probability events, as defined by the IAEA[23], particularly if the reactor operator(s) were ignorant of the value of masking the diversion via thermal output manipulation or unable to execute masking with the necessary precision.

The safeguards performance of the antineutrino detector suite tended to perform better for UCFR monitoring than for AFR monitoring. This is due to a combination of the higher signal to background ratio provided by the tenfold higher reactor power and the more sudden and complete transition of the fissile core inventory from initial loading to isotopes bred *in situ*. Core-center diversions tended to be more visible per SQ removed than those from the core periphery.

Unless otherwise indicated, all sensitivity calculations are carried out for 3-month count integrations of three 42%-efficient detectors with 5-ton fiducial masses observing reactors operating at a power which minimizes the difference in detector signal from a standoff of 17 m (AFR) or 25 m (UCFR) with background from cosmogenic neutrons of the same scale as at HFIR and an allowed false positive rate of 5%. No reduction in the uncertainty of antineutrino yields has been assumed, although some amount of reduction is likely available for installations of cores which are not first-of-a-kind.

Table 18: Safeguards test sensitivity for the UCFR-1000 diversion scenarios with 1-, 2-, and 3-month count integration periods. The last column is the 3-month count period, but with no attempt made to mask the diversion via power manipulation.

ID	1 month	2 months	3 months	No masking
1a	1.149×10^{-10}	4.276×10^{-6}	1.541×10^{-4}	0.255
1b	2.943×10^{-5}	3.257×10^{-3}	1.676×10^{-2}	0.523
2a	0	0	0	0
2b	0	0	0	0
3a	0	0	0	2.154×10^{-4}
3b	0	0	0	7.685×10^{-4}

6.1 UCFR diversion scenarios

The UCFR diversions which took place in the core center (1a and 1b) were more visible to antineutrino detectors by a very large margin than those from the core periphery. The primary reason for this dichotomy is that the 0^{th}-order Bessel shape of the radial flux distribution arising from the flat enrichment scheme of the initial core loading. This flux shape is responsible for the much earlier availability of 1 SQ of plutonium in the core center as well, so it is a double-edged sword in terms of maintaining a long breakout period for the user nation of a UCFR-like reactor: SQ-level plutonium is available only a couple of years after reactor startup, but visibility of any missing plutonium is significantly higher. The safeguards test sensitivities for integration times spanning up to the weapon conversion time for plutonium obtained from irradiated fuel are compiled in Table 18, and the fractional power change required to minimize the goodness-of-fit function and its minimized and unminimized values are shown in Table 19. The nuisance factor is the fraction by which reactor power was temporarily increased or decreased following the diversion in order to minimize the difference in detector signal between the reference and perturbed signals.

The sensitivities for non-masked diversions were included at the 3-month mark

Table 19: Goodness-of-fit minimization parameters and χ^2 values for the UCFR-1000 diversion scenarios for count integration periods of 3 months.

ID	Power adjustment	Minimized χ^2	Un-minimized χ^2
1a	-1.031×10^{-3}	0.25	1.99
1b	-1.469×10^{-3}	0.59	4.07
2a	-7.031×10^{-5}	1.16×10^{-3}	7.19×10^{-3}
2b	7.813×10^{-5}	9.86×10^{-4}	8.52×10^{-3}
3a	-4.063×10^{-4}	4.11×10^{-2}	0.26
3b	4.531×10^{-4}	3.53×10^{-3}	0.31

to illustrate the necessity of some level of masking to the diverting actor's ability to remain covert; in the cases with core-center diversions, masking efforts are the difference between almost certainly remaining undetected and being caught with likelihood in the tens of percent. Figures 38 to 43 illustrate the minimization difference by comparing the contribution to the goodness-of-fit summation contributions of each bin from the minimized and un-minimized functions for each of the diversion scenarios. A set of minimized nominal counts which aligned perfectly with the horizontal centerline would indicate perfect spectral agreement with the reference case values, and alignment of un-minimized nominal counts would indicate both spectral and reactor thermal power agreement.

Although antineutrino safeguards were insufficient to provide assurance of the core fissile inventory within the 3-month conversion time, count integration duration was varied smoothly out to 1 EFPY in order to assess a secondary value of continuous monitoring: confidence that such a diversion has not taken place further than 3 months in the past. The improvement in safeguards test sensitivity as integration times increase (Figure 44) indicates that, even with ideal masking, core-center diversions approach 20% visibility, and for replacement with natural uranium, exceeds the threshold after about 10 months. Detection of 6-SQ diversions from the least-important assembly locations in the UCFR enters the realm of possibility with

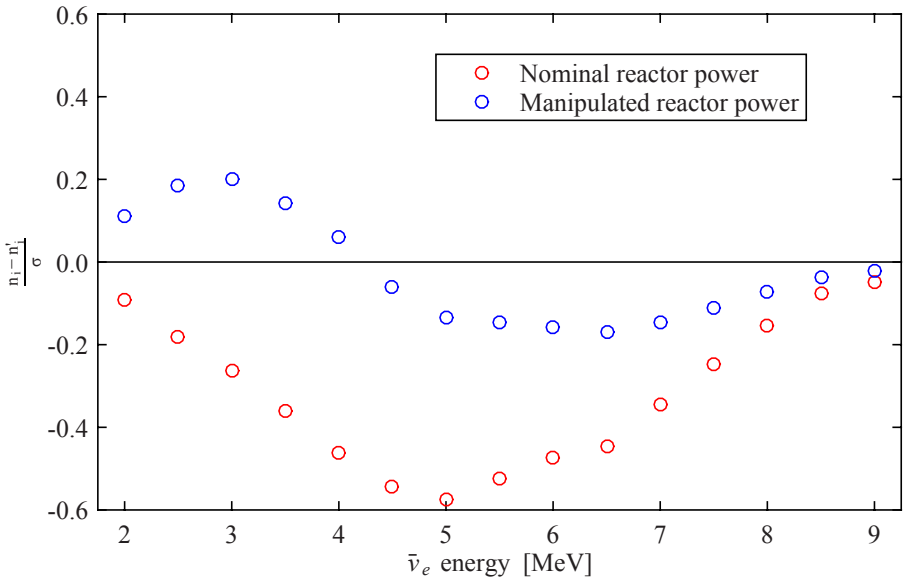

Figure 38: Effect of minimization on the contribution to the goodness-of-fit function from each bin for diversion UCFR-1a.

several months of observation, although sensitivity to the single-assembly, 1-SQ diversion cases is still numerically indistinguishable from zero.

6.2 AFR diversion scenarios

The antineutrino safeguards test sensitivities to the AFR-100 diversion scenarios were much lower than for the UCFR-1000 scenarios, largely resulting from a substantially lower signal-to-background ratio ($\sim$ 1.5 vs $\sim$ 8). None of the sensitivities for diversions of material from the core periphery were distinguishable from zero at count integration times of 3 months if properly masked. The test was substantially more sensitive to core-center diversions, just as for the UCFR-1000 diversion scenarios. However, because the AFR-100 has a flatter radial flux distribution and less concentrated power production, the breakout period is not shortened to less than 10 years for single-assembly diversions (despite their invisibility to antineutrino safeguards). The safeguards test sensitivities for integration times spanning up to 3 months post-diversion are compiled in Table 20, including the 3-month sensitivity with no masking;

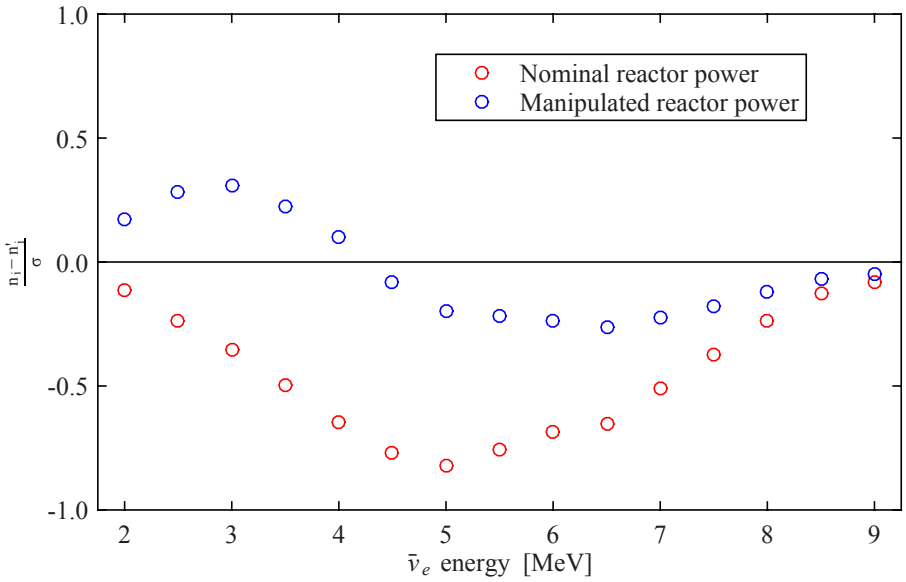

Figure 39: Effect of minimization on the contribution to the goodness-of-fit function from each bin for diversion UCFR-1b.

the parameters used in the 3-month calculations are shown in Table 21. The small difference in un-minimized signal magnitudes compared to background rates keep the diversions invisible to antineutrino safeguards even though the test sensitivity is improved by several orders of magnitude.

Increasing the count integration time (Figure 51) provides $1/\sqrt{n}$ improvement in the count statistics, but remains insufficient to resolve SQ-level diversions after 1 year without improvement of detector hardware or data processing techniques. The use of antineutrino detectors for safeguarding the inventory of small, fast-spectrum cores with low power density against 1-SQ diversions remains contingent on either substantial improvement of the technology or increases in total detector suite fiducial mass.

The overall features of the un-minimized and minimized spectral differences for the AFR-100 diversion scenarios (Figures 45 to 50) are the same as the UCFR-1000 scenarios. However, the smaller signal-to-background ratio is evident in the jagged behavior between 5-7 MeV.

Table 20: Safeguards test sensitivity for the AFR-100 diversion scenarios with 1-, 2-, and 3-month count integration periods. The last column is the 3-month count period, but with no attempt made to mask the diversion via power manipulation.

ID	1 month	2 months	3 months	No masking
1a	0	0	2.516×10^{-13}	2.213×10^{-2}
1b	0	0	6.344×10^{-12}	8.562×10^{-4}
2a	0	0	0	5.626×10^{-12}
2b	0	0	0	0
3a	0	0	0	4.687×10^{-12}
3b	0	0	0	0

Table 21: Goodness-of-fit minimization parameters and χ^2 values for the AFR-100 diversion scenarios for count integration periods of 3 months.

ID	Power adjustment	Minimized χ^2	Un-minimized χ^2
1a	-1.469×10^{-3}	6.82×10^{-2}	0.64
1b	-9.531×10^{-4}	7.72×10^{-2}	0.32
2a	-5.313×10^{-4}	8.06×10^{-3}	7.69×10^{-2}
2b	4.063×10^{-4}	3.71×10^{-3}	4.60×10^{-2}
3a	-5.000×10^{-4}	7.31×10^{-3}	7.63×10^{-2}
3b	3.750×10^{-4}	2.22×10^{-3}	3.73×10^{-2}

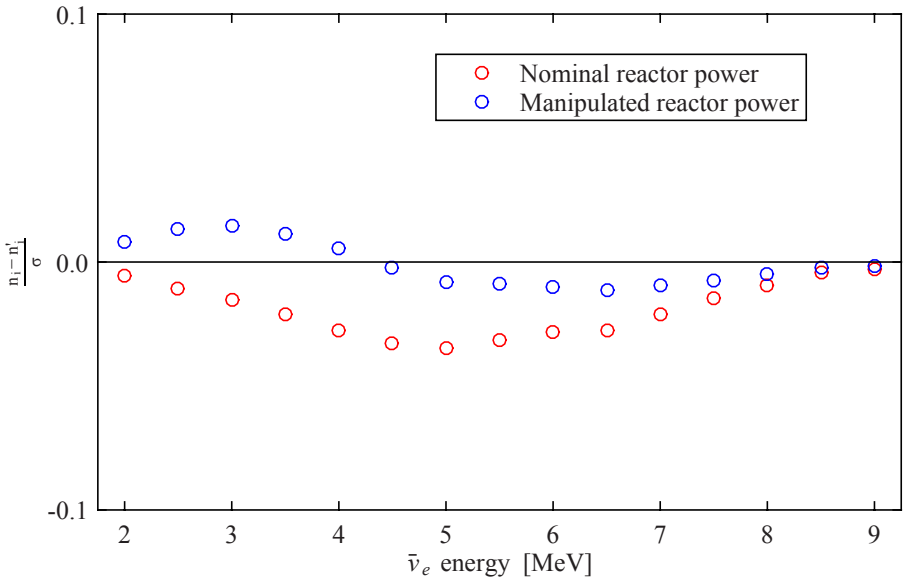

Figure 40: Effect of minimization on the contribution to the goodness-of-fit function from each bin for diversion UCFR-2a.

6.3 Variation of test parameters

Parameters which serve as inputs to the goodness-of-fit test between the reference and perturbed antineutrino signals were varied about their values for the nominal test. In some cases, the response of the test sensitivity gives insight into the direction which optimization efforts would yield the largest returns. In others, particularly the required true negative rate, the sensitivity response indicates potential value of antineutrino safeguards as red-flag indication or exclusion of diversion without access to enriched materials. Parameter variation which results in lower test sensitivity is used to assess elasticity to potential limitations of antineutrino safeguards imposed by reactor plant design and siting.

Variation of the parameters about their nominal values was performed for a single parameter at a time; although many of their effects on detector event rates can be

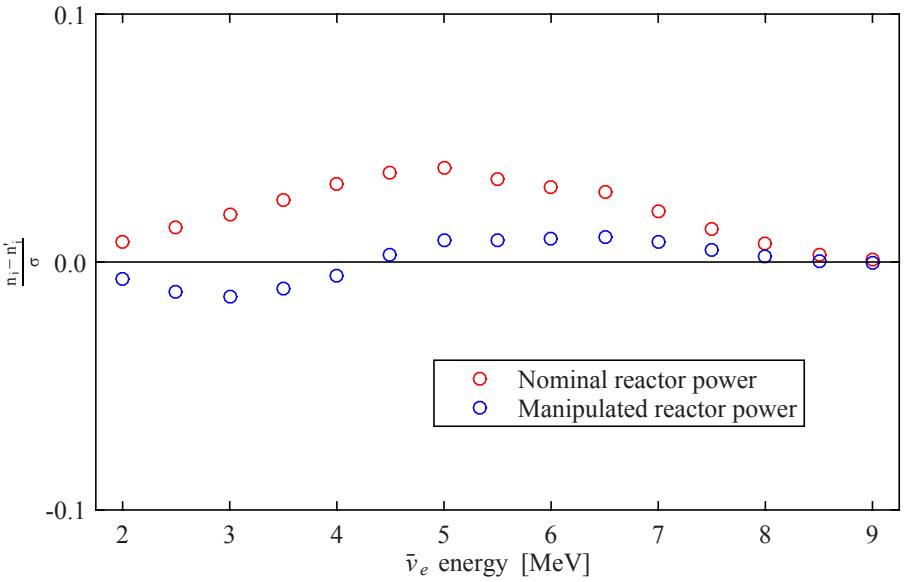

Figure 41: Effect of minimization on the contribution to the goodness-of-fit function from each bin for diversion UCFR-2b.

described without undue mathematical vigor, the resulting test sensitivity is an integrated Gaussian distribution whose mean and standard deviation change with parameter variation and with integration limits that shift depending on the requirements by the monitoring agent. Behavior therefore is highly non-linear and behaves differently across the range of variation of even a single parameter. 2- and higher-dimensional response surfaces mapped out by simultaneous variation of multiple parameters consequently provides reduced insight.

The UCFR-1000 diversion scenario results indicate that relatively modest improvements of multiple parameters would allow them to protect high-power cores from early-cycle diversions, while more significant improvements and perhaps flagging-only use are required for near-term application near low-power cores.

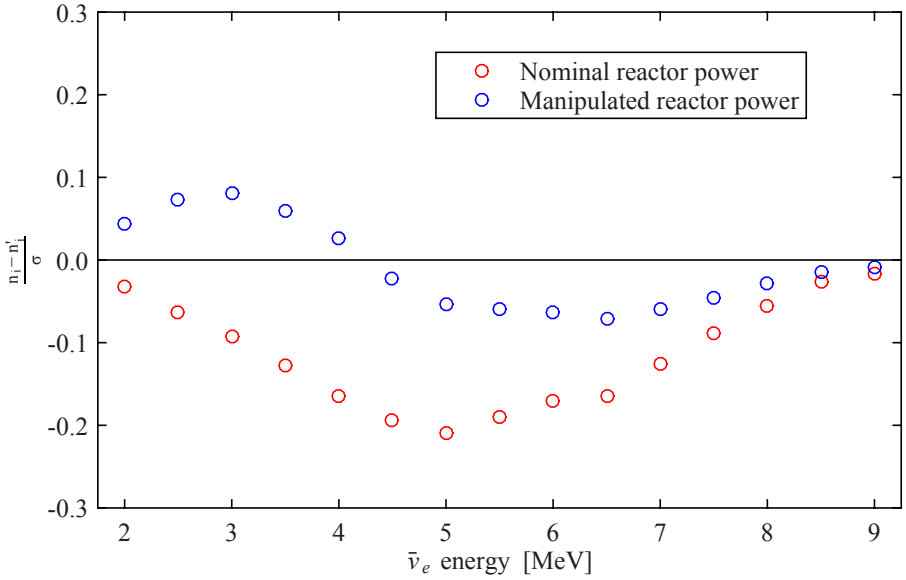

Figure 42: Effect of minimization on the contribution to the goodness-of-fit function from each bin for diversion UCFR-3a.

6.3.1 Detector background

Reduction of the background that is indistinguishable from the reactor inverse beta decay signal offers non-linear improvement in the signal-to-background ratio via $1/(1+x)$-like behavior. The effect on the ratio in the goodness-of-fit test is more pronounced because the numerator is the difference in signals rather than the magnitude of the signal itself—resembling instead $1/(a+x)$ for large a and x—and the resulting difference in signal shifts the limits on integration of a Gaussian, which is well-known to have highly non-linear effects. Safeguards test sensitivity as a function of background level relative to that present at HFIR is shown in Figure 52.

Sensitivities to both the UCFR and AFR center-core diversions improve markedly with background reduction. Because the UCFR signal magnitude is already substantially above background, detection test power is enhanced by factors of a few for diversions that are within reach of detection in the nominal tests. The returns on background reduction reach multiple orders of magnitude for AFR diversions due to their much lower raw differences in signal magnitude. While background reduction is

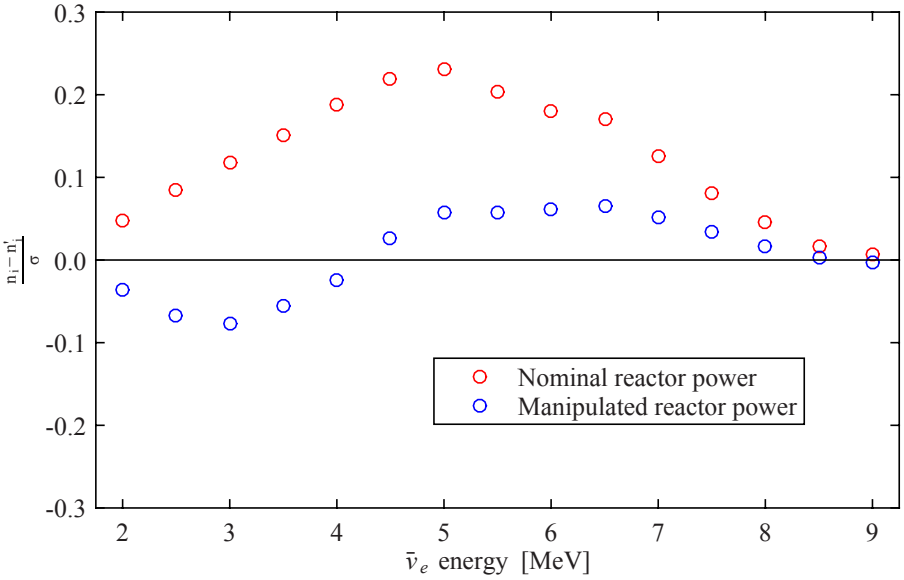

Figure 43: Effect of minimization on the contribution to the goodness-of-fit function from each bin for diversion UCFR-3b.

useful for large-core safeguards, it is an absolute necessity for small-core safeguards since it affects the ratio of differences in small signals to background so drastically.

Some reduction in background through improved rejection techniques is expected to be available within the next few years as experience with safeguards-scale segmented detectors is accumulated in the PROSPECT and SOLI∂ neutrino physics experiments. These will likely also be able to reduce the cosmogenic background through by a small factor further optimization of shielding. Low-hanging fruit in cosmogenic background reduction is built into reactors at lower altitudes than HFIR (259 m above sea level) by virtue of having more atmosphere above them, although installations at higher altitudes are correspondingly worse off. Depending on the extent of achievable improvements in rejection and installable passive reduction, antineutrino safeguards may only prove to be useful for low-lying reactor sites. If a detector can be installed without issue directly below the core, as was done in the ROVNO (citation) experiment, cosmogenic background would be substantially reduced, although the reactor-detector standoff may prove to be less than desirable.

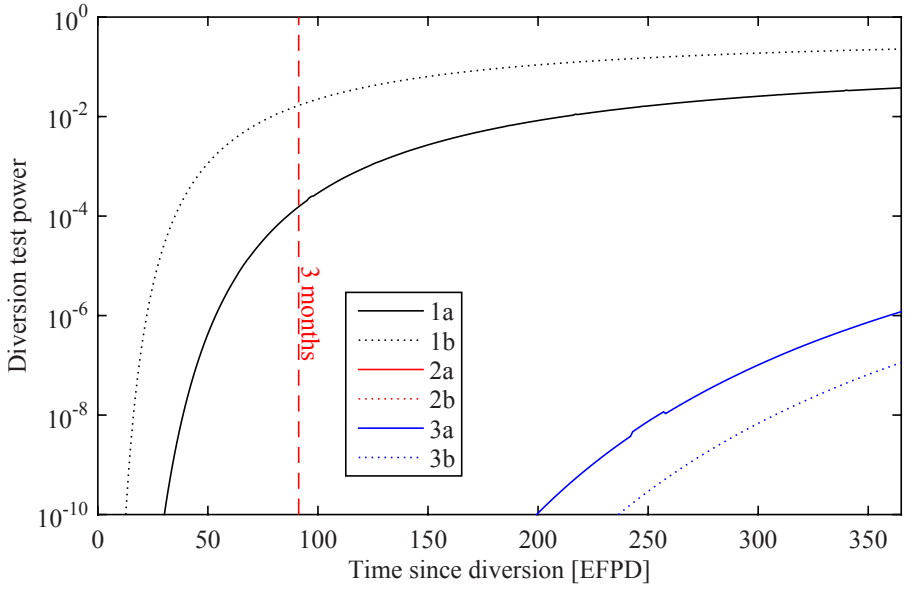

Figure 44: Improvement of safeguards test sensitivity as count integration times are lengthened for the UCFR-1000 diversion scenarios.

Since the scale of core-catcher apparatus, below-vessel instrumentation, and containment building foundation are unknown at this point, analysis on below-core detector placement was not studied.

6.3.2 Fiducial mass

Altering the total fiducial mass of the safeguards detector suite linearly scales both the signal and background event rates, with corresponding $1/\sqrt{n}$ improvement in the count statistics. In this respect, increases in detector fiducial mass improve reactor state discrimination in the same manner as lengthening count integration periods. The effect of reasonable changes to total fiducial mass on safeguards test sensitivity is shown in Figure 53.

For diversion of a center-core assembly from the UCFR, replacement with natural uranium fuel can be detected by tripling the detector suite fiducial mass, and replacement with LEU is over 2 orders of magnitude closer to visibility. Peripheral-assembly diversions, even for multiple SQ, remain essentially impossible to resolve. Sensitivity

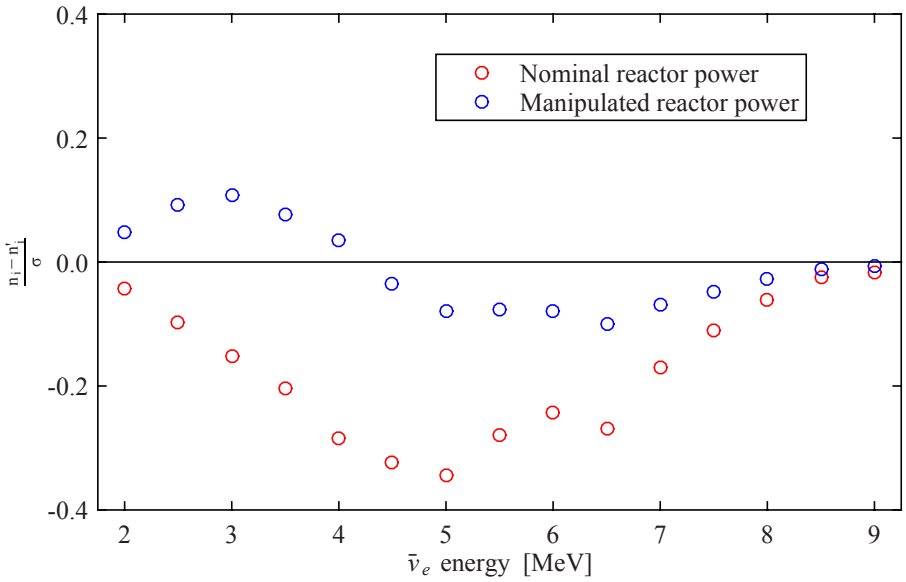

Figure 45: Effect of minimization on the contribution to the goodness-of-fit function from each bin for diversion AFR-1a.

to the AFR center-core diversions, while showing marked improvement relative to the nominal fiducial mass, are still at least 2 orders of magnitude from detectability.

It is unlikely that the amount of detector fiducial mass which could be incorporated into plant designs is less than nominal (3×5 tons), but any reductions should be offset by improvements in other signal-magnitude-related parameters to retain performance. For a given detector size, the accumulation of experience with segmented antineutrino detectors may yield improved fiducialization techniques that allow use of a larger fraction of total detector mass. While fiducial mass increase should not be relied upon to shift antineutrino safeguards into viability, if the space is available for some combination of more or larger detectors, adding mass is a financial, rather than technical, solution that could be applied whenever necessary in order to preserve or bolster safeguards performance.

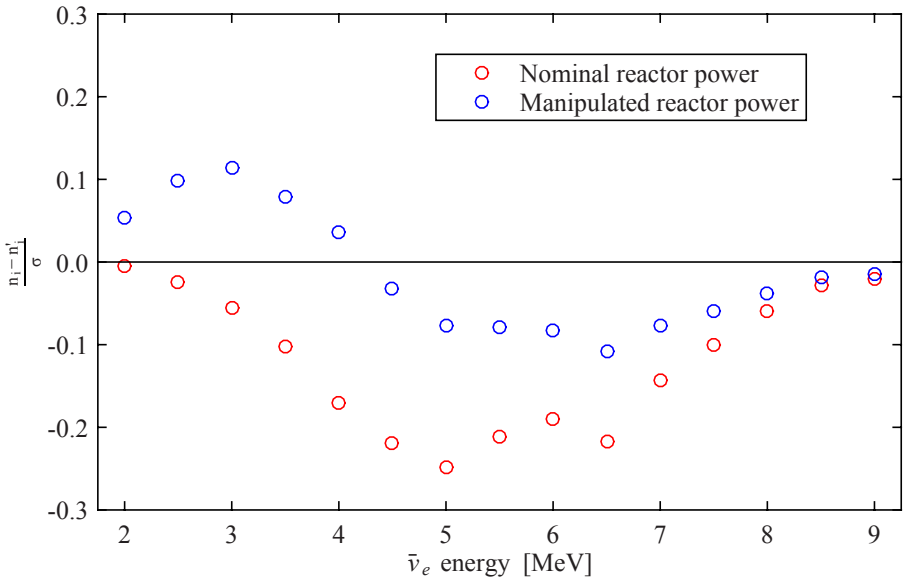

Figure 46: Effect of minimization on the contribution to the goodness-of-fit function from each bin for diversion AFR-1b.

6.3.3 Detector efficiency

The intrinsic efficiency within the fiducial mass of surface-level, safeguards-scale antineutrino detectors has improved approximately fourfold in the last 15 years [9, 12, 8, 13, 5]. This pace of efficiency increase has largely run its course, and only minor increases are expected in the future as the 100% limit is approached. The efficiency for PROSPECT is dominated by the ability to distinguish neutron capture events [5], so materials, segment sizing, and multiple-segment event summation techniques are where further gains most likely lie. Nonetheless, further improvements in detector efficiency offer correspondingly better reactor state discrimination according to $1/\sqrt{n}$ count statistics, as illustrated in Figure 54.

Efficiency improvements alone are insufficient to resolve any of the studied diversion scenarios, even at the 100% limit. They will likely provide modest improvements in detector statistics and may allow for cost optimization of the detector suite for particular reactor sites.

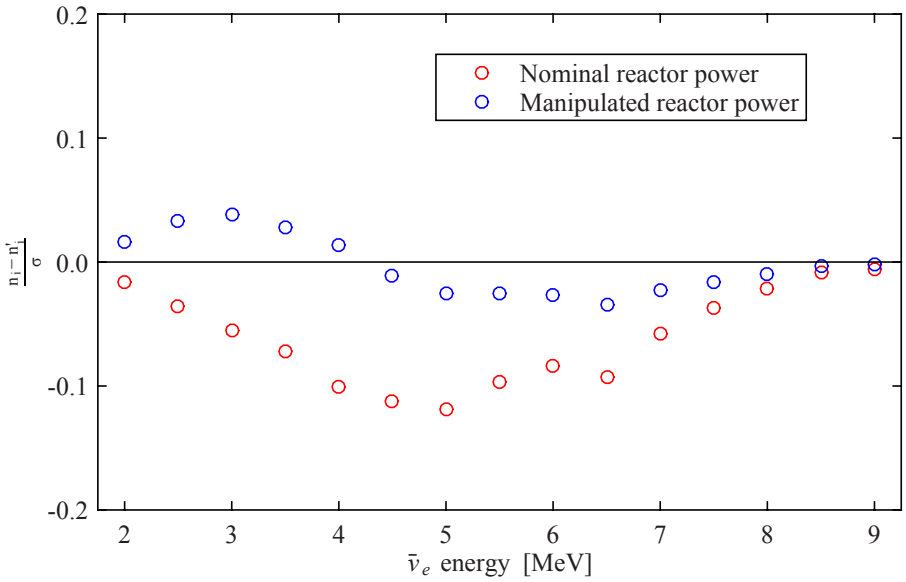

Figure 47: Effect of minimization on the contribution to the goodness-of-fit function from each bin for diversion AFR-2a.

6.3.4 Reactor-detector standoff

The reactor-detector standoff because of $1/r^2$ geometric attenuation and, to a lesser degree, any short-range neutrino oscillation physics, is one of the most important factors which impacts the signal to background ratio. The reactor-detector standoff for the UCFR and AFR scenarios was varied from 1.5 times its nominal value, within which detectors could almost certainly be placed, down to 0.5 times its nominal value, at which point further reductions in standoff would likely place the detector inside the guard vessel. The dependence of safeguards test sensitivity on standoff over this range is shown in Figure 55.

The maturity of the AFR-100 design provides assurance that 17 m is a maximum value for its standoff and likely represents a near-minimum for all small, fast, sodium-cooled cores. The UCFR-1000 scenarios were studied with a standoff based on commercial PWR plant layouts, so its nominal figure is less certain. Unless the standoff is able to be reduced to $\sim$ 15 m, none of the detection scenarios become sufficiently visible. However, due to the higher scaling of safeguards test power with standoff

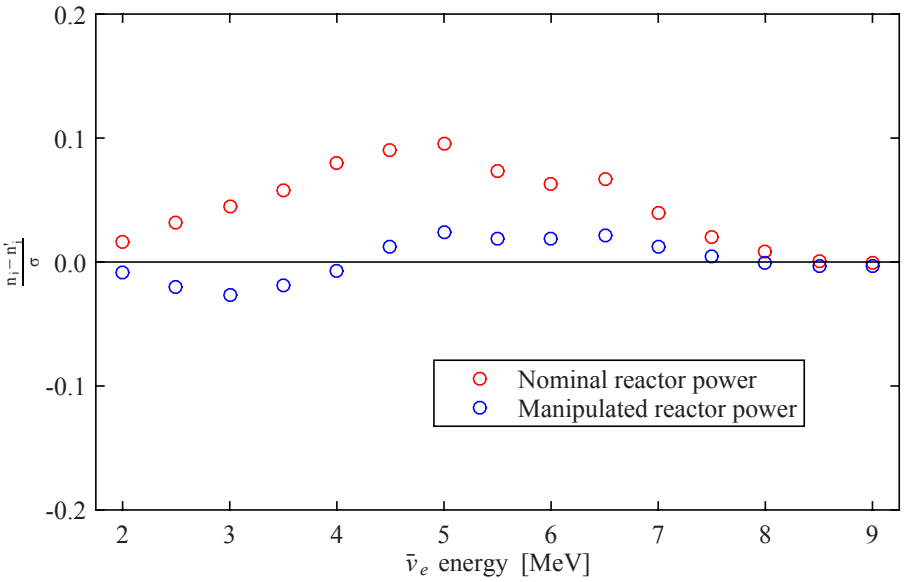

Figure 48: Effect of minimization on the contribution to the goodness-of-fit function from each bin for diversion AFR-2b.

improvements, small changes in containment building design could substantially improve the viability of antineutrino safeguards. If, as discussed in 6.3.1, placement of the detector directly underneath the core is possible, its standoff may differ substantially from detectors co-planar with the core midline (the reactor-detector standoff at Rovno was 18 m), but this is not a surety.

Variation of the reactor-detector standoff changes the in-plane space available for antineutrino detectors. The circumference around which the detector suite is distributed grows in direct proportion to the standoff; this is slower than the loss of reactor signal magnitude, but implies that if a larger standoff proves necessary, some of the loss in safeguards test sensitivity can be offset by adding fiducial mass.

6.3.5 Reactor operator power manipulation

It was assumed when calculating nominal safeguards test sensitivities that the reactor operator was compliant with the diverting actor's desire to remain covert and had

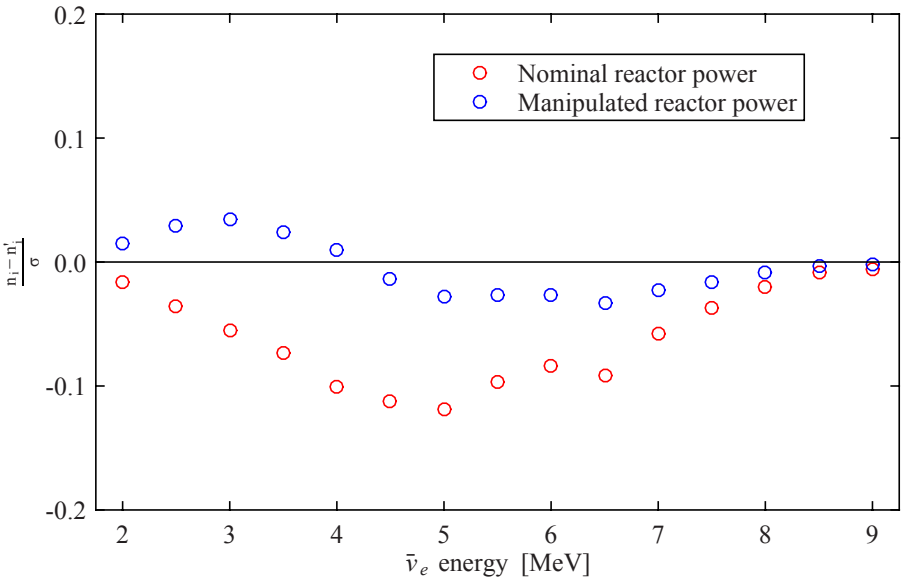

Figure 49: Effect of minimization on the contribution to the goodness-of-fit function from each bin for diversion AFR-3a.

the perfect information and operational precision necessary to fully minimize the difference in expected detector event rates. However, the imprecision of instantaneous power measurements (order of percent deviation from nominal) and the fact that no single person is responsible for direct operation makes power-masking efforts extremely difficult to execute in practice. Power manipulation is further complicated by the lack of immediate feedback on the scale of the average 0.1% level required in the absence of large short-term power swings that also run the risk of being identified by antineutrino monitoring equipment—the operator would not necessarily know that they performed any particular manipulation correctly. The non-masked versions of nominal sensitivities are orders of magnitude higher, indicating that this is a key factor in the success of antineutrino safeguards to determine the core fissile inventory on a 1-SQ level. The nuisance factor applied to represent thermal power manipulation was varied smoothly from zero to twice its nominal values for each diversion scenario; the resulting safeguards test sensitivity response is shown in Figure56.

In the absence of masking attempts, both center-core diversions from the UCFR

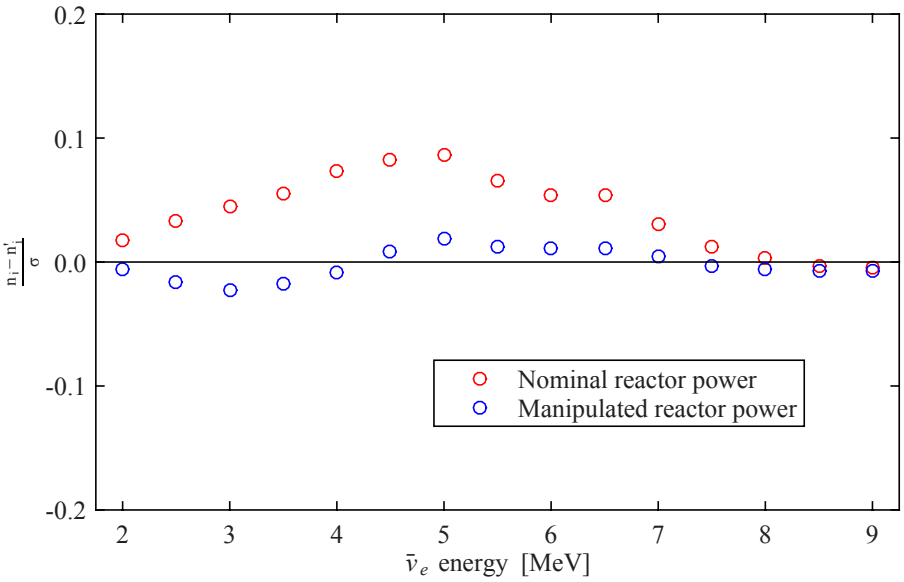

Figure 50: Effect of minimization on the contribution to the goodness-of-fit function from each bin for diversion AFR-3b.

become detectable by 3 months after the diversion. If minimization is not precisely performed, the chance of maintaining covertness drops dramatically. Masking, even if carefully orchestrated, is unlikely to be perfectly executed. Furthermore, if perfect information is not obtained and the average power is varied too far or in the wrong direction from nominal, antineutrino safeguards are more likely than not to indicate that a diversion has occurred. The AFR diversion scenarios do not become visible with zero masking, but the visibility of the core-center diversions increases by several orders of magnitude. The severity of consequences for improper masking for some diversion scenarios may sufficiently restrict operator behavior within those scenarios to using methods which risk detector by means other than antineutrinos.

It should be noted that the scaling of test sensitivity to operation with off-nominal power are for core states that are perturbed, not for a reference core with expected amounts of uncertainty on its thermal power. Cores with none of their fissile inventory altered have identical expected antineutrino spectra to the reference case, and the operating power can be verified by comparing total detector counts with their

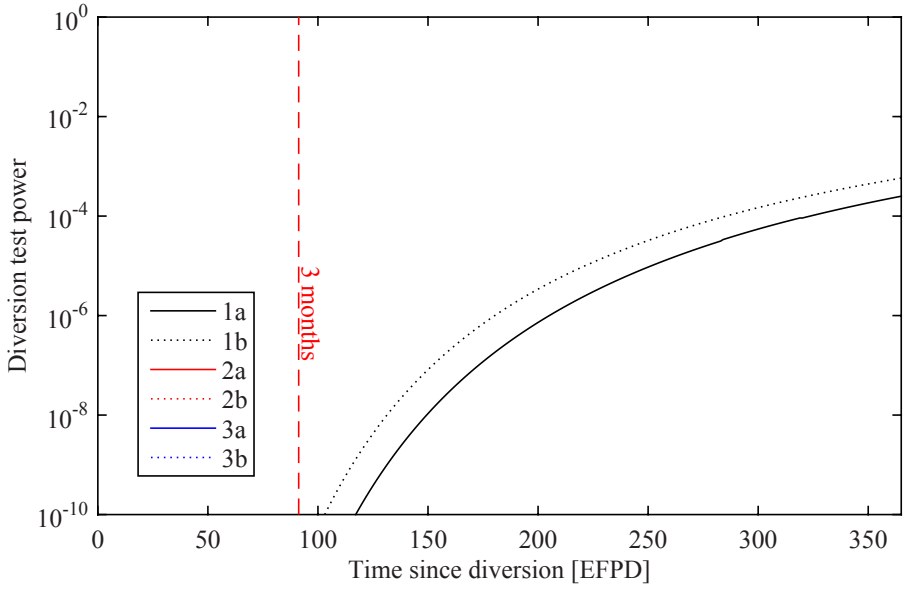

Figure 51: Improvement of safeguards test sensitivity as count integration times are lengthened for the AFR-100 diversion scenarios.

expected values, a much more expeditious determination.

6.3.6 Required true negative rate

The IAEA requires safeguards tests to have at most a 5% false positive rate to avoid costly deployments of inspectors to a large number of situations in which no material has been diverted. However, non-invasive continuous monitoring of functioning reactors may provide red-flagging functionality which has been previously unavailable that does not prompt inspector deployment, but which does initiate deeper study. Conversely, if other parameters can be improved to the point where false positive rates below 5% are achievable without sacrificing test sensitivity, antineutrino safeguards could act as a standalone indicator of the integrity of the declared reactor fissile inventory.

Variation of the required true negative rate of the safeguards test shifts the integration limits of the Gaussian distribution describing the perturbed signal (Equation 14), which captures much more of the area underneath if the nominal limits are near its

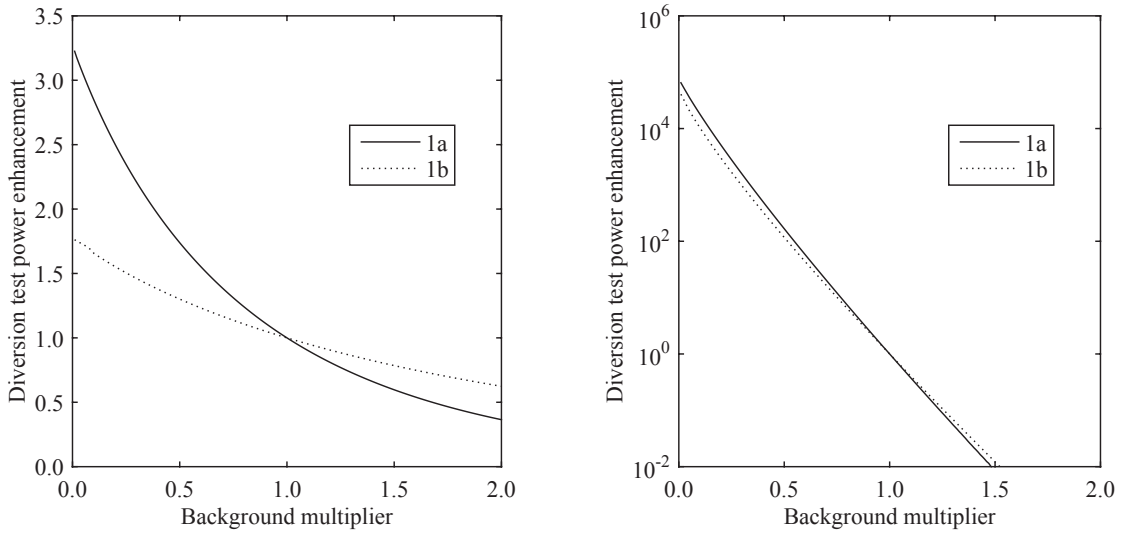

(a) UCFR (b) AFR

Figure 52: Effect on the safeguards sensitivity test to background levels at the detector installation. Only center-core diversions are shown for numerical reasons.

mean—this occurs in diversion scenarios which are within an order of magnitude or so of visibility under nominal parameters.

Depending on the willingness of the monitoring agent to sacrifice the rate of true negatives, the true positive rate can be dramatically improved. For continuous monitoring, this behavior provides the ability to set a variety of conditions based on time since last reactor shutdown, time since last on-site inspection, or confidence that LEU above a certain enrichment is unavailable, etc., for which high sensitivity is achievable without undue increase in expenditure of logistical resources or inspector manpower. The effect is strong enough that UCFR-1000 scenario with 6-SQ diversion from the core edge approaches visibility, albeit at the cost of falsely flagging the site under half of the tests in which the null hypothesis (no diversion) remains true. The AFR scenarios require similarly unacceptable sacrifices of true negative rates in order to achieve visibility of single-SQ diversions, indicating that antineutrino safeguards require significant improvement before they could possibly be used as standalone indicators of fissile inventory integrity.

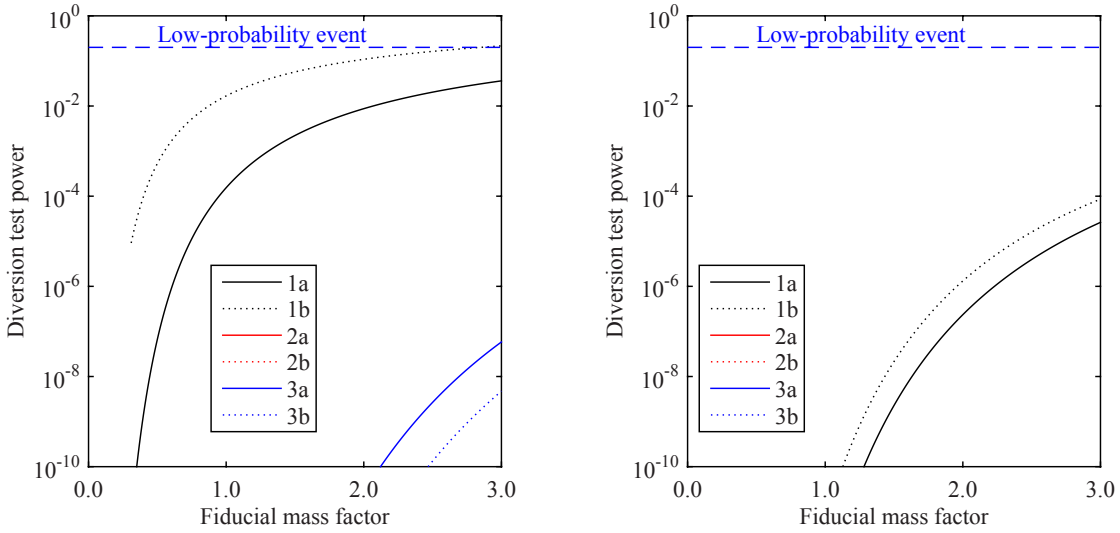

(a) UCFR (b) AFR

Figure 53: Effect on the safeguards sensitivity test to variation of the total fiducial mass of the detector suite.

6.3.7 Uncertainty reduction

The nominal safeguards test results conservatively assumed that there would be no reduction in the detector event rate uncertainties between now and when near-field antineutrino safeguards might be implemented. This gap is likely at least a few years, perhaps over a decade in length, and during this time data will be gathered by multiple near-field neutrino physics experiments. Coupled with the reasonable assumption that any reactor installation in a non-nuclear state would not be a first-of-a-kind system, but rather a well-understood plant with at least a few reactor-years' worth of operational experience, there are almost certainly going to be some refinements of the reactor antineutrino source measurement and modeling. Since the uncertainty on the detector event rates would be reduced by a factor of $^2/_3$ for a perfectly characterized antineutrino source term and over half the remaining magnitude of σ_{norm} is due to uncertainty on the IBD cross section—which is also likely to be reduced to some extent by upcoming near-field experiments—reductions in event rate uncertainties up to an order of magnitude may be achievable prior to antineutrino safeguards deployment.

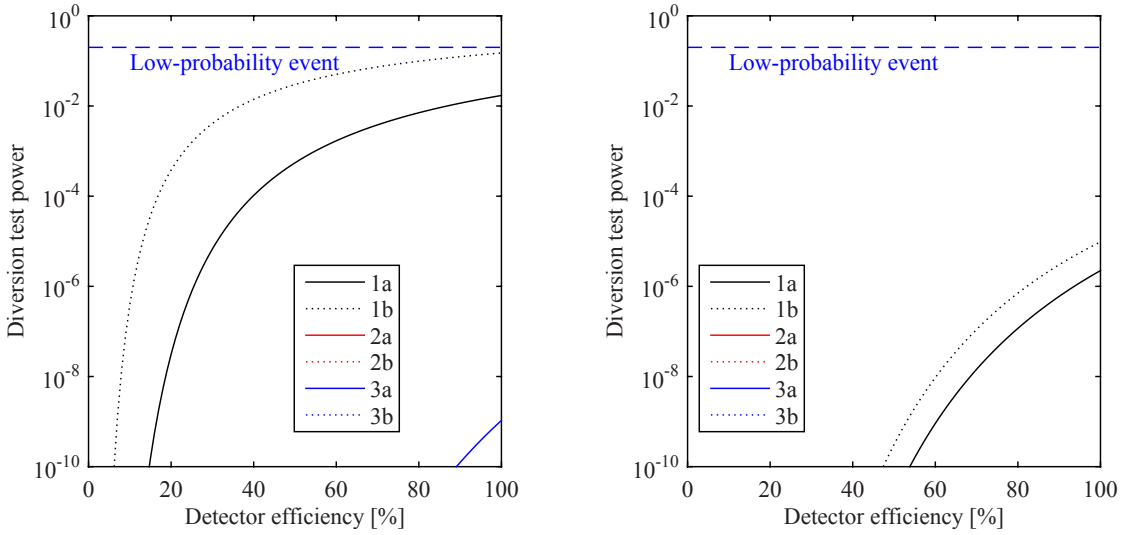

(a) UCFR (b) AFR

Figure 54: Effect on the safeguards sensitivity test to improvements in the detector efficiency within the fiducial mass.

The response of safeguards test sensitivity to reductions in σ_{norm} is shown in Figure 58.

The signal-to-background ratio plays a large role in the amount of reduction in σ_{norm} required before the test sensitivity becomes elastic to changes in the parameter. This behavior is a result of the formulation of the goodness-of-fit summation in which the normalized and minimized count rate differences form most of the terms, to which is added a "penalty" term accounting for prolonged average reactor operation which departs from declared nominal values. For the UCFR, the signal to background ratio is sufficiently high that the bulk of the chi-square summation is due to differences in detector counts, with only a small contribution from the penalty term. It does not contribute significantly to the sum until reduction by approximately a factor of 5. The AFR, with a fivefold smaller signal-to-background ratio, has a low minimized difference in detector counts, so safeguards test sensitivity is more elastic to the diversion scenarios from its core.

Improvements to the detector apparatus and background rejection will tend to shift the region of elasticity toward requiring larger reductions in σ_{norm} and provide

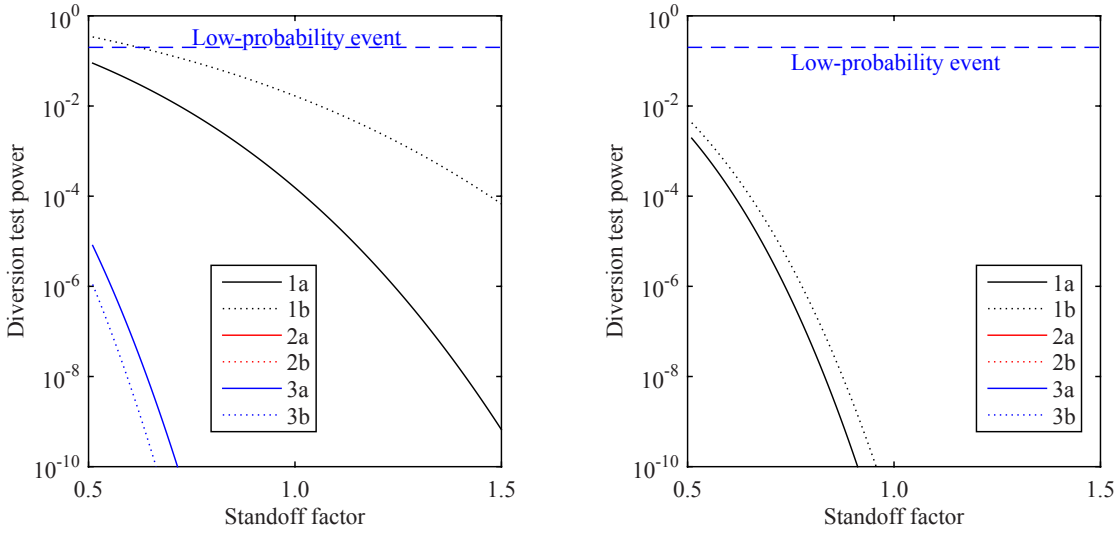

(a) UCFR (b) AFR

Figure 55: Effect on the safeguards sensitivity test to variation of the reactor-detector standoff.

less return for doing so. However, reductions to σ_{norm} will correspondingly tend to strengthen the test sensitivity the most for diversions which appear closest to the reference antineutrino signature when minimized and those which require larger levels of power manipulation to achieve minimization of the detector count differences.

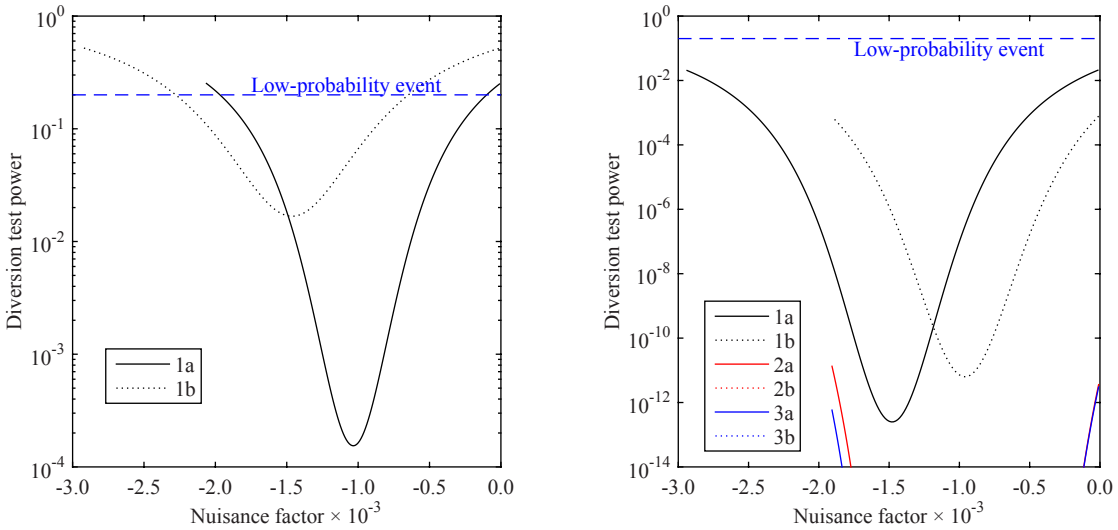

(a) UCFR (b) AFR

Figure 56: Effect on the safeguards sensitivity test to masking efforts undertaken by the reactor operator(s).

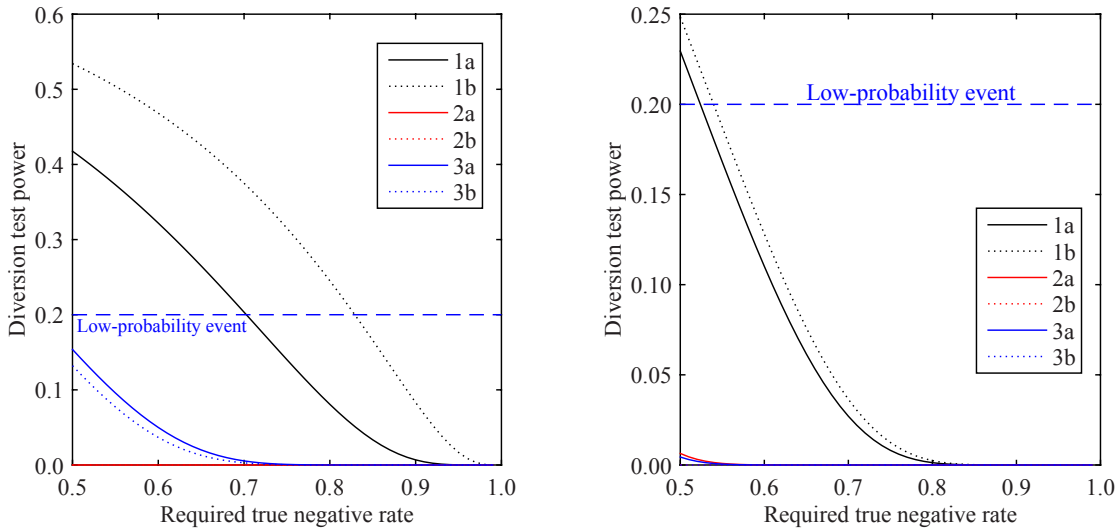

(a) UCFR (b) AFR

Figure 57: Effect on the safeguards sensitivity test to the required false negative rate of the test.

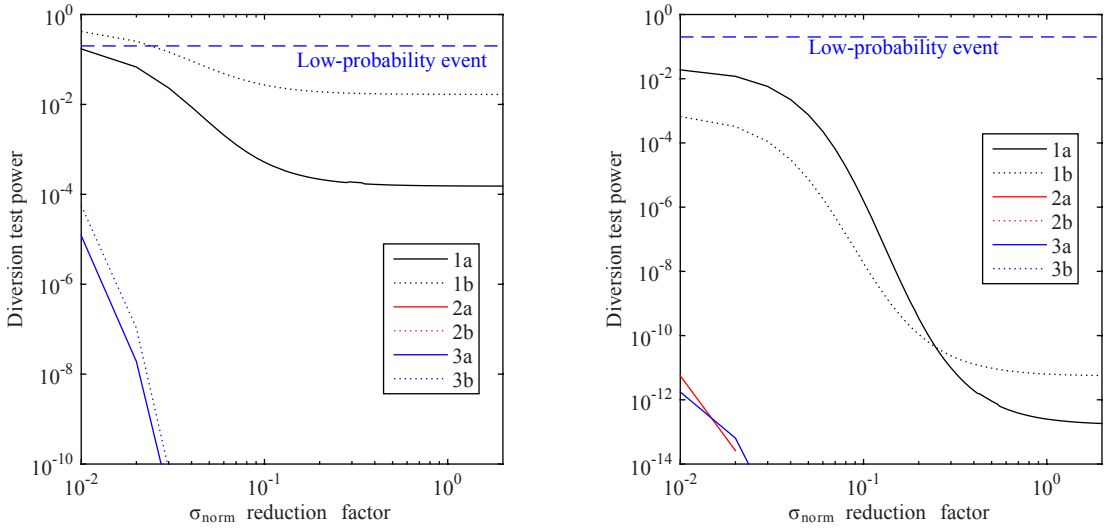

(a) UCFR (b) AFR

Figure 58: Effect on the safeguards sensitivity test to the relative reduction in the uncertainty captured in σ_{norm}.

CHAPTER VII

CONCLUSION

Nuclear energy generation is likely to expand in the coming decades to meet the demand for a substantial base electricity source which does not emit copious levels of CO_2. Nuclear safeguards institutions have identified continuous monitoring as a key capability to combat nuclear proliferation which would both better ensure that nonproliferation goals are met and reduce the stress on the safeguards infrastructure that a large number of nations in possession of nuclear reactor facilities would pose. Near-field antineutrino detectors have previously been shown to provide safeguards-usable information on the on/off power state of a reactor, its approximate operating power, and the bulk evolution of core isotopics within a timely manner for a commercial LWR. Their ability to protect against small changes to the core fissile inventory for reactor types with more subtle isotopic evolution than GW-scale LWR's is a stringent test which indicates their readiness for deployment for continuous monitoring safeguards missions.

To that end, the signal in an antineutrino detector suite with the characteristics of a current-generation detector design was modeled for reference nominal progression of low- and high-power long-life fast reactors from which irradiated fuel is not normally discharged. Scenarios in which a determined, technologically proficient, and well-supplied actor removed single-SQ amounts of plutonium were devised based upon prioritizing both short-term availability of the plutonium and making the smallest possible perturbations to the core composition to avoid detection. The estimated antineutrino signal in these scenarios resulting from the perturbed core states was compared with the reference signal via a goodness-of-fit test incorporating estimates

of the uncertainty on the detector signal that were precise where able and conservative in assumption where precision was precluded.

The goodness with which the perturbed signal fit the reference signal was high enough that reasonable confidence of the integrity of the core fissile inventory was unable to be ascertained. However, this depended very strongly on the reactor operator's ability and willingness to hide the diversion; in the early-acquisition scenarios with a high-power core, it was the difference between covertness and a detection probability of above 20%.

While antineutrino detectors are not yet sufficiently advanced to provide standalone protection against small, covert diversions of nuclear material in the most difficult scenarios in which diversion might occur, there are advances to the technology and its operational experience within reach in the near term that would substantially improve their efficacy in continuous reactor safeguards. It is not unreasonable to expect that the maximum amount of covertly-obtainable plutonium from a reactor will drop below one SQ in the coming decade, provided the core has a sufficiently high power and even distribution of fissions.

The capabilities, as developed today, of ton-scale segmented antineutrino detectors allow for the exclusion of certain material diversions within meaningful amounts of time after such diversion may have occurred. Some qualifications regarding a cap on the amount of material removed and the neutronic properties of replacement material can be made, providing for their use in concert with information on other aspects of a nation's nuclear program—for example, if their access to uranium enriched above a certain degree can be excluded. Relaxation of requirements on false positive rates could be useful for remotely red-flagging facilities and the direction and coordination of other safeguards efforts, perhaps informing the deployment of inspectors.

7.1 Future work

In addition to the basic science measurements which would improve the efficacy of antineutrino safeguards as inputs—it really would be helpful to have a base of ILL-like experimental measurements for fast fission of at least the uranium and plutonium isotopes—there are extensions of the signal comparison approach that can occur at the fine-grained modeling level which would not necessarily offer any refinement of these results, but lay the groundwork for the measurement of finer details regarding core state.

The focus of this work has been analysis of the reaction rate differences between reference and perturbed cores which have yielded to a malicious actor a weaponizable quantity of plutonium. The core of a nuclear reactor is, in every sense of the term, a non-linear system with a staggering number of feedback mechanisms spanning at least a few dimensions. That truth guided the simulated measurement of the core as a gestalt object even as perturbations to it accounted for a finer structure, and since the counting statistics of current-generation antineutrino detectors are quite low, meaningful differences in core state can currently only be measured on the core-level. Should the application of near-field antineutrino detectors for safeguards proceed toward large-scale implementation, the entire space of possible diversions will require mapping. Separation of the difference from reference antineutrino signal into components based on the composition of the altered assemblies and those resulting from the altered neutron flux in unperturbed assemblies would provide guidance into many types of multiple-assembly diversion scenarios.

The restriction to single-assembly diversions with no shuffling was made in order to limit the permutations of core perturbations to infinite in only the dimension of replacement assembly enrichment. Diversion scenarios in which removals are masked by shuffling fuel around, multiple highly-differing assemblies are removed and their

plutonium content combined during reprocessing, etc., are all viable paths a proliferator might take if given the chance. While changing particular parts of the core and measuring the whole-core effect gives insight into the strengths and weaknesses of the technology and informs us about how the technology might be applied to protect against certain eventualities, the library of possible real-world diversion scenarios is vast and if a signal comparison approach to antineutrino safeguards is adopted in practice, modeling a great number complex scenarios to determine the minimum spanning set and which types of diversions resemble each other is a necessary block in the foundation of antineutrino safeguards.

REFERENCES

[1] Abe, S., Ebihara, T., Enomoto, S., Furuno, K., Gando, Y., Ichimura, K., Ikeda, H., Inoue, K., Kibe, Y., Kishimoto, Y., and others, "Precision measurement of neutrino oscillation parameters with kamland," *Physical Review Letters*, vol. 100, no. 22, p. 221803, 2008.

[2] Ahn, J., Chebotaryov, S., Choi, J., Choi, S., Choi, W., Choi, Y., Jang, H., Jang, J., Jeon, E., Jeong, I., and others, "Observation of reactor electron antineutrinos disappearance in the reno experiment," *Physical Review Letters*, vol. 108, no. 19, p. 191802, 2012.

[3] An, F., Balantekin, A., Band, H., Beriguete, W., Bishai, M., Blyth, S., Brown, R., Butorov, I., Cao, G., Cao, J., and others, "Spectral measurement of electron antineutrino oscillation amplitude and frequency at daya bay," *Physical review letters*, vol. 112, no. 6, p. 061801, 2014.

[4] Ashenfelter, J., Balantekin, B., Baldenegro, C., Band, H., Barclay, G., Bass, C., Berish, D., Bowden, N., Bryan, C., Cherwinka, J., and others, "Background radiation measurements at high power research reactors," *Nuclear Instruments and Methods in Physics Research Section A: Accelerators, Spectrometers, Detectors and Associated Equipment*, vol. 806, pp. 401–419, 2016.

[5] Ashenfelter, J., Balantekin, B., Band, H., Barclay, G., Bass, C., Berish, D., Bowden, N., Bowes, A., Bryan, C., Brodsky, J., and others, "The prospect physics program," *arXiv preprint arXiv:1512.02202*, 2015.

[6] Association, W. N. and others, "Generation iv nuclear reactors," *updated June*, 2010.

[7] Bernstein, A., Baldwin, G., Boyer, B., Goodman, M., Learned, J., Lund, J., Reyna, D., and Svoboda, R., "Nuclear security applications of antineutrino detectors: current capabilities and future prospects," *Science & Global Security*, vol. 18, no. 3, pp. 127–192, 2010.

[8] Bernstein, A., Bowden, N., Misner, A., and Palmer, T., "Monitoring the thermal power of nuclear reactors with a prototype cubic meter antineutrino detector," *Journal of Applied Physics*, vol. 103, no. 7, p. 074905, 2008.

[9] Bernstein, A., Wang, Y.-f., Gratta, G., and West, T., "Nuclear reactor safeguards and monitoring with antineutrino detectors," *Journal of Applied Physics*, vol. 91, no. 7, pp. 4672–4676, 2002.

[10] Bjornard, T., Schanfein, M., Hebditch, D., Bari, R., and Peterson, P., "Improving the safeguardability of nuclear facilities," *Jnmm*, vol. 37, no. 4, p. 74, 2009.

[11] Blennow, M., Coloma, P., Huber, P., and Schwetz, T., "Quantifying the sensitivity of oscillation experiments to the neutrino mass ordering," *Journal of High Energy Physics*, vol. 2014, no. 3, pp. 1–41, 2014.

[12] Bowden, N., "Reactor monitoring and safeguards using antineutrino detectors," in *Journal of Physics: Conference Series*, vol. 136, p. 022008, IOP Publishing, 2008.

[13] Bowden, N., Bernstein, A., Dazeley, S., Svoboda, R., Misner, A., and Palmer, T., "Observation of the isotopic evolution of pressurized water reactor fuel using an antineutrino detector," *Journal of Applied Physics*, vol. 105, no. 6, p. 064902, 2009.

[14] Chadwick, M., Herman, M., Obložinskỳ, P., Dunn, M. E., Danon, Y., Kahler, A., Smith, D. L., Pritychenko, B., Arbanas, G., Arcilla, R., and others, "Endf/b-vii. 1 nuclear data for science and technology: cross sections, covariances, fission product yields and decay data," *Nuclear Data Sheets*, vol. 112, no. 12, pp. 2887–2996, 2011.

[15] Christensen, E., Huber, P., and Jaffke, P., "Antineutrino reactor safeguards: A case study of the dprk 1994 nuclear crisis," *Science & Global Security*, vol. 23, no. 1, pp. 20–47, 2015.

[16] Clement-Nyns, K., Haesen, E., and Driesen, J., "The impact of charging plug-in hybrid electric vehicles on a residential distribution grid," *Power Systems, IEEE Transactions on*, vol. 25, no. 1, pp. 371–380, 2010.

[17] Cochran, T. B., "Adequacy of iaeas safeguards for achieving timely detection," *and Robert Zarate,The NPT, IAEA Safeguards and Peaceful Nuclear Energy: An Inalienable Right,But Precisely to What*, pp. 221–290, 2008.

[18] Council, U. S., "A joint comprehensive plan of action (jcpoa), vienna, 14 july 2015," 2015.

[19] Diakov, A. and Rybachenkov, V., "Disposition of excess weapon grade plutonium: New developments," tech. rep., 2014.

[20] Djurcic, Z., Detwiler, J. A., Piepke, A., Foster, V., Miller, L., and Gratta, G., "Uncertainties in the anti-neutrino production at nuclear reactors," *Journal of Physics G: Nuclear and Particle Physics*, vol. 36, no. 4, p. 045002, 2009.

[21] Eyer, J. and Corey, G., "Energy storage for the electricity grid: Benefits and market potential assessment guide," *Sandia National Laboratories*, pp. 69–73, 2010.

[22] Galeotti, M. and Lanza, A., "Richer and cleaner? a study on carbon dioxide emissions in developing countries," *Energy Policy*, vol. 27, no. 10, pp. 565–573, 1999.

[23] Glossary, I. S., "edition, international nuclear verification series no. 3," *IAEA, Austria*, 2001.

[24] Haag, N., Gütlein, A., Hofmann, M., Oberauer, L., Potzel, W., Schreckenbach, K., and Wagner, F., "Experimental determination of the antineutrino spectrum of the fission products of u 238," *Physical review letters*, vol. 112, no. 12, p. 122501, 2014.

[25] Hahn, A., Schreckenbach, K., Gelletly, W., von Feilitzsch, F., Colvin, G., and Krusche, B., "Antineutrino spectra from 241 pu and 239 pu thermal neutron fission products," *Physics Letters B*, vol. 218, no. 3, pp. 365–368, 1989.

[26] Harding, J., "Economics of nuclear power and proliferation risks in a carbon-constrained world," *The Electricity Journal*, vol. 20, no. 10, pp. 65–76, 2007.

[27] Huber, P., "Determination of antineutrino spectra from nuclear reactors," *Physical Review C*, vol. 84, no. 2, p. 024617, 2011.

[28] Huber, P. and Schwetz, T., "Precision spectroscopy with reactor antineutrinos," *Physical Review D*, vol. 70, no. 5, p. 053011, 2004.

[29] Kim, T. Personal communication, 2014.

[30] Kim, T., Grandy, C., and Hill, R., "A 100 mwe advanced sodium-cooled fast reactor core concept," tech. rep., American Nuclear Society, Inc., 555 N. Kensington Avenue, La Grange Park, Illinois 60526 (United States), 2012.

[31] Kummu, M., Ward, P. J., de Moel, H., and Varis, O., "Is physical water scarcity a new phenomenon? global assessment of water shortage over the last two millennia," *Environmental Research Letters*, vol. 5, no. 3, p. 034006, 2010.

[32] Mian, Z. and Nayyar, A., "Playing the nuclear game: Pakistan and the fissile material cutoff treaty," *Arms Control Today*, vol. 40, no. 3, p. 17, 2010.

[33] Mueller, T. A., Lhuillier, D., Fallot, M., Letourneau, A., Cormon, S., Fechner, M., Giot, L., Lasserre, T., Martino, J., Mention, G., and others, "Improved predictions of reactor antineutrino spectra," *Physical Review C*, vol. 83, no. 5, p. 054615, 2011.

[34] Narayan, P. K. and Narayan, S., "Carbon dioxide emissions and economic growth: panel data evidence from developing countries," *Energy policy*, vol. 38, no. 1, pp. 661–666, 2010.

[35] Nephew, R., "Based on breakout timelines, the world is better off with the iran nuclear deal than without it," 2015.

[36] Nikou, S. N., "Timeline of irans nuclear activities," *United States Institute of Peace,¡ http://iranprimer. usip. org/resource/timeline-irans-nuclear-activities¿,[Access Date: 11/10/2014]*, 2013.

[37] Nisan, S. and Dardour, S., "Economic evaluation of nuclear desalination systems," *Desalination*, vol. 205, no. 1, pp. 231–242, 2007.

[38] Palmiotti, G., Lewis, E., and Carrico, C., "Variant: Variational anisotropic nodal transport," in *Proceedings of the international conference on mathematics and computations, reactor physics, and environmental analyses. Volume 1 and 2*, 1995.

[39] Palmiotti, G. and Salvatores, M., "Proposal for nuclear data covariance matrix," *JEF/DOC-1063 Rev*, vol. 1, 2005.

[40] Philipp, E., "N. korea claims hydrogen bomb test," *Arms Control Today*, vol. 46, no. 1, p. 36, 2016.

[41] Rimpault, G., Plisson, D., Tommasi, J., Rieunier, J., and Jacqmin, R., "The eranos code and data-system for fast reactor analyses," in *Proc. Int. Conf. New Frontiers of Nuclear Technology: Reactor Physics, Safety and High-Performance Computing (PHYSOR 2002)*, pp. 7–10, 2002.

[42] Ryabtsev, A., Kotsupalo, N., Titarenko, V., Igumenov, I., Gelfond, N., Fedotova, N., Morozova, N., Shipachev, V., and Tibilov, A., "Development of a two-stage electrodialysis set-up for economical desalination of sea-type artesian and surface waters," *Desalination*, vol. 137, no. 1, pp. 207–214, 2001.

[43] Şahin, S. and Ligou, J., "The effect of the spontaneous fission of plutonium-240 on the energy release in a nuclear explosive," *Nuclear Technology*, vol. 50, no. 1, pp. 88–94, 1980.

[44] Schaper, A., "Principles of the verification for a future fissile material cutoff treaty (fmct)," 2001.

[45] Schreckenbach, K., Colvin, G., Gelletly, W., and Von Feilitzsch, F., "Determination of the antineutrino spectrum from 235 u thermal neutron fission products up to 9.5 mev," *Physics Letters B*, vol. 160, no. 4, pp. 325–330, 1985.

[46] Schrock, V. E., "Evaluation of decay heating in shutdown reactors," *Progress in Nuclear Energy*, vol. 3, no. 2, pp. 125–156, 1979.

[47] Sekimoto, H., Ryu, K., and Yoshimura, Y., "Candle: the new burnup strategy," *Nuclear Science and Engineering*, vol. 139, no. 3, pp. 306–317, 2001.

[48] Smith, D. L., "Covariance matrices for nuclear cross sections derived from nuclear model calculations," tech. rep., Argonne National Laboratory, Argonne, Illinois, 2004.

[49] Stauffa, N., Kima, T., Taiwoa, T., Buironb, L., Varaineb, F., and Gullifordc, J., "Evaluation of sodium-cooled fast reactor neutronic benchmarks," in *Proc. Int. Conf. Fast Reactors and Related Fuel Cycles (FR13), Paris, France*, 2013.

[50] Stewart, C. and Erickson, A., "Antineutrino analysis for continuous monitoring of nuclear reactors: Sensitivity study," *Journal of Applied Physics*, vol. 118, no. 16, p. 164902, 2015.

[51] Tak, T., Lee, D., and Kim, T., "Design of ultralong-cycle fast reactor employing breed-and-burn strategy," *Nuclear Technology*, vol. 183, no. 3, pp. 427–435, 2013.

[52] Technology, E., "Ej-309 liquid scintillator pulse-shape discrimination properties," 2010.

[53] to the 2010 Nuclear Nonproliferation Treaty Review Conference, U. D., "Treaty on the non-proliferation of nuclear weapons," tech. rep., 2010.

[54] United States, R. F., "Agreement between the government of the united states of america and the government of the russian federation concerning the management and disposition of plutonium designated as no longer required for defense purposes and related cooperation," tech. rep., 2000.

[55] Vishwanathan, A., Chandrashekar, S., Krishnan, L., and Sundaresan, L., "North korea's 2016 nuclear test: An analysis (isssp report no. 01-2016)," 2016.

[56] Vogel, P., Schenter, G. K., Mann, F. M., and Schenter, R., "Reactor antineutrino spectra and their application to antineutrino-induced reactions. ii," *Physical Review C*, vol. 24, no. 4, p. 1543, 1981.

[57] Von Feilitzsch, F., Hahn, A., and Schreckenbach, K., "Experimental beta-spectra from 239 pu and 235 u thermal neutron fission products and their correlated antineutrino spectra," *Physics Letters B*, vol. 118, no. 1, pp. 162–166, 1982.

[58] Vyrodov, V., Declais, Y., De Kerret, H., and Kozlov, Y. V., "Precise measurement of the cross section for the reaction v˜ e+ p-¿ e^++ n at the bourges reactor," *JETP LETTERS C/C OF PIS'MA V ZHURNAL EKSPERIMENTAL'NOI TEORETICHESKOI FIZIKI*, vol. 61, pp. 163–163, 1995.

[59] Yudin, Y., *Multilateralization of the nuclear fuel cycle: Assessing the existing proposals*. United Nations Institute for Disarmament Research, 2009.

[60] Zimmerman, P. D., "Proliferation: Bronze medal technology is enough," *Orbis*, vol. 38, no. 1, pp. 67–82, 1995.